TU Delft

Rijkswaterstaat
Ministerie van Infrastructuur en Waterstaat

CLEARANCE MEASUREMENT VALIDATION FOR HIGHWAY INFRASTRUCTURE WITH USE OF LIDAR POINT CLOUDS

J.P. Meinderts

Geoscience & Remote Sensing
Delft University of Technology

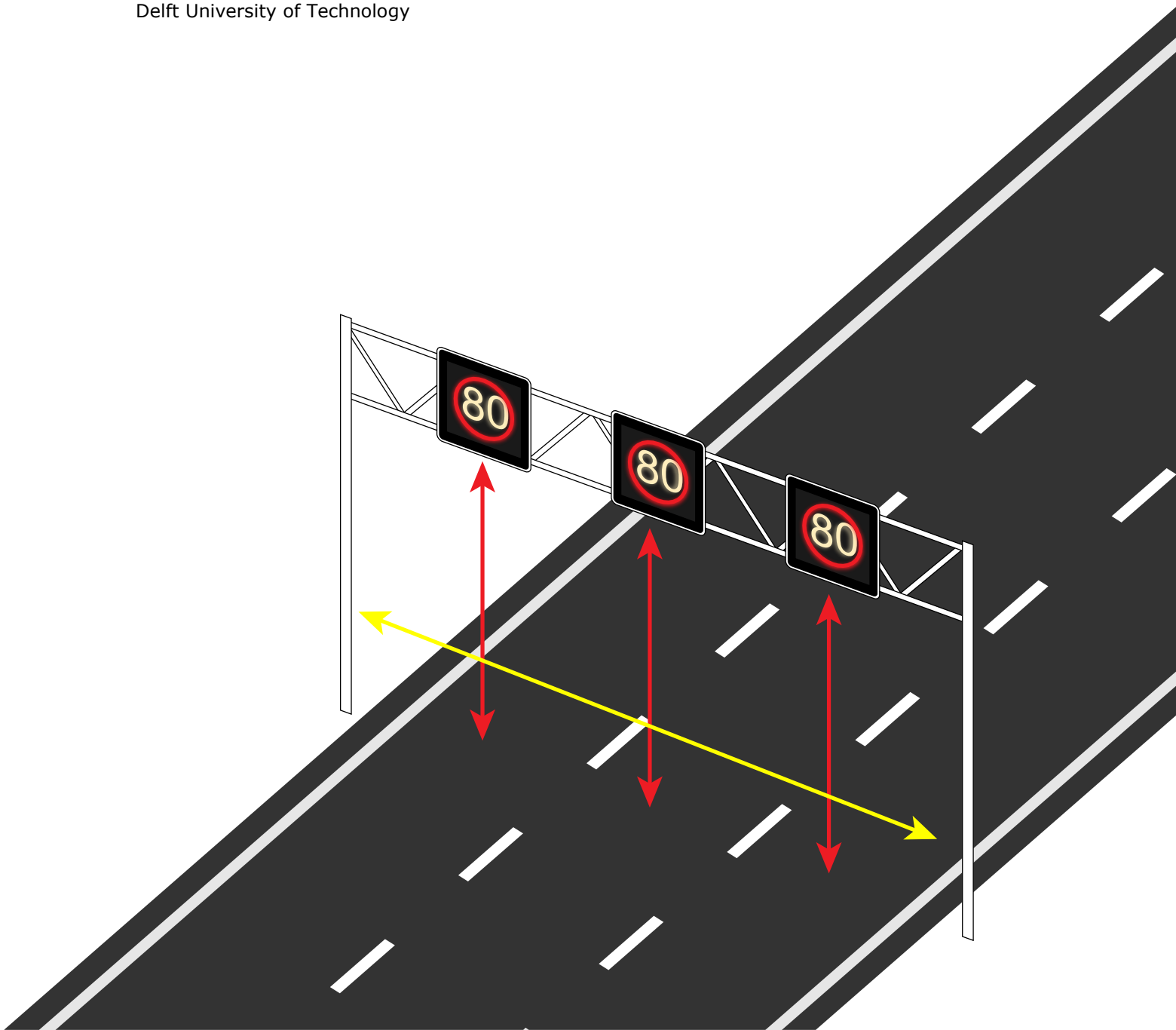

CLEARANCE MEASUREMENT VALIDATION FOR HIGHWAY INFRASTRUCTURE WITH USE OF LIDAR POINT CLOUDS

by

J.P. Meinderts

to obtain the degree of Master of Science at the Delft University of Technology,
to be defended publicly on January 16th, 2023 at 11:00.

Student number:	4305779	
Project duration:	April 18th, 2022 – January 16th, 2023	
Thesis committee:	Dr. R. C. Lindenbergh,	TU Delft, chair
	Dr. A. R. Amiri-Simkooei,	TU Delft
	Ir. D.H. van der Heide,	Rijkswaterstaat

TU Delft Delft University of Technology

Rijkswaterstaat
Ministerie van Infrastructuur en Waterstaat

Abstract

The Dutch highway network contains more than 3.000 kilometers of roads. Along these roads are thousands of overhead objects such as viaducts and traffic sign gantries. It is essential to have recent and accurate data on the clearances under these objects. This data is important for maintenance and routing oversized transports. Obtaining clearance measurements can be time consuming, costly and in involves a lot of manual labor. The aim of this study is to develop a method that automatically estimates vertical and horizontal clearances of highway viaducts and gantries from Mobile Laser Scanning (MLS) point clouds. The proposed method takes a point cloud of an infrastructure object as input, and as output provides the user with a concise overview of the estimated horizontal and vertical clearances under the object.

A point cloud of a highway viaduct or gantry is segmented into different clusters relevant for determining the clearances. The discrete points in these clusters are then used to approximate their corresponding surfaces with B-splines. Subsequently the minimal clearances can be estimated. These clearances are estimated at certain pre-specified locations according to guidelines from the highway authority, Rijkswaterstaat. To validate the proposed method a case study is performed on two sections of Dutch highway containing a total of 20 viaducts and 50 gantries. For the viaducts and gantries along these highway sections there are clearance measurements available from third-party contractors. After processing the point clouds in the case study, the obtained clearance estimations are compared to the third-party measurements. This comparison gives a quantitative analysis of the estimated clearances and shows that the proposed method produces similar results to the third-party measurements. On average the proposed method overestimates the vertical clearances and underestimates the horizontal clearances. A sensitivity analysis is performed to confirm that the proposed method can produce consistent results. When performing clearance estimations on a different dataset containing point clouds with an up to 20 times higher point density, the estimation differences with the third-party measurements become even smaller.

Contents

1. Introduction

1.1 Highway infrastructure clearance measurements

The Dutch highway network contains more than 3.000 kilometers of highways (Rijkswaterstaat, 2021). It is essential to have accurate data on the vertical and horizontal clearances at overhead objects along these roads. 'Objects' in this case could refer to via-, eco- or aqueducts, tunnels, or gantries wielding traffic signs or lane control signs. This data can be used for determining routes for oversized transports, infrastructure reconstruction after accidents, maintenance and preventing or settling legal claims after an incident. Oversized transports rely on the assumption they receive valid clearance data when routing their cargo. When the provided clearance data is inaccurate it can have great (financial) consequences for either the cargo or highway infrastructure.

For all overhead structures along the Dutch highway network the clearances are documented according to specifications issued by the executive organization of the Dutch ministry of Infrastructure and Waterways: Rijkswaterstaat. These specifications describe at what locations under an overhead infrastructure object and with what margin of error the clearances should be measured.

Traditionally these measurements are taken in the field with usage of geodetic measurement devices such as a rangefinder, theodolite, total station or laser scanner. The measurements and processing of the data is usually executed by third party contractors and subsequently validated by Rijkswaterstaat. Since the documentation process of the measurements involves a lot of manual work it is important that this validation process occurs thoroughly. Currently this validation process is meant to prevent blunders in the documented clearances. One of the tools available for validation is a large point cloud dataset covering all the highways in the Netherlands. The validation occurs by manually selecting points that approximately restrict the clearance in either horizontal or vertical direction whereafter the distance between those points is calculated. This is not a thorough procedure as it is prone to user error. Furthermore, it is difficult to obtain reproducible results this way since no solid workflow is in place.

This research uses an independent point cloud dataset that offers great potential for developing an automated process that can validate clearance data provided by third party contractors. Point clouds contain a lot of (geo-)information and therefore provide a well-suited environment for validating real world measurements. However, it is important that these validations are accompanied by a quality assessment to make sure the validation verdict is sound.

With the fast-paced development of point cloud technology, clearance measurement validation can greatly benefit from the automatic segmentation, classification and surface estimation of available point cloud datasets. Since the available data is so abundant, the goal is to achieve a method that is applicable to a large variety of situations that can be encountered on the road. Different types of viaducts, different road layouts and different types of traffic gantries.

1.2 Research objective

The main objective for this study is to develop a method for validating vertical and horizontal clearance measurements of highway infrastructure with use of LiDAR point cloud data. The method should take a point cloud of an infrastructure object as input, and as output provide the user with a concise overview of the horizontal and vertical clearances of the object (Figure 1.1). Since the method should fit into the workflow Rijkswaterstaat uses for validating clearance measurements, it is important that the output is analogous with currently used clearance reports.

A point cloud of an overpass or gantry should first be segmented into the different components relevant for determining the clearances. Geometric models will then be fitted to these segmented clusters after which the clearances can be computed. These clearances should be calculated at certain pre-specified locations according to Rijkswaterstaat's guidelines.

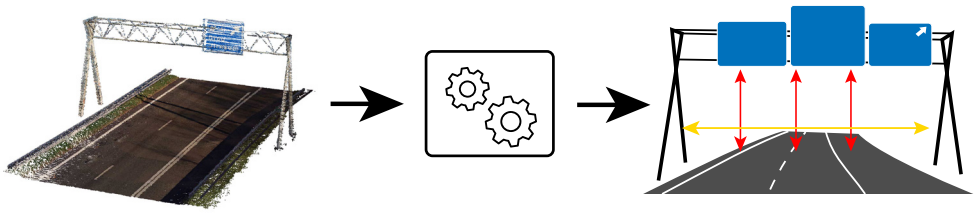

Figure 1.1: A simplification of the tool to be developed in this research. A point cloud of a traffic gantry is taken as input and processed. The result is a visualization of the horizontal and vertical clearances.

1.3 Research questions

Taking the previously mentioned objectives in consideration, the following main research question is defined:

- *How to improve the approach for validating clearance measurements of highway infrastructure with the usage of LiDAR point clouds?*

To find an answer to this main research question a method will be developed to automatically estimate the clearances of a viaduct or gantry from available point clouds. This method involves multiple steps which can help to answer the following sub-questions:

- *How to segment and classify different viaduct and gantry components from the point cloud data?*
- *How to obtain the highway lane boundaries from the point cloud data?*
- *What objects restrict the horizontal clearances under a gantry or viaduct and how can they be segmented from the point cloud?*
- *What are the geometric characteristics of a structure's components that determine the clearances?*
- *How to estimate and locate the minimal vertical and horizontal clearances from the point clouds?*
- *How to assess the quality of the inferred clearances and what is the quality difference between data providers?*

1.4 Thesis outline

This thesis is structured as follows:

Section 2 presents background information about the current requirements for clearances on Dutch highways, related research, and an overview of some point cloud processing techniques that are used in this research. Section 3 gives a summary on the characteristics of the point clouds dataset that were used in this research. Section 4 explains the workflow of the proposed method for estimating clearances under viaducts and gantries. A step-by-step guide is provided with intermediate results. Section 5 presents the case study on a selection of viaducts and gantries and their results. These results are compared with third-party measurements that were obtained by contractors. In Section 6 some problems with the data and the applicability of the method are discussed. Finally, in Section 7 the research is concluded and the research questions from Section 1.3 are answered one-by-one. Several recommendations are provided for potential future research.

2. Background

Section 2.1 covers the current requirements that apply to clearance measurements. Following is Section 2.2 that introduces laser scanning and point clouds. Section 2.3 presents a selection of related research on estimating clearances under overhead infrastructure objects. Lastly, Section 2.4 covers the clustering, detection and approximation principles used in the proposed method.

2.1 Current standards for determining clearances

This subsection gives an overview of the requirements for clearance measurements as composed by Rijkswaterstaat. It covers the definitions that are important to understand what is meant by a minimal clearance. The information here is based on the product specifications for clearance measurements (Rijkswaterstaat, 2019).

2.1.1 Vertical clearance

The **vertical clearance** is a measurement perpendicular to the road surface between an object and the underlying pavement. The minimal vertical clearance is found where this distance is the smallest. Objects are defined as highway bridges, wildlife bridges, navigable aqueducts, tunnels, and road sign gantries. For this thesis the focus will be on highway bridges and road sign gantries. These are also the most common objects.

The vertical clearance measurements must meet the following requirements: The precision σ should be $\leq 1.0\ cm$ and the measurements should be presented with 3 decimals. The locations of the clearance heights have different requirements for viaducts and traffic gantries.

2.1.1.1 Highway viaducts

For a highway viaduct the following applies:

- The vertical clearance should be determined on each lane marking.
- For each driving direction two clearance cross sections should be provided. The first one at beginning of the object and the second one at the rear of an object. The location of the front is determined by in what direction the hectometer signs along the road are increasing in value. This is illustrated in Figure 2.2.
- Double highway bridges less than 3 meters apart are seen as one object. When the gap in between the two viaducts is larger than 3 meters, both bridges are seen as individual objects.

The vertical clearances must be determined at:

- The road markings such as:
    - Continuous lines
    - Dashed lines
    - Block markings
- 1 meter outside from the edge of the continuous markings (edge markings). This is only needed when this location is still on the pavement.
- The edges of the asphalt.
- Suspended signage on the structure if these signs hang lower than the structure itself.

Many highway bridge superstructures have a bridge deck with decreasing thickness towards the sides. For these bridges the vertical clearances should be determined at lines AA’ and BB’ as shown in Figure 2.2.

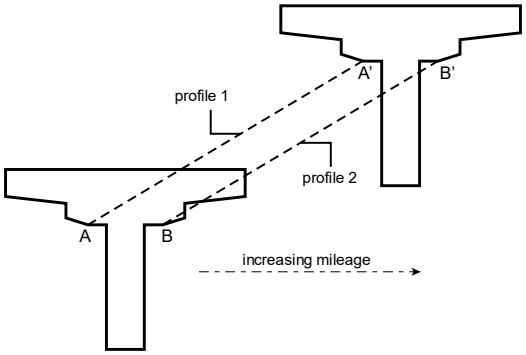

Figure 2.2: Cross sections along which the vertical clearances should be determined for a highway bridge with a non-constant deck thickness.

2.1.1.2 Traffic sign gantries

For these structures the minimal vertical clearances should be determined per lane including rush hour lanes, entry or exit lanes and emergency lanes. If there is no road sign or lane control sign directly above a lane the vertical clearance is determined from the pavement to the gantry's suspension superstructure.

2.1.1.3 Important difference between viaducts and gantries

The approach in determining the minimal clearances under a viaduct and a gantry is different. For viaducts Rijkswaterstaat requires that the vertical clearance is determined on the location of each road marking that is intersecting cross sections AA' and BB' in Figure 2.2. For gantries this is not the case since here the **minimal** clearance should be determined for each lane which can be located on the edge, in the middle of somewhere in between. The location for this minimal clearance greatly depends on the signage that is suspended above.

2.1.2 Horizontal clearance

The **horizontal clearance** is the minimal horizontal distance perpendicular to the driving direction between obstacles that are positioned alongside the pavement. Obstacles here are defined as objects or vegetation that can cause severe damage or injuries to a vehicle or passengers when a collision occurs.

The horizontal clearance measurements must meet the following requirements: The precision σ should be $\leq 5.0\ cm$ and the measurements should be presented with 2 decimals. For the location of the horizontal clearance the following applies:

- The horizontal clearance must be determined at a height between $0.5\ m$ and $1.0\ m$ above the pavement. The height of the guardrail should fall within this range.
- In case there is no guard rail on one or either side of the road, the width of the roadway cannot always be clearly defined. If the boundary of the passage width on one or both sides of the road cannot clearly be indicated, for instance due to the absence of obstacles as stated previously, the edge of the pavement is taken as the boundary.

2.1.3 Final clearance product

The final product containing the obtained clearance measurements consists of one or more photographs depicting evaluated structure with the clearance dimensions visualized and indicated by the red and yellow arrows. An example is given in Figure 2.3. The photograph is accompanied by metadata that gives information about the road name, the direction, the location, the measurement date, the asset number of the gantry or viaduct and the minimal clearance. The figure shows a gantry with five lanes (four regular lanes and an emergency lane). The horizontal clearance here is bounded by the guard rails that are present on both sides of the road.

Figure 2.3: Example of the final product containing the clearance measurements in meters.

2.2 Point clouds and laser scanners

A point cloud is a collection of data points in 3D space with each point defined separately in a coordinate system. Since point clouds are well suited to describe structures and its surface properties, they are used widely in metrology or other forms of infrastructure inspections. General methods for obtaining point clouds are either using 3D laser scanners or photogrammetry.

When using a 3D laser scanner to obtain a point cloud of an object, each point in the cloud represents a real point on the surface of the scanned object. The scanner calculates a coordinate for each point based on the vertical and horizontal angle of the scanner combined with the time of flight of the laser pulse it sends out for each point (Figure 2.4). This technique is also called LiDAR (**Li**ght **D**etection **A**nd **R**anging).

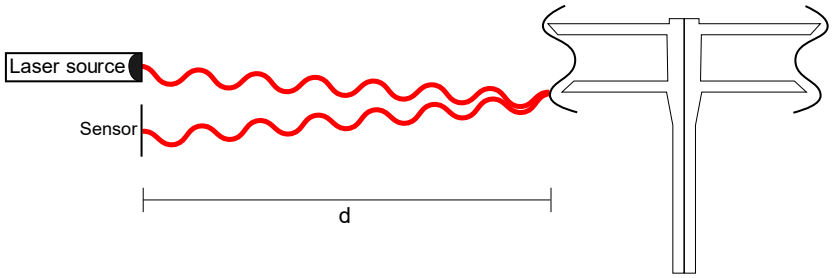

Figure 2.4: A schematic overview of a laser pulse reflecting on a guard rail

Mobile LiDAR presents multiple benefits (Puente et al., 2013): data is captured at high speed, measurements can be performed remotely, the obtained datasets have a much higher point density compared to traditional measurement techniques and the abundance of data and 3D visualizations can provide added confidence that the mapped objects correspond to the actual existing conditions.

Besides the laser scanner, a mobile LiDAR system also includes several other subsystems: a digital camera to map colors, an Inertial Measurement Unit (IMU), a Global Navigation Satellite System (GNSS) receiver and a control unit that ensures that all subsystems acquire synchronized data and data is recorded (Heikkilä et al., 2010).

A LiDAR uses a laser to obtain range and angle measurements. Currently there are two different techniques that are used in mobile laser scanning systems for range measurements: time-of-flight (TOF) and phase shift based systems (Figure 2.5). A TOF system measures the time difference between an emitted and a received laser pulse. The distance d (see Figure 2.4) can be calculated as:

$$d[m] = \frac{ct}{2} \qquad (1)$$

where $c[m/s]$ is the speed of light and $t[s]$ is the time in seconds the laser pulse takes to travel from the laser source via the reflecting surface into the sensor. Phase based laser scanners determine the range as the difference between the emitted and received backscattered signal of an amplitude modulated continuous wave (Puente et al., 2013). This technique uses a continuous signal, which enables a much higher measurement frequency since the scanner does not need to wait for the return signal before sending a new pulse as is the case with TOF scanners. Phase based systems achieve in general a better accuracy but their range is shorter compared to TOF systems (Soudarissanane, 2016). The relationship between the phase shift $\Delta\phi$ and range d is provided in the following equation:

$$d[m] = \frac{\Delta\phi}{2\pi}\frac{\lambda}{2} + \frac{\lambda}{2}n \qquad (2)$$

Here λ is the modulation wavelength and n is the unknown number of full wavelengths between the system sensor and the reflecting object. The measurement of the phase difference can be ambiguous when there is an uncertainty in the number of periods n that is measured. This ambiguity can be avoided by measuring the phase difference of multiple signals with different wavelengths.

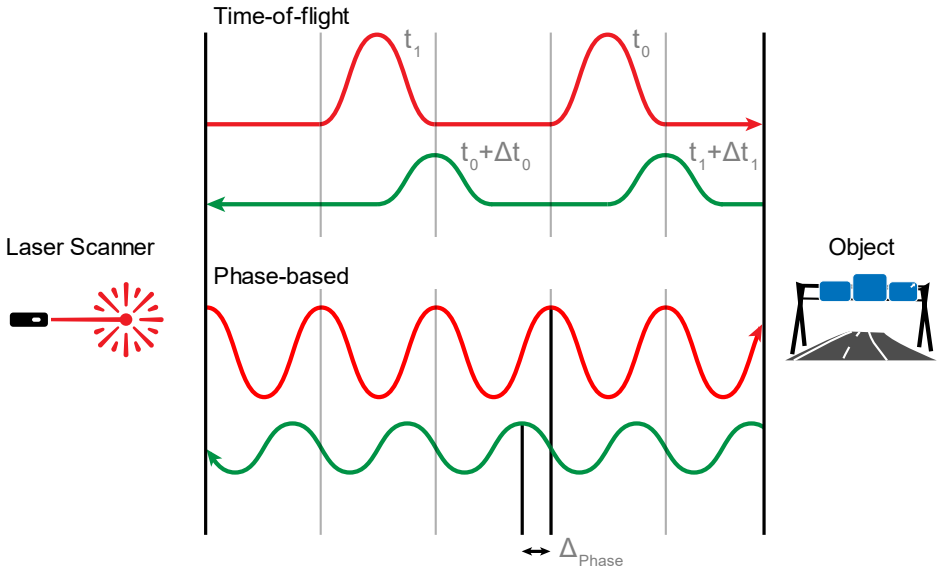

Figure 2.5: Distance measurement principle of time-of-flight laser scanners and phase based laser scanners. The red signal is the emitted signal, and the green signal is the received signal.

The point density or resolution of a point cloud is mainly dependent on how many laser pulses per second the laser scanner can transmit. Scanners can generate hundreds of thousands of points per second which comes at the downside that the file sizes of the generated point clouds can get out of hand quickly. To make the point cloud data easier to manage 'down sampling' can be used to reduce the number of points to an arbitrary amount.

For this research point clouds with different resolutions are used. Low- and high-resolution point clouds each have their own advantages and disadvantages. A tradeoff is made between storage size and point cloud detail.

2.3 Estimating clearances of highway bridges from point cloud data

Multiple researches have already been successful in estimating clearances along highways from point cloud data. This section presents recent research on clearance estimations as well as some other closely related recent research.

2.3.1 Trajectory definition

Both the vertical and horizontal clearances are dependent on the orientation of the road axis. The horizontal clearance is determined perpendicular to the road axis in the horizontal plane and the vertical clearance is determined perpendicular to the road axis in the vertical plane. Hence, determining the orientation of the road is an important first step.

When a point cloud is obtained from a Mobile Laser Scanner (MLS)-system, often the angle of the scanner is also recorded as an attribute for each point in the cloud alongside intensity, time, etc. With this information it is possible to find points parallel to the road's axis by removing all points that fall out of the nadir plane of the MLS (Gargoum et al., 2018). It is important to note that this method works best when the point cloud consists of one continuous scan. If the point cloud is constructed from multiple co-registered scans, multiple trajectories can be found. The trajectory only gives information on the trajectory of the MLS and this will not necessarily follow the road axis. This means the MLS vehicle should remain in the same lane while scanning or the obtained trajectory will not give a good estimation of the road axis.

This method does not give any information on the number of lanes and width of the road surface. This information is necessary since vertical clearances must be determined for every lane.

2.3.2 Road marking detection

A second method for determining the trajectory of a road involves the segmentation of road markings. There are several methods to detect road markings from LiDAR data. These methods can be roughly divided into two categories: real-time detection and non-real-time detection. Real-time detection is mainly used for car safety systems and asks for lightweight code whereas the other category gives room to sacrifice some processing time for improved detection accuracy.

Prochazka et al. (2019) propose a method that processes a point cloud obtained from LiDAR measurements and provides an output file with vectors containing the road lane polygons, specifically dashed and continuous markings. Initially the segmentation of the point cloud starts based on reflectance values and after this step a ground detection algorithm (Landa et al., 2013) is applied. With use of standard Euclidean distance segmentation, the extracted ground points are further segmented. Points that satisfy an empirically determined limit of maximal distance between points are considered as belonging to a single segment. The resulting segments are filtered based on four conditions: the minimal number of points in a segment, the maximal number of points in a segment, the maximal size of an enveloping rectangle in x or y direction and a minimal percentage of planar points using RANSAC algorithm.

2.3.3 Vertical bridge clearance estimation with terrestrial laser scanning

In Zhang et al. (2013) a method is proposed to estimate vertical bridge clearances by using static terrestrial laser scanners (TLS). The study introduces an approach to reduce data noise caused by passing and obstructing the laser scanner. The filtered point cloud is used to manually infer the vertical clearances from. The proposed method is validated in a case study of a large interchange. However, no detailed accuracy assessment is provided.

2.3.4 Railway tunnel clearance estimation

Railway tunnel clearance is directly related to the safe operation and freight capacity of trains. In (Zhou et al., 2017) a tunnel clearance inspection approach is presented based on 3D point clouds obtained by a mobile laser scanner system. A dynamic coordinate system for railway tunnel clearances is introduced. By using a 3D linear fitting algorithm on a segmented point cloud, the rail line can be extracted and is used to seamlessly connect all rail segments. Based on the rail alignment and the clearance coordinate system different types of clearance frames are introduced to perform the tunnel clearance inspection. The claimed precision reaches $0.03\ \mathrm{m}$.

2.3.5 Impact of point density reduction

Point clouds often contain differences in point density. This variation is expected to affect the quality of the information that is inferred from the point clouds. Gargoum & El-Basyouny (2022) investigates the impacts of point density reduction on the extraction and assessment of different geometrical features. The different geometrical features were extracted from a point cloud at varying levels of point density and on a selection of different Canadian highway segments. It was found that clearance assessments on viaducts had low sensitivity to reductions in point density. Reductions to 10% of the original data yielded comparable results to what was obtained at 100% point density. A possible explanation for this could be that the clearance estimation procedure involves rasterizing the point cloud, which uses a collection of points that fall within a raster cell to estimate the surface elevation properties at that location. Even when the number of points that fall within a raster cell is greatly reduced, the elevation estimate of that cell is not impacted significantly.

Low point density can however cause an inability to detect accurate clearances under short span overhead objects e.g. power cables or gantries. The proposed method for short span overhead objects does involve any form of surface reconstruction. As a result, the vertical clearance only depends on the single lowest point in a segmented overhead object.

2.3.6 Review of mobile mapping and surveying technologies

In Puente et al. (2013) an analysis is introduced on the performance of some modern mobile terrestrial laser scanning systems. The study presents an overview of the positioning, scanning and imaging devices used in these systems. A systematic comparison of the navigation and LiDAR specifications from the manufacturers is provided. Based on the accuracy requirements for a mapping or surveying project a best solution is found considering all scanner specifications.

2.3.7 Vertical clearance estimation of highway bridges

An approach for estimating the vertical clearance under highway bridges is to segment an initial point cloud of the road plus the bridge into two segments. One segment representing the road surface and one segment representing the underside of the bridge. The vertical distance between these point clouds represents the vertical clearance. A problem with point clouds however is that often there is no point available at the exact location where a clearance should be estimated. A laser scanner only samples physical surfaces at random locations. Even more, scanned data can contain a variety of deficiencies and therefor it could be beneficial to use a multiple of nearby points to estimate a surface at a given location.

Clearance estimation with B-Splines

An example for a surface approximation method is using B-splines. This method is relatively simple to implement, gives generally good results and not too computationally intensive (Kineri et al., 2012). Truong-Hong et al. (2022) propose a cubic B-spline method that firstly divides the area of the surface of interest (road or bridge) into 5x5 meter patches and subsequently applies third degree B-splines to obtain cubic splines. Next a least squares problem should be solved for each patch to obtain a final surface approximation. Since a B-spline approximation usually results in a, to a certain degree, smoothened surface, the approximated surface can have some inaccuracies at locations with rough surface features. For example, locations on the bridge surface where cement leaked during construction or local asphalt imperfections on the road surface.

Cell based clearance estimation

Another method that calculates the vertical distance between a specific point *p* on the road and the underside of the bridge approximates a section around point *p* as a plane. The normal of this reference plane is then projected on the bridge surface (Kretschmer et al., 2002). This approach can be complemented with another method that subdivides a point cloud into 2D cell-grids with a certain cell size and determines the vertical clearance for each individual cell (Paffenholz et al., 2008). Truong-Hong et al. (2022) uses a similar approach to this based on the assumption that the road and bridge surfaces can be represented by multiple local planes for each cell in a 2D cell-grid. The distance between the local road and bridge planes is the vertical clearance.

2.4 Clustering, detection and approximation principles

This paragraph will show some insight into different algorithms that are widely used for different clustering, detection and approximation purposes.

2.4.1 DBSCAN

The Density-Based Spatial Clustering of Applications with Noise or DBSCAN (Ester et al., 1996) is a widely used clustering algorithm. It is an unsupervised machine learning method that can identify distinctive clusters in a, in this application, geo-spatial dataset or point cloud. It is based on the concept that clusters in the data space are represented as a contiguous regions of high point density separated by regions of low point density. The algorithm takes two input parameters: The maximum distance between two points to have them considered as being in each other's neighborhood (ϵ) and the number of points in a neighborhood for a point to be considered as a core point (*min_pts*). It then starts at an arbitrary point in the dataset and looks how many other points are in its neighborhood. If the number of points in the neighborhood is larger than *min_pts* (including the original point itself) all points in the neighborhood are considered to be part of a cluster. This cluster is expanded by recursively checking the neighborhoods of the newly added points. Once there are no more points to be added to the cluster the algorithm picks a new arbitrary point that has not previously been assessed and repeats the process. It can however be that the neighborhood of a point contains fewer than *min_pts* points. If the point is not already part of a cluster this point will be considered as a 'noise' point and thus is not assigned to a cluster.

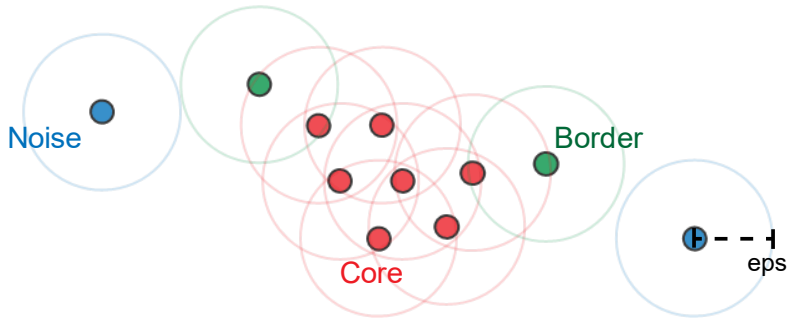

Figure 2.6: Example of DBSCAN algorithm with min_pts = 3.

Figure 2.6 shows a simple example of the DBSCAN algorithm applied to a small set of points. The red points serve as core points and all of them have at least three other points within their neighborhood as illustrated by the red circular borders. All red points belong to a single cluster. The green points contain fewer than 3 points in their neighborhood, but they are part of the neighborhood of another red core point. This makes the green points also part of the main cluster. The blue points have fewer than 3 points in their neighborhood, but they do not belong to the neighborhood of another red core points. Hence, the blue points are classified as noise.

A disadvantage of DBSCAN is that it can give bad results when the data contains clusters of varying density. Point clouds do however sometimes spatially vary in density since the point clouds are usually composed of different co-registered scans. MLS point clouds can also experience temporary occlusions by traffic that passes the laser scanner. This often causes spatially varying point densities.

2.4.2 Principal component analysis (PCA)

Principal component analysis is a technique applied for multivariate analysis. PCA is widely used in classification problems to project data on a new orthonormal basis in the direction of the largest variance (Bellekens et al., 2015). The principal components of a cluster of points in a $\mathbb{R}^3$ coordinate space give information on the orientation of the group of points. The principal components are the eigenvalues and eigenvectors of the covariance matrix of the data where the largest eigenvector corresponds to the direction of the largest variance. The magnitude of this variance is defined by the corresponding eigenvalue.

PCA is often performed with use of singular value decomposition (SVD) as is the case in `scipy`'s implementation of `PCA` (Pedregosa et al., 2012). The singular value decomposition is a factorization of a real or complex matrix. For a real matrix $\boldsymbol{X}$ the SVD is a factorization of the from:

$$\boldsymbol{X} = \boldsymbol{U}\boldsymbol{\Sigma}\boldsymbol{V}^T \tag{3}$$

Here $\boldsymbol{U}$ and $\boldsymbol{V}$ are both orthogonal matrices. The columns of $\boldsymbol{U}$ are called the left-singular vectors of $\boldsymbol{X}$ and the columns of $\boldsymbol{V}$ are called the right-singular vectors of $\boldsymbol{X}$. $\boldsymbol{U}$ and $\boldsymbol{V}$ contain the principal components or eigenvectors of $\boldsymbol{X}\boldsymbol{X}^T$ and $\boldsymbol{X}^T\boldsymbol{X}$ respectively. $\boldsymbol{\Sigma}$ is a diagonal matrix containing the singular values or eigenvalues of $\boldsymbol{X}$.

2.4.3 Straight line Hough transform

The Hough transform (Hough, 1962) in its simplest explanation is a procedure for detecting straight lines in pictures. The original patent for this method uses slope-intercept parameters to define a straight line as $y = ax + b$ with slope a and intercept b. However, the problem with this approach is that when defining a vertical line the slope a will go to infinity. Duda & Hart (1972) propose a method where the vertical line is defined with use of angle-radius parameters where vertical lines do not cause a problem. The line is now defined in the Hesse normal form $r = x\cos\theta + y\sin\theta$ where r is the length of a line from the origin perpendicular to the line $y = ax + b$. θ is the angle between the x axis and the line through the origin perpendicular to the line $y = ax + b$. This is illustrated in Figure 2.7.

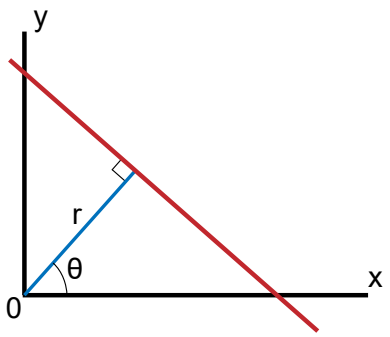

Figure 2.7: Relation of r and θ parameters to the line y=ax+b in red.

The parameter space of the Hough transform is constructed as an $m * n$ matrix for an arbitrary amount m different values of the radius r and n different values for the angle θ. Every combination of m and n represents a line in the image space and the amount of non-zero pixels each individual line intersects in the image space decides the intensity of the pixel (m,n) in the parameter space. This is carried out recursively. The final plot of the Hough space shows many sinusoids which intersect in different knots. These knots represent the strongest signals and thus represent the

detected lines. A threshold can be set to remove lines that are detected with only a weak signal. This is illustrated in Figure 2.8.

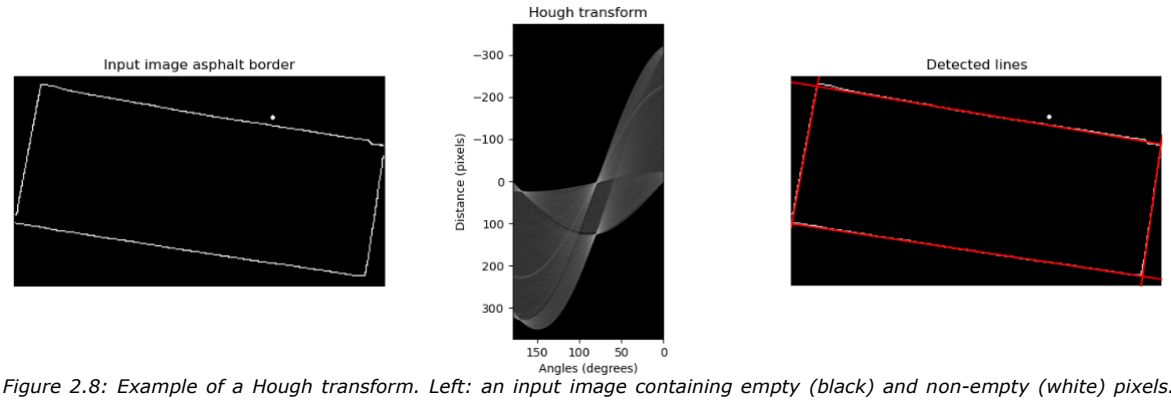

Figure 2.8: Example of a Hough transform. Left: an input image containing empty (black) and non-empty (white) pixels. Middle: The Hough parameter space with on the x and y-axis the distance rand angle θ. Right: The image space containing the input image with the detected lines superimposed.

This method relies on a 2D-image as input which means that it cannot take a 3D point cloud directly as input. The point cloud should first be projected to a 2D image to serve as input for the Hough transform.

2.4.4 Alpha shape

The alpha shape, first defined by Edelsbrunner et al. (1983), is a generalization of the convex hull of a finite set of points. *The convex hull of a set of points S may be defined as the intersection of all closed halfplanes that contain all points of S* (Edelsbrunner et al., 1983). The convex hull can be visualized as the shape of a rubber band that is stretched to enclose S. Figure 2.9 shows a visualization of this rubber band analogy in blue. The alpha shape has a comparably more detailed and rougher surface. The general idea behind the alpha shape is that a circle with radius $1/\alpha$ is moved inwards until it is obstructed by two points. These two points then form part of the alpha shape edge. This then continues recursively until an enclosed polygon is obtained. When the radius $1/\alpha$ goes to infinity, the alpha shape will have an identical shape to the convex hull.

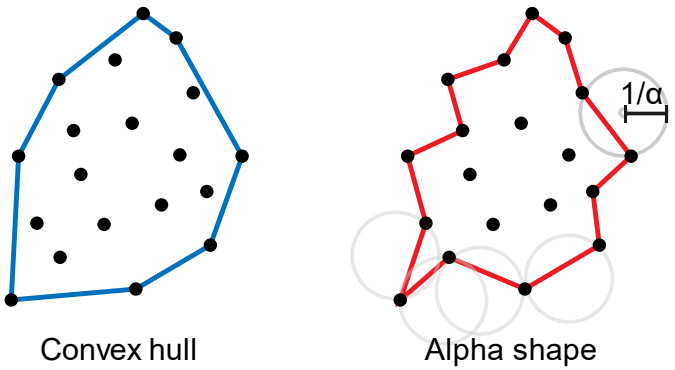

Figure 2.9: A convex hull and alpha shape polygon of an identical set of points in 2D.

2.4.5 B-spline

A spline in the general sense is a function consisting of multiple pieces of smooth functions that are seamlessly concatenated. A large variety of spline species exists, where the most popular splines are piecewise algebraic polynomials (Kunoth et al., 2017). When working with splines it is important to find an efficient and suitable basis for their representation. B-splines, sometimes called basis splines, are among the most useful spline basis functions since they have several properties are important from both theoretical and computational point of view. The B-spline function is a combination of flexible bands that passes through a number of knots or control points (Talebitooti et al., 2015). It is a piecewise polynomial that is differentiable up to a prescribed degree. The simplest example is a 1st degree piecewise linear spline. Other examples are a 2nd degree piecewise spline or a 3rd degree piecewise cubic spline. The degree determines the degree of the polynomial pieces. Examples of simple B-splines are given in Figure 2.10. The j^{th} basis function for a set of knots ξ and degree p is recursively defined by Equation (4) from Kunoth et al. (2017):

$$B_{j,p,\xi}(x) \coloneqq \frac{x-\xi_j}{\xi_{j+p}-\xi_j} B_{j,p-1,\xi}(x) + \frac{(\xi_{j+p+1}-x)}{\xi_{j+p+1}-\xi_{j+1}} B_{j+1,p-1,\xi}(x), \tag{4}$$

Starting with

$$B_{i,0,\xi}(x) \coloneqq \begin{cases} 1, \text{ if } x \in [\xi_i, \xi_{i+1}), \\ 0, \text{ otherwise.} \end{cases} \tag{5}$$

The splines are fit to the data by solving a constrained optimization problem, where a smoothing term is minimized while keeping the residual error under a specified value (Dierckx, 1982). A smoothing condition of $s = 0$ would correspond to the splines passing exactly through all points in the original data. A B-spline with degree $p = 3$ is used to obtain a cubic spline. k is the number of total segments the B-spline has. This gives the number of B-splines equal to:

$$n = (k + p) \tag{6}$$

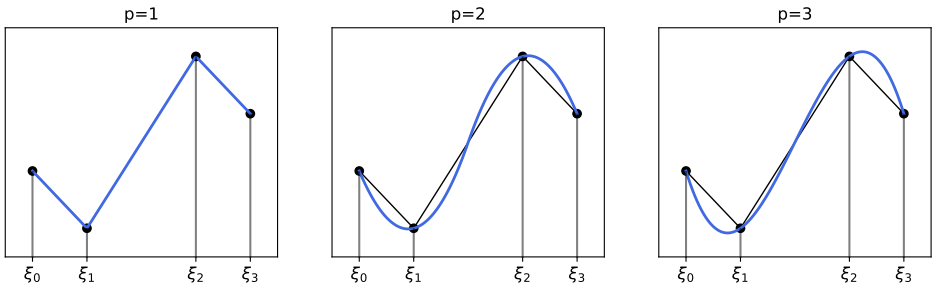

Figure 2.10: Spline functions of degree (p) 1, 2 and 3 through the knots $\xi_0, \ldots, \xi_m$.

In this research `scipy's` function `splprep` (Virtanen et al., 2020) was used to fit the B-splines.

2.4.6 Image processing

Morphological transformations are common operations based on the shape of an image. It is usually performed on a binary image with only empty and full pixels. As input, two items are needed: a binary image and secondly a kernel or structuring element. This kernel will decide the nature of the transformation.

Erosion and **dilation** are two basic morphological operations. Erosion of an image involves the removal of pixels around the edges of an object in the image. Dilation does the opposite in the sense that it grows out from the boundary of an object. Through combinations of these two processes, it is possible to remove noise from images or clean up their edges. This is visualized in Figure 2.11.

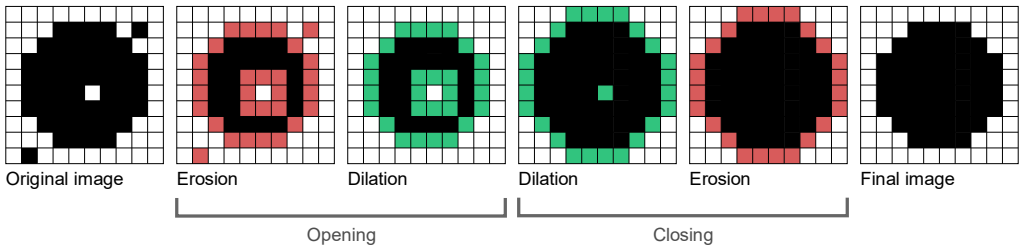

Figure 2.11: A combination of erosion and dilation operations on a raster image. Red pixels are removed, and green pixels are added. The final image is cleared from noise. A 1x1 kernel is used.

A **TopHat** operation is used to extract small elements and details from a given image. Figure 2.12 shows that narrow parts and small details from the original image are preserved. The result from this operation can also be described as the difference between the input image and opening of the image.

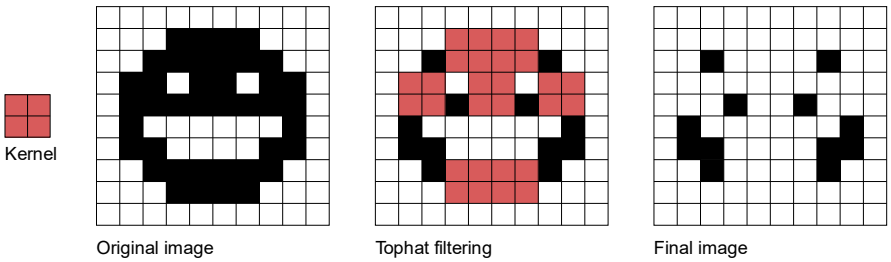

Figure 2.12: A TopHat operation. The red pixels are removed from the image.

To detect edges in an image a **Canny edge detector** (Canny, 1986) can be applied. This is an algorithm that detects edges based on the intensity gradients in an image. The algorithm consists of noise reduction and threshold steps, but the fundamental part is the gradient calculation. The gradient calculation detects the intensity of an edge and the direction by calculating a local gradient. The gradient will return a high value when there is an edge present and a low value if there is no significant change in intensity (Figure 2.13).

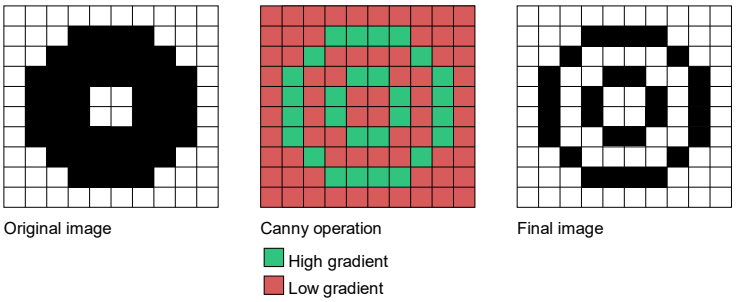

Figure 2.13: A Canny edge detection operation. The final image only contains the edges of the original image.

3. Data

This chapter presents the properties of the data that is used in this project. A description of the different datasets is given along with a subsection dedicated to the difference in average point density between the datasets.

3.1 Data description

For this study the focus is on using point clouds from a database that contains all Dutch highways and has a temporal resolution of 1 year. This data is referred to as **dataset A**. The point clouds are obtained using a Velodyne HDL-32E TOF LiDAR sensor which can generate 695.000 points per second with a claimed relative accuracy of ±2 cm (Velodyne, n.d.). GNSS combined with an Intertial Measurement Unit is used to present the xyz-coordinates in the RD-New (EPSG:28992) reference frame. The point cloud is stored as a .laz file and for all points it contains five attributes: intensity, number of returns, return number, GPS time and RGB color. Figure 3.14 shows the layout of the mobile mapping system used to acquire the point clouds. Point clouds of a road section are obtained from only a single pass. While scanning, the road is open to other traffic users.

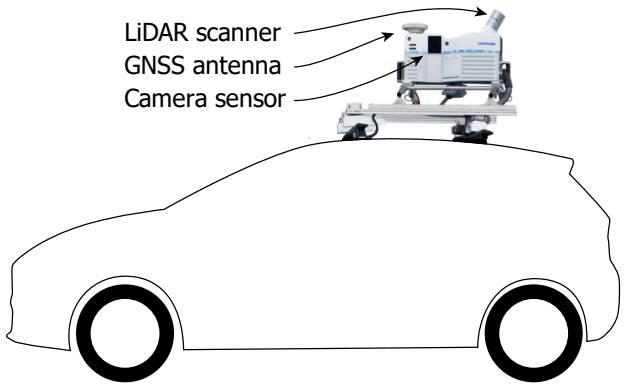

Figure 3.14: A mobile mapping system from Cyclomedia [1].

The different attributes that are available in the point cloud dataset can give different information. The **intensity** value gives information about the reflectivity of the scanned point. A road marking has a higher reflectivity, even so a higher intensity, compared to the surrounding asphalt which makes them clearly distinguishable in the right illustration in Figure 3.15. Furthermore, traffic signs also have very reflective surfaces which is visible in the figure. The laser scanner measures the return strength of the laser pulse to obtain a relative value for the intensity. This can be considered a very important attribute since it reveals important information in complex scenes.

[1] *Image source: https://www.cyclomedia.com/us/capturing-and-processing-data*

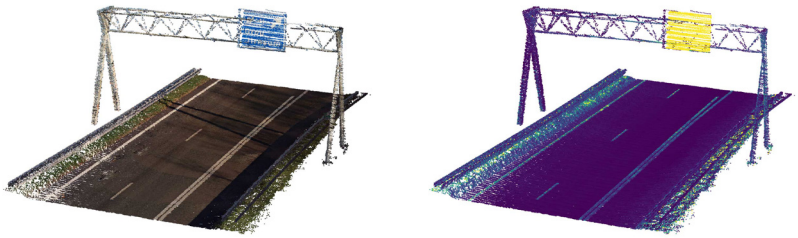

Figure 3.15: A typical point cloud of a traffic gantry. Left: RGB values. Right: Intensity values

The **number of returns** attribute stores information on the number of reflected signals that were recorded for a single pulse. On solid surfaces the laser scanner will generally only record a single backscattered signal, but semitransparent thin surfaces such as foliage can cause multiple backscattered signals for a single pulse. The **return number** is similar to the number of return attributes but here the order of the returns is stored. The first return is flagged as return number one, the second as return number two, and so on. **GPS time** is a time stamp at which the pulse was emitted from the laser scanner. This time is stored in GPS seconds of the week. This is also useful when segmenting point clouds that contain multiple passes from the mobile laser scanner. **PointsourceID** is an attribute that is present when a point cloud consists of multiple co-registered scans. This is a useful addition to the GPS time attribute when a scanning system contains multiple scanners. Then only the GPS time is not sufficient anymore to distinguish the different scans. The **Scan angle** stores the angle of the laser scanner with respect to the nadir at the instance the pulse was emitted from the laser scanner. The **RGB color** attribute stores the red, green and blue value for a point. These color values are usually derived from 360° panoramic images captured simultaneously with the LiDAR point cloud on a separate sensor. An overview of the attributes for each dataset is shown in Table 1.

For validation of the method proposed in this research there are point clouds available of 10 highway gantries with a much higher point density. These point clouds are obtained with a StreetMapper IV mobile mapping system and referred to as **dataset B**. This system has a claimed relative accuracy of 5 mm (StreetMapper, n.d.) and used two laser scanners to obtain a combined measurement rate of 2.000.000 point per second. Just like the first system the StreetMapper IV uses GNSS and a IMU to georeferenced the obtained point cloud in a RD-New (EPSG:28992) reference frame. The data is stored as a .laz file and each point contains multiple attributes: intensity, pointsourceID, scan angle, number of returns, return number, GPS time and RGB color. When a road section is scanned, the MLS makes 5 passes. The data obtained from these 5 passes is then coregistered into a single point cloud. The road is closed for other traffic during the scanning.

Table 1: Overview of the characteristics of each dataset.

Attribute	***Dataset A***	***Dataset B***
Intensity	X	X
Number of returns	X	X
Return number	X	X
GPS time	X	X
PointsourceID		X
Scan angle		X
RGB Color	X	X
Typical gantry[1]	±700.000 points	±10.000.000 points
Typical viaduct[1]	±1.100.000 points	-[2]

[1]this includes points on the asphalt.
[2]Dataset B contains only traffic gantries

3.2 Point density

Dataset A has a significantly lower point density than dataset B. This is illustrated for a gantry superstructure in Figure 3.16. The figure shows that even when dataset B is subsampled to 20% of the original point cloud, it still contains almost 6 times more points. In the top image the separate scanlines of the laser scanner are just visible, but the bottom image does not show this separation between points. Nonetheless both datasets seem to cover all structural elements.

Both point clouds have been acquired with a different purpose in mind. The point clouds in dataset A can be considered as 'general purpose' data since they were not obtained with a specific purpose in mind. The point clouds in dataset B were specifically obtained with the purpose of obtaining clearance measurements. Spatially, dataset A has a great advantage since it covers all roads in the Netherlands, whereas dataset B only has coverage of the specific gantries for which clearance measurements needed to be taken.

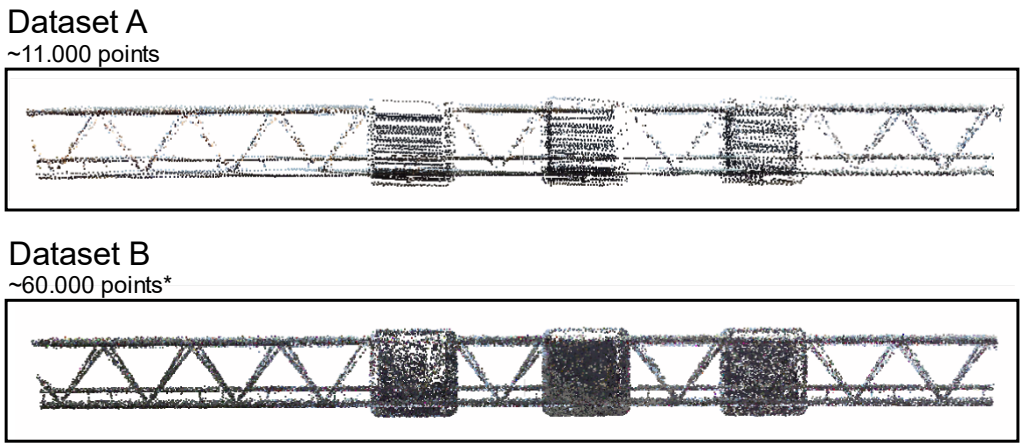

Figure 3.16: Difference in point density when looking at the same gantry superstructure.

4. Method

This section will give a step-by-step explanation of the method that is developed for this thesis. Figure 4.17 shows a schematic overview of the method. To estimate the clearances under a viaduct or gantry, the proposed method is divided into three components: (i) Horizontal clearance estimation, (ii) vertical clearance estimation under a highway viaduct and (iii) vertical clearance estimation under a traffic gantry. All three components require the location and orientation of the road markings. Therefore, the segmentation of the road surface and the classification of the road markings is the first step. The first subsection in this chapter covers the extraction of the horizontal surfaces in a point cloud. Following is a section on road marking classification, and the subsections from there on will cover the three horizontal and vertical clearance components.

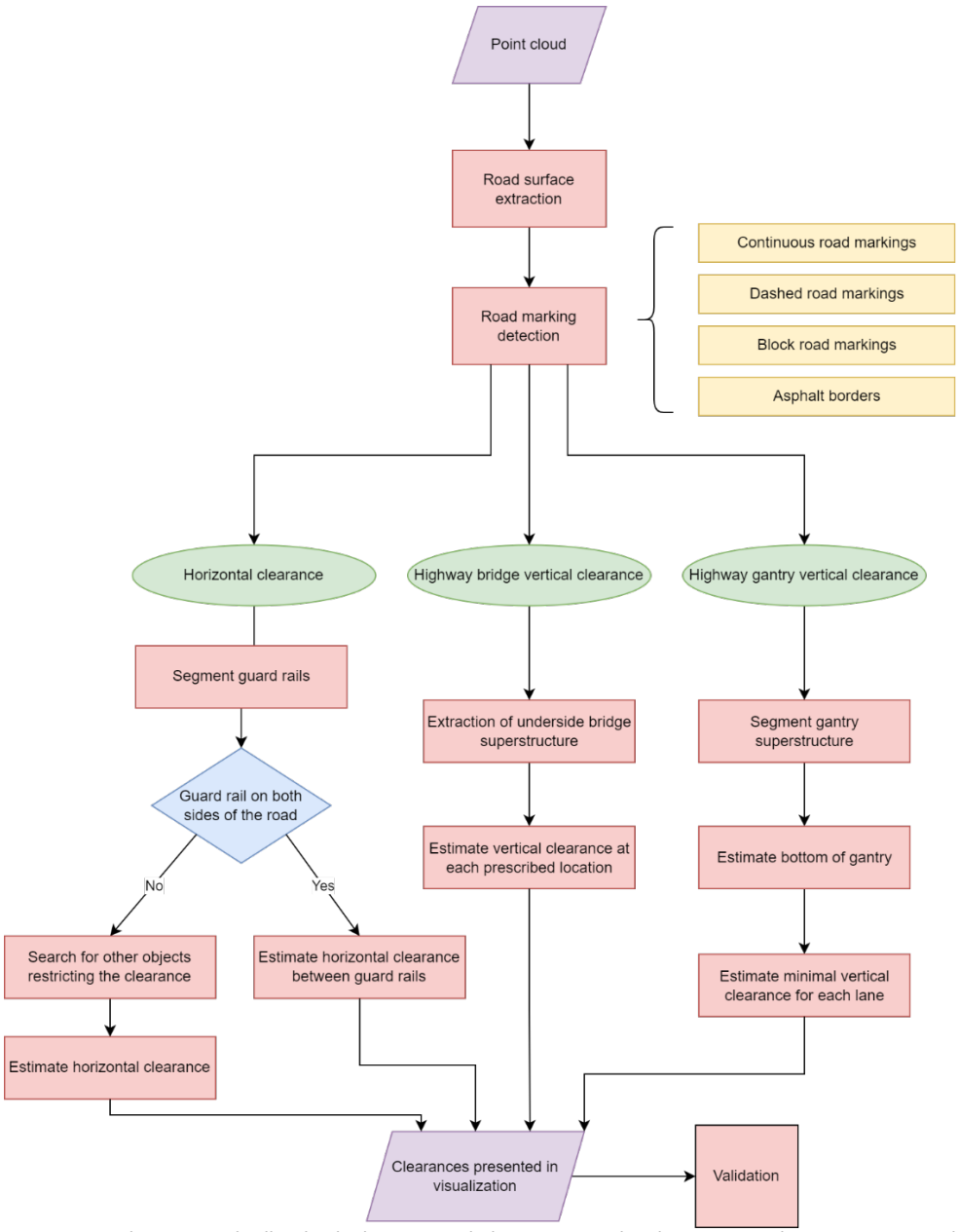

Figure 4.17: A schematic with all individual steps needed to estimate the clearances under a gantry or viaduct.

4.1 Horizontal surface segmentation

The workflow for extracting the road surface consists of multiple steps. Three assumptions are made:

Assumption 1: The road surface has a minimal width of $5.7\ m$ (approximately 2 lanes).
Assumption 2: The underside of the bridge superstructure can be planar or curved but a small area of the surface can be approximated by a plane
Assumption 3: Vertical clearance is only estimated in areas that contain both road and bridge surfaces. The distance between the road and the bridge is larger than a predefined arbitrary height; $3.25\ m$.

1. **Quadtree representation**
   A Quadtree representation (Truong-Hong & Lindenbergh, 2022) aims to reduce the complexity of the initial point cloud. The quadtree is carried out to recursively subdivide the initial point cloud into increasingly smaller 2D cells. This is carried out until the termination criterion is reached that is triggered when a subdivided cell contains fewer points than a predefined threshold. Since a cell is only useful if it contains both the road surface and the underside of the bridge surface, all cells must have a minimal height according to Assumption 3. Cells that do not satisfy this requirement are discarded (Figure 4.18).

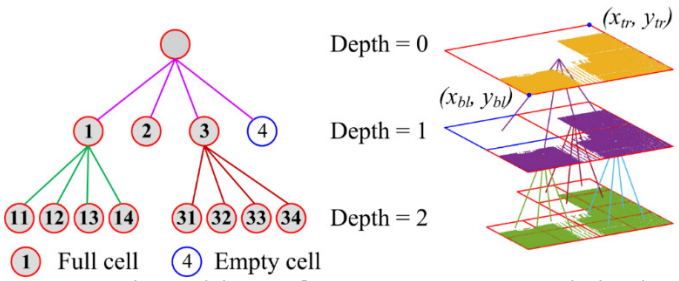

Figure 4.18: Quadtree subdivision. [Source: Truong-Hong & Lindenbergh, 2022*]*

2. **Local surface extraction**
   For all remaining cells the local surfaces are extracted. When the input point cloud contains a viaduct, the remaining cells can contain multiple horizontal surfaces; the road pavement and the bridge superstructure. Since the surfaces are expected to be concentrated in different groups in vertical direction, a kernel density estimation (KDE) (Truong-Hong & Lindenbergh, 2022) is used to establish the location of the local surfaces. These local surfaces are assumed to be nearly horizontal.
3. **Cell-based region growing (CRG)**
   In this step planes are fitted to the different surfaces in each cell. Cell-based region growing (Truong-Hong & Lindenbergh, 2022) is applied to group the planes from the different patches that belong to the same surface. Some additional patch filtering is applied to obtain appropriate surface edges.
4. **Surface classification**
   Now that multiple surfaces have been extracted it is necessary to classify them with the correct class. Road and bridge surfaces are extracted from the set of surfaces derived in the previous step.

When an input point cloud contains a traffic gantry, the output for the horizontal surface segmentation will only contain a single horizontal surface: the asphalt. When the input point cloud contains a highway bridge, the surface extraction will result in two segmented horizontal surfaces: the road surface and the bottom of the bridge superstructure. This is shown in Figure 4.19.

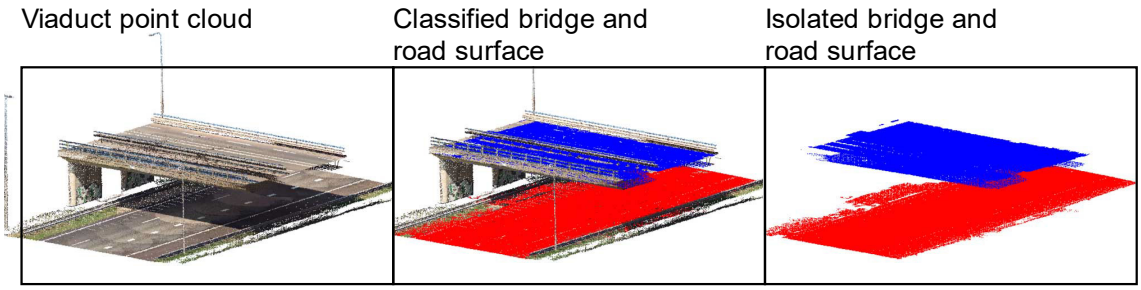

Figure 4.19: Classified road and viaduct surfaces.

4.2 Road marking classification

The locations of the different road markings are important because they specify at what location the clearance measurements should be inferred as explained in Section 2.1. Road markings are located on the asphalt surface, which means this step will disregard all other points but the segmented road surface from the previous section. A step-by-step explanation will be given in this subsection.

With the asphalt surface segmented from the point cloud, the next step is to segment and classify the road markings. The lane markings are generally very visible in the point cloud since the points that are located on the road markings have a much higher intensity than the points on the dark asphalt. Three different types of road markings are classified:

1. Dashed lines
2. Blocked markings
3. Continuous lines
4. The edge of the asphalt

The asphalt edge is technically not a painted-on road marking, but it often defines the outside border of an emergency lane. To find the minimal clearance on the emergency lane, under a gantry, it is thus important that the location of the asphalt edge is known. For viaducts it is explicitly demanded that the vertical clearance should be determined on the asphalt edge.

4.2.1 Dashed lines

The road markings in the point cloud have high intensity values. With an intensity filter most of the darker asphalt can be filtered out. Remaining is a point cloud with most of the black asphalt removed. This remaining point cloud is very well suited to deploy a DBSCAN algorithm on. The algorithm will remove noise and assign each remaining point to a cluster.

After the DBSCAN algorithm is finished, the resulting point cloud can still contain irrelevant clusters. It is needed to setup a Cluster-based feature filter that can remove the irrelevant clusters from the dataset. The features for this filter are created using PCA. The filter is intended to remove all clusters that do not contain a road marking. Different features are calculated for each cluster and from there the clusters with features exceeding predefined thresholds are removed. Several PCA features have already been proposed (West et al., 2004 and Hackel et al., 2016). The following geometrical features are selected and can give information whether a cluster is potentially a dashed line:

- **Orientation:** With the assumption that all road markings are parallel (only small sections of road are considered at once) all markings should have the same orientation. The orientation is defined by the first eigenvector corresponding to the largest eigenvalue λ_1.
- **Length:** The largest eigenvalue λ_1 of a cluster gives information about the variance in the direction of the first eigenvector. Dashed lines as well as block markings have generic dimensions which should suggest that all dashed markings and all block markings should have similar characteristics.
- **Width:** Similar to the length, the second eigenvalue λ_2 gives information about the variance in the direction of the second eigenvector perpendicular to the first eigenvector.
- **Roughness/height:** The third eigenvalue λ_3 gives information about the variance in the direction of the third eigenvector. Since road markings usually 2D planes on the road surface, the variance in the direction of the third eigenvalue should be very small ($\lambda_3 \ll \lambda_1$).

- **Linearity:** The linearity of a cluster is a geometrical feature that can be derived from the eigenvalues. To describe the linearity of a cluster:

$$\text{linearity} = \frac{\lambda_1 - \lambda_2}{\lambda_1}$$

- **Planarity:** The planarity is a cluster is described as:

$$\text{planarity} = \frac{\lambda_2 - \lambda_3}{\lambda_1}$$

4.2.2 Block markings

The segmentation of block markings has a similar approach to the segmentation of the dashed markings in the previous section. The PCA filter uses similar features, but different thresholds are set since a block marking has different geometrical characteristics compared to a dashed line.

4.2.3 Continuous lines

For continuous lines it would also be possible to segment and classify them from the point cloud using a similar method to the method explained for the dashed and block markings. However, an approach using the Hough transform for detecting lines is simpler and gives more reliable results. The Hough method takes as input a 2D image. The point cloud itself is a collection of points in 3D space, so some preprocessing must be done to obtain a 2D projection of the point cloud that can be used as input for the Hough algorithm.

To obtain a 2D image that is suitable for the Hough transform algorithm, the 3D point cloud is ideally project into a 2D binary image with full and empty pixels. The road surface point cloud is first converted to a 2D image by projecting it from a bird's eye perspective. To remove some noise from the image a few basic image processing steps are taken. An overview of the processing steps is shown in Figure 4.20. The individual morphological transformations are explained in Section 2.4.6.

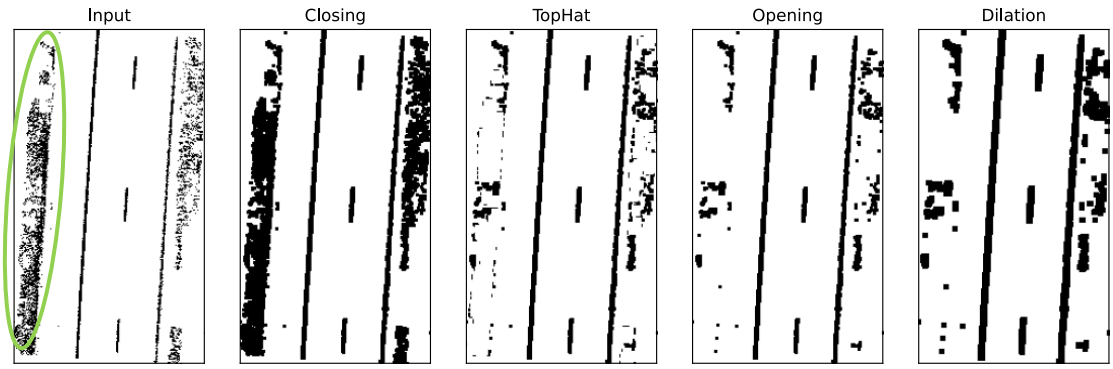

Figure 4.20: The morphological transformations applied to an input image. The operations are performed in order from left to right. These operations improve the visibility of the road markings. The green area shows vegetation which could be mistaken for a road marking.

The goal of the morphological transformations applied in Figure 4.20 is to improve the visibility of the road markings and to decrease the visibility of vegetation. This workflow is robust and will also work on point clouds where the road markings have a varying point density when the road markings are (partly) occluded from the MLS system by a passing vehicle.

Hough Transform

Now that the input image has been preprocessed, the Hough transform algorithm will attempt to find straight lines for a given intensity threshold in the Hough feature space (Figure 4.21). This threshold is arbitrary and can be tuned based on trial and error. The lower the threshold, the higher the number of detected lines. When detecting road markings, the assumption can be made that the detected lines should be parallel since they belong to the same section of road. Another boundary condition that applies to the solid road markings is that there should be at least two detected lines. Using these two conditions increases the chance that the correct lines are detected. The detected lines in Figure 4.21 are roughly vertical with an angle of approximately 180 degrees. This is also visible in the Hough feature space.

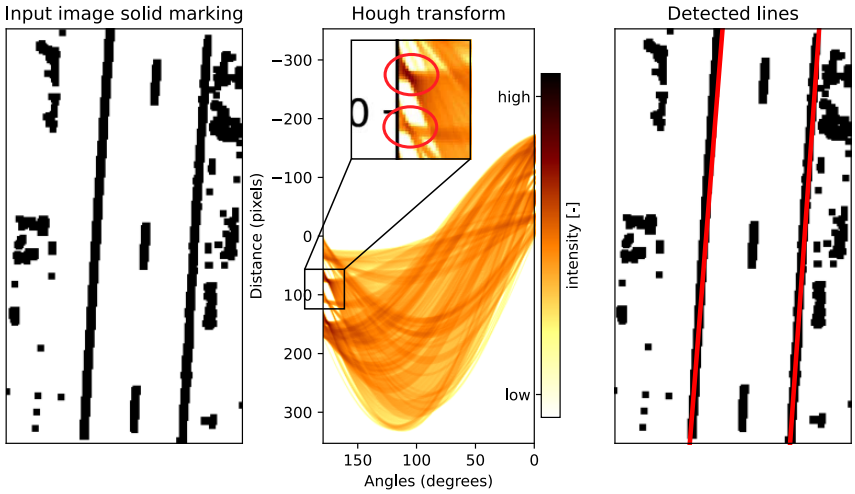

Figure 4.21: (left) The input image for the straight-line Hough transform. (middle) The Hough feature space. The knots of the detected lines are circled in red. (right) The detected lines superimposed on the input image.

When the Hough transform would be applied on the left input image from Figure 4.20, the green circled vegetation area would also show up as a knot in the Hough feature space. Figure 4.22 shows three detected lines instead of two. The extra line compared to Figure 4.21 does not represent an actual road marking in reality. It represents vegetation alongside the pavement which just like road markings contains high intensity values in the point cloud.

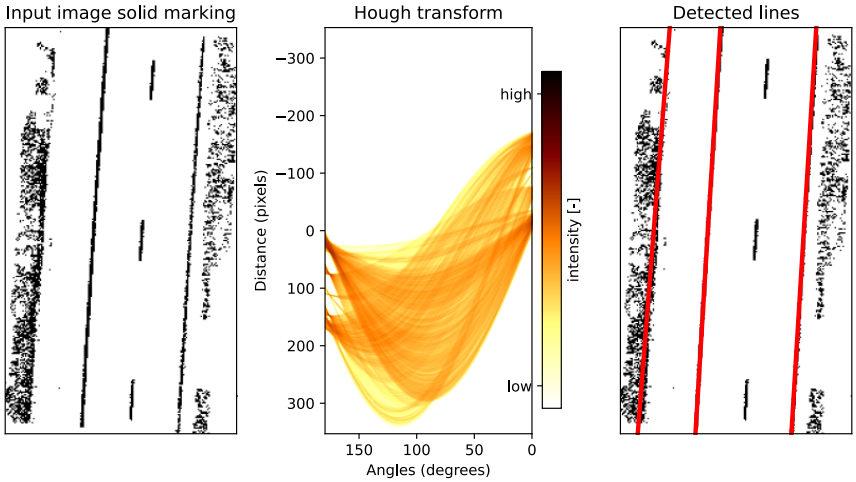

Figure 4.22: The result of the Hough transform on an input image with no preprocessing.

4.2.4 Asphalt edges

To find the edges of the asphalt, a similar approach to the previous section is taken. The preprocessing of the input 2D image now focusses on making the asphalt edges clearly visible. The individual processing steps are shown in Figure 4.23. The opening and closing steps are used to remove noise and road markings from the image. The erosion step is used to make sure that the asphalt outline in the last step lies **on** the asphalt and not **adjacent** to the asphalt. This satisfies the standards for determining vertical clearances as explained in Section 2.1.

The Canny operation in the last preprocessing step is necessary since the Hough transform algorithm detects lines and not edges. By applying the Canny edge detection the outline of the asphalt surface remains. This outline however also includes the edge of the asphalt along the point cloud border perpendicular to the side edges. An example is circled in light blue in Figure 4.24. This knot in the Hough feature space has an angle perpendicular to the other two asphalt edges circled in red. Since the two red lines return a higher intensity value in the Hough space than the line circled in blue, a threshold can be set to exclude the blue circled line.

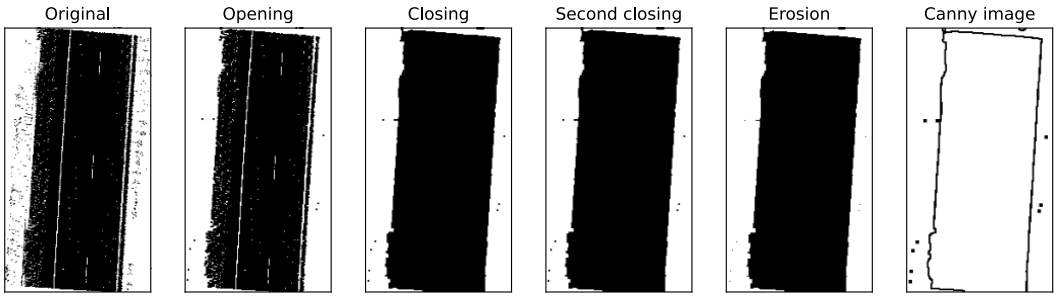

Figure 4.23: The morphological transformations applied to an input image. These operations improve the visibility of the asphalt edge and remove other features such as road markings from the image.

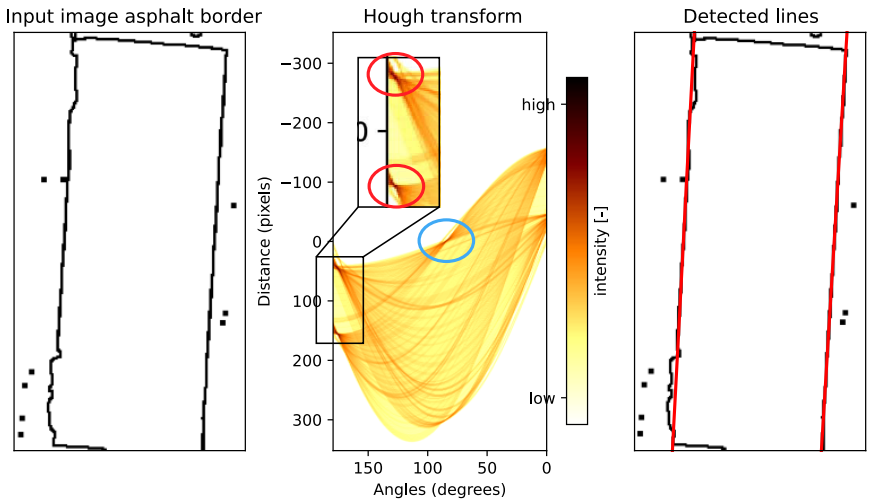

Figure 4.24: (left) The input image for the straight-line Hough transform. (middle) The Hough feature space. The knots of the detected lines are circled in red. The light blue circle also highlights a knot for a detected line at a different angle. (right) The image space containing the detected lines superimposed on the input image.

4.2.5 Lane identification

Individual dashed and block markings do not give sufficient information needed for constructing the lane borders. All separate markings need to be grouped to reconstruct the lane borders. To identify which markings belong to the same border a similar version of a spanning tree algorithm from Prochazka et al. (2019) is used. A first random individual road marking is selected, and its end points are connected to all end points of the other remaining markings. The link that has the smallest angle and the smallest distance is then connected to the initial road marking. This process continues until all road markings are connected. Figure 4.25 gives a visualization of this process. This process is similar for block markings.

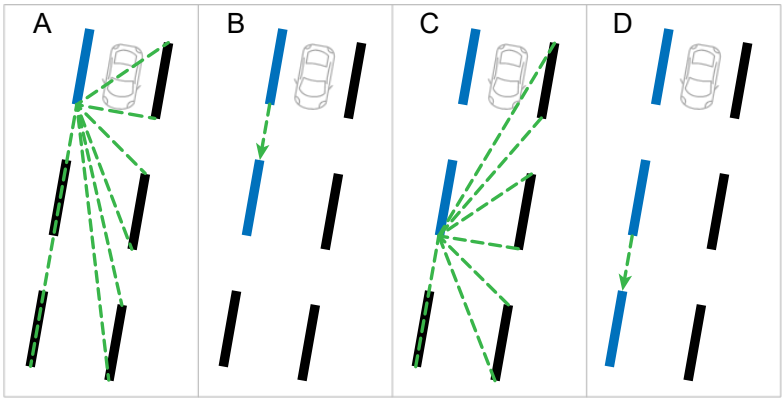

Figure 4.25: The operations used to identify the different lane borders. (a) Connecting the initial road marking to all other markings. (b) The connection with the lowest distance and angle is selected. (c) The operation continues and the next road marking is connected to the remaining markings. (d) All road markings belonging to the same lane border are connected.

4.2.6 Final detected lines

All different road markings can now be represented as a straight line as is shown in Figure 4.26. Each marking was classified correctly here. The road marking information is stored in an array with attributes for the slope and intercept parameters and the line type. The slope parameters give information on the orientation of the road, which becomes useful information later on when the road name and location are determined.

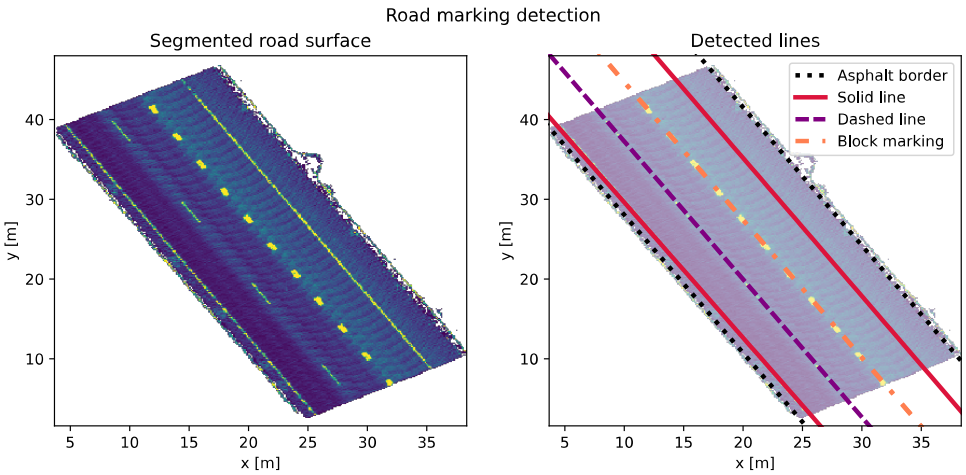

Figure 4.26: Example of a road section with different classes of detected lines.

4.3 Gantry vertical clearance estimation

This paragraph is intended to explain the method for segmenting the gantry superstructure from the input point cloud. The segmentation of the gantry superstructure aims to discard the irrelevant points. This way only the relevant points for determining the vertical clearance remain.

4.3.1 DBSCAN

To extract the superstructure of the gantry from the point cloud the following assumption is used:

Assumption 1: The superstructure of the gantry is at a height of more than $3\,m$ above the road surface.

This assumption already removes a lot of the irrelevant points and gives a good starting point for the DBSCAN algorithm. DBSCAN removes most of the noise and is very suitable to segment the gantry structure from the point cloud. Figure 4.27 shows the input point cloud, the input point cloud after the height threshold and the results of the DBSCAN clustering algorithm.

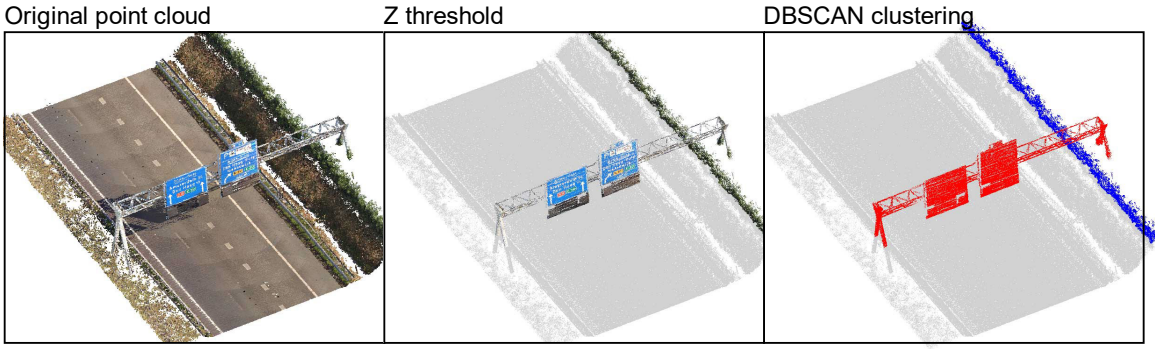

Figure 4.27: Initial clustering of the point cloud to obtain the gantry superstructure after a height threshold is applied.

4.3.2 Gantry orientation

By performing a Hough transform on a 2D projection of the segmented gantry it is possible to estimate its orientation in the horizontal plane. With this information a local reference frame can be constructed for the gantry. This local reference frame makes it easier to process the data. Figure 4.28 shows the result of the Hough transform on the 2D projection of the gantry cluster.

Figure 4.28: Detected line by a Hough transform. The angle of the detected line is the orientation of the gantry in the horizontal plane.

4.3.3 Probability density function of z-values

The columns at either end of the gantry structure are not relevant when determining the vertical clearances. Therefor they are removed from the cluster by removing $0.5\,m$ from both ends. The suspension structure of a gantry can be characterized as an extruded triangle with the point facing downwards (See Figure 4.29). Along the extruded edges there are steel tubes. The bottom steel tube is often the lowest point of a gantry whenever there are no road signs mounted to the superstructure.

Figure 4.29: Superstructure of a traffic gantry mounted on a temporary column.
[source: https://www.gsbirkhoff-staalwerken.nl/projecten/78-tijdelijke-ondersteuning-verkeersportaal]

A kernel density estimation, or KDE (Truong-Hong & Lindenbergh, 2022), is used to identify the approximate location of the bottom steel tube. This location corresponds to a local maximum in the probability density function (PDF) of the z-values of the points in the gantry superstructure. This PDF should have a distinguishable peak at the height of the bottom tube since this tube is generally well represented by points in the point cloud. The points above the bottom tube are removed from the cluster. The remaining cluster contains all points on and below the bottom tube. These points are shown in red in Figure 4.30.

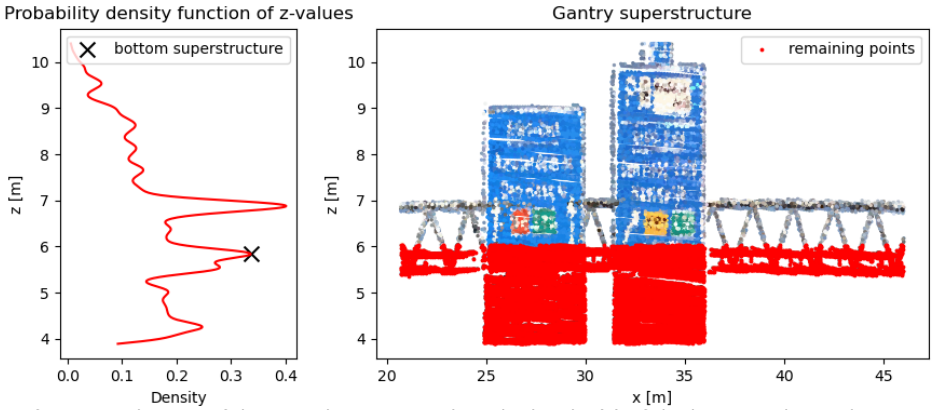

Figure 4.30: Left image: The PDF of the KDE showing a peak at the height (z) of the bottom tube. Right image: The gantry superstructure with the columns on each end removed (right).

4.3.4 Alpha shape

The alpha shape enables the possibility to find the edge points of the remaining cluster. When computing the alpha shape of a set of points it is important to choose a suitable α parameter. This can be any arbitrary value. Here it is important to obtain a single alpha shape that encloses the entire point cluster. Figure 4.31 (top illustration) shows that a too high value for α will result in multiple alpha shape polygons. These alpha shapes are very rough and do not exclusively include points that are on the edge of the gantry structure. When choosing a lower value for α the obtained polygons will have fewer cavities and protrusions and an overall smoother edge. A good value for α results in a single alpha shape polygon.

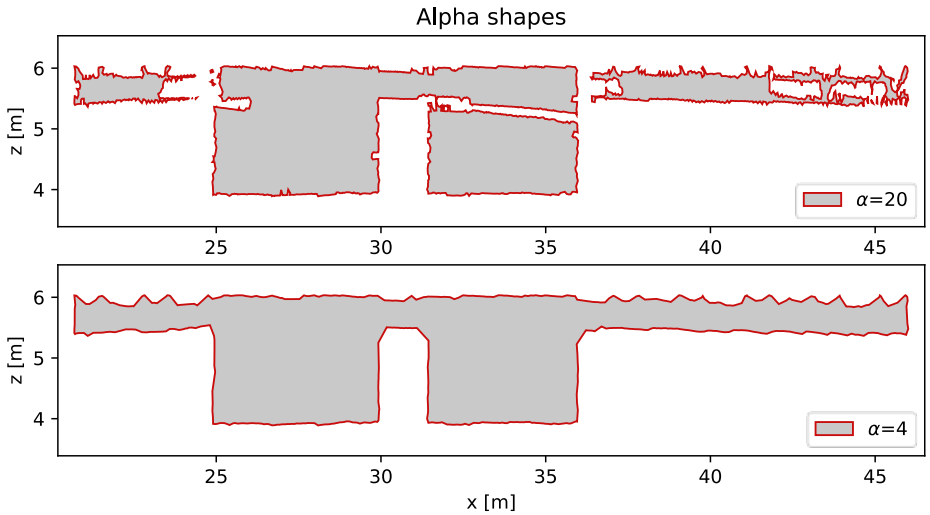

Figure 4.31: Alpha shapes for two different values of α. A larger α value will result in more rough edges and multiple separate polygons.

4.3.5 B-spline approximations

Bottom edge of the gantry superstructure

The obtained alpha shape polygon describes the bottom edge of the gantry, but this alpha shape is defined in $\mathbb{R}^2$ whereas the gantry superstructure in reality spans 3D space, $\mathbb{R}^3$. The points along the edge of the alpha shape represent the bottom of the gantry superstructure. The first step is to cluster the edge points of the alpha shape in 3D space using DBSCAN. The resulting clusters are shown in Figure 4.32.

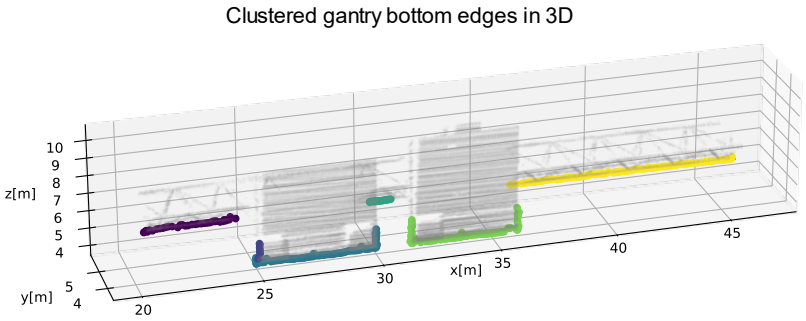

Figure 4.32: Along the x-axis the separate-colored clusters define a continuous line, but in the y direction this line is not continuous.

The remaining point clusters represent the bottom of the gantry superstructure. These are however discrete points where in reality this should be a continuous line. In an effort the estimate the superstructure's bottom edge a B-spline is introduced to obtain a continuous approximation. For each individual cluster in Figure 4.32 a B-spline is computed. The final B-spline is shown in Figure 4.33. This B-spline is defined in $\mathbb{R}^3$. A smoothing parameter of $s = 0.005$ was used which results in a B-spline knot approximately every $10\ cm$.

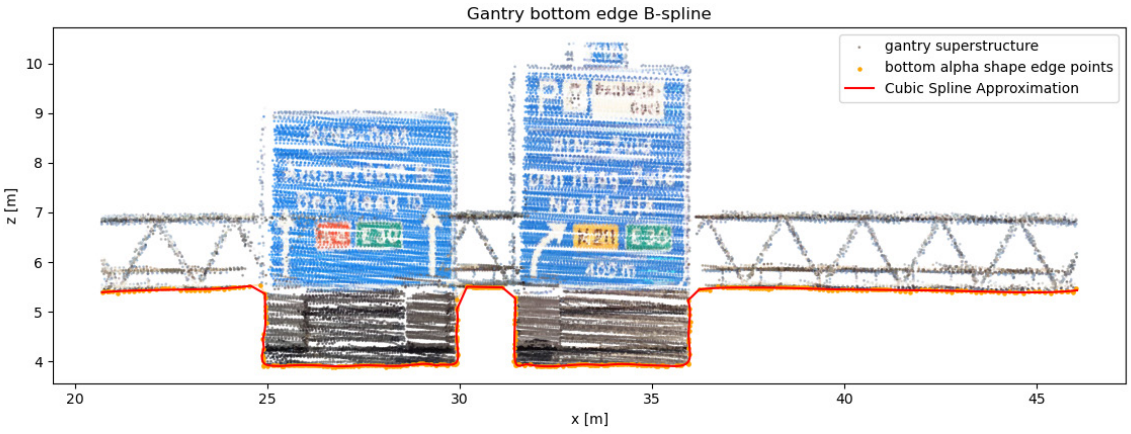

Figure 4.33: Gantry superstructure with the B-spline approximation of the bottom edge.

Road surface

The road surface can also be approximated with B-splines but in this instance bivariate B-splines will be used to approximate the road surface as a slightly curved plane. It is not necessary to approximate the entire the road surface present in the point cloud. Only the surface directly under the gantry is of importance. The segmented road surface points from Figure 4.34 are used to estimate the road surface with B-splines. A smoothing parameter of $s = 0.05$ was used which results in a B-spline knot approximately every $50\,cm$. Since the road surface is very smooth it is not necessary to have the knots as close as is the case with the bottom of the gantry. Opting for a larger smoothing parameter can improve the performance significantly.

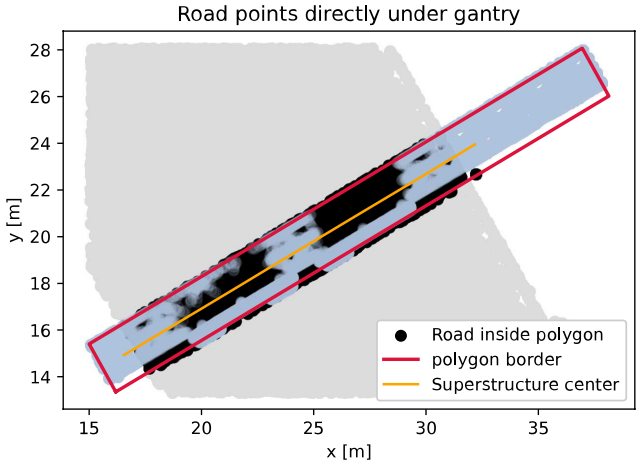

Figure 4.34: The red polygon encloses the superstructure of the gantry. All road points inside the red polygon are segmented from the road surface and used for the B-spline estimation.

4.3.6 Vertical clearance estimation

To estimate the vertical clearances under a gantry, three components are needed:

- The bottom edge estimation of the gantry
- The road surface estimation
- The location of the road markings

The road markings represent the lane borders. Since the minimal vertical clearance should be determined for each lane, a loop iterates over each lane and estimates the minimal vertical distance between the sections of the gantry edge and road surface that are located inside the evaluated lane. The vertical clearance c_V is minimal distance $\perp$ between the road surface and the gantry bottom edge. A visualization of the estimated vertical clearances is presented in Figure 4.35.

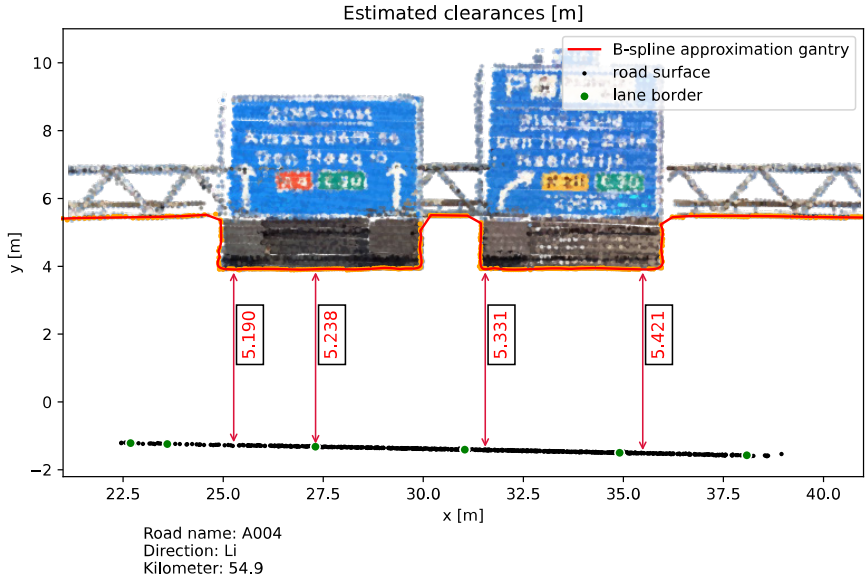

Figure 4.35: The estimated vertical clearances for a traffic gantry. The road has four lanes (3 + 1 emergency lane), so four clearances are estimated.

4.4 Viaduct vertical clearance estimation

The steps described in Section 4.1 describe how the horizontal surfaces can be segmented from a viaduct point cloud. This results in two horizontal surfaces: the road and the bottom surface of the viaduct superstructure. In this section the process on how to infer the vertical clearances from these two surfaces is described.

4.4.1 Viaduct convex hull

The vertical clearances under a viaduct must be determined on the intersections of the detected road markings and the edge of the viaduct superstructure. Finding the intersection between a set of lines, the road markings, and a set of points, the viaduct, can be computationally intensive if the bridge surface consists of many points. A good solution here is to first compute the convex hull of the viaduct (Figure 4.36). This convex hull describes the edge of the bridge as if the cluster of points was enclosed by a rubber band. Since this convex hull is a polygon, it is possible to compute the intersections with all road marking lines. These intersections give a location in the horizontal plane with a x and y coordinate where the vertical clearance should be estimated. To estimate the heights of the road surface and the viaduct at the intersections both horizontal surfaces are estimated with a B-spline and the obtained B-splines are evaluated on the locations of the intersections.

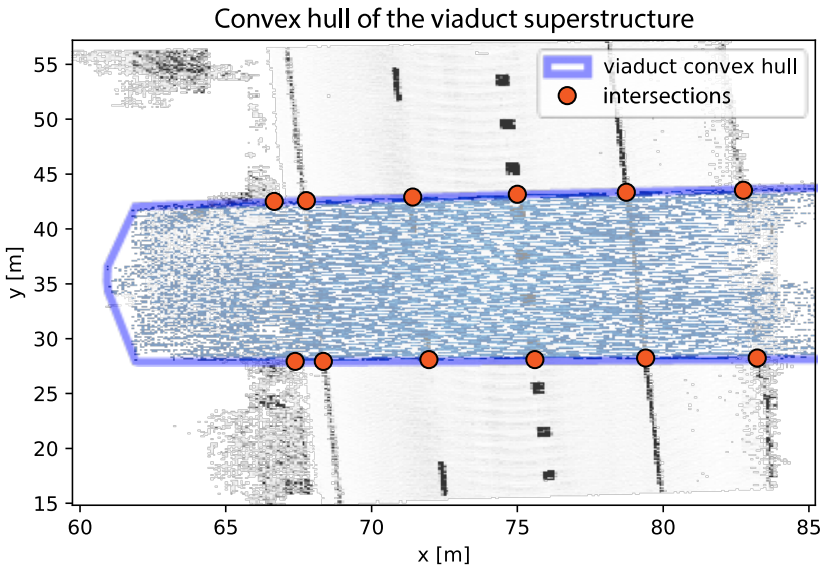

Figure 4.36: Convex hull of the viaduct superstructure that bridges the highway. The noisy shaded area inside the polygon is the segmented viaduct bottom surface. The convex hull represents the edge of the bridge superstructure.

4.4.2 Vertical clearance estimation

To estimate the vertical clearances under a viaduct, three components are needed:

- *The estimation of the viaduct bottom surface*
- *The estimation of the road surface*
- *The location of the road markings*

The road markings represent the lane borders. Since the vertical clearance should be determined on each lane border, each lane border is processed recursively and ethe vertical distance c_V between the road surface and the viaduct surface is estimated. This distance $\perp$ is determined twice for each lane border as illustrated in Figure 2.2. A visualization of the estimated vertical clearances is presented in Figure 4.37. The figure shows that the location on the hectometer signs (215.9) is increasing in the North direction. This indicates that the clearances at the bottom of the figure represent profile number one and the top clearances represent profile number two.

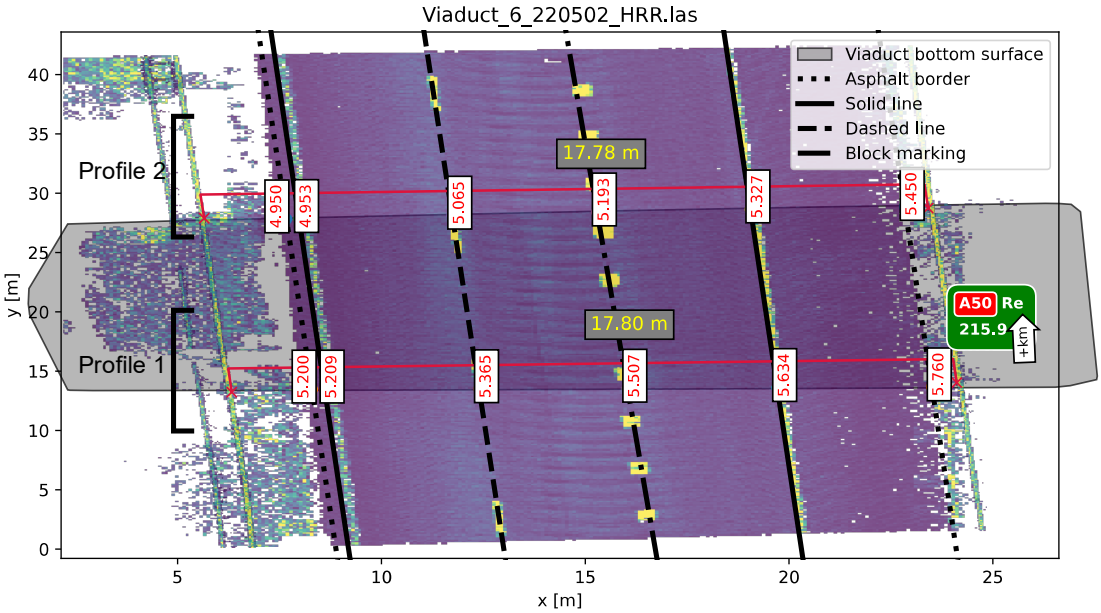

Figure 4.37: Estimated clearances under a viaduct. The dark shaded area represents the projection of the viaduct bottom surface convex hull on the road.

4.5 Horizontal clearance estimation

When determining the horizontal clearance, it is necessary to determine what objects or locations serve as a boundary. The type of boundary for is determined by following schematic in Figure **4.38**. When the boundary is determined on each side of the road, the horizontal clearance can be estimated.

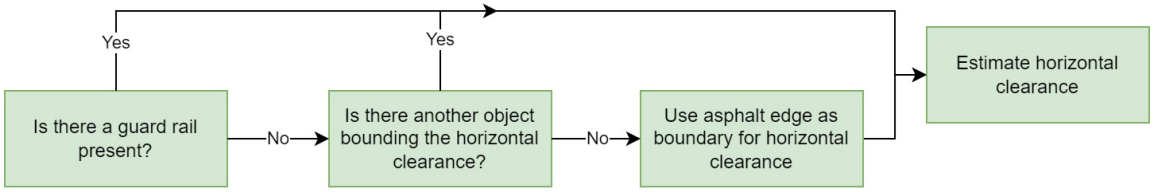

Figure 4.38: Path that is followed when determining what the boundary is for the horizontal clearance.

4.5.1 Location

The horizontal clearance is estimated at the same location as the vertical clearance estimations. Most often there are guard rails present on both sides of the road meaning that the horizontal clearance is defined as the distance between the guard rails that are parallel to the road surface. Under a gantry a single horizontal clearance is estimated, but under a viaduct the horizontal clearance is determined twice: once at the front and once at the back of the viaduct (see the two profiles in Figure 4.37).

4.5.2 Segmentation of guard rails

Guard rails are predictable structures. Their height relative to the road surface and distance from the asphalt border does not vary a lot. A first step in segmenting the guard rails from the point cloud is by using the DBSCAN clustering algorithm. Before using the clustering algorithm a few assumptions are applied to the point cloud:

- *Assumption 1*: The guard rail is located at a height of at least $20\,cm$ above the road surface.
- *Assumption 2*: Points more than $2\,m$ above the road surface are not considered for the horizontal clearance.
- *Assumption 3*: The road surface is already classified in the lane detection step. These points can be disregarded when searching for the guard rails.

The clustering algorithm can do a good first segmentation step, but often the clusters potentially containing the guard rails also contain a lot of vegetation. This is not odd since vegetation can easily grow high enough to make it difficult for the clustering algorithm to find a border between the guard rail and the vegetation. To resolve this problem some knowledge of the dimensions of standard guard rails is used.

A candidate cluster possibly containing a guard rail and some grass noise is divided into multiple sections with a length of approximately $25\,cm$. For each section a Kernel Density Estimation (KDE) is performed of the z-values with a Top-hat filter (Figure 4.39). This Top-hat filter has a total bandwidth of $30\,cm$. Since the height of a guard rail bumper is also $30\,cm$ the KDE should give the highest signal on a height equal to the center of the bumper which is represented by the peak of the probability density shape (PDS).

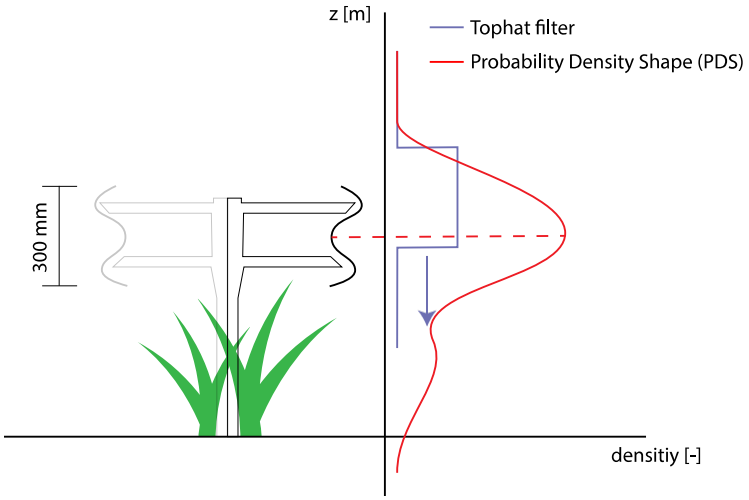

Figure 4.39: PDS of the KDE along the z-axis with a Top-hat filter for a single section of a guard rail cluster containing vegetation.

This information on the approximate center of the guard rail bumper can be used to improve the clustering results for the guard rails. The guard rail clusters in Figure 4.40 still contain some unwanted points from vegetation. When performing the KDE for each guard rail cluster and removing all points that fall outside the Top-hat filter centered at the peak of the PDS, the vegetation is mostly removed. The black points in the right panels are discarded. When high grass is present in a point cloud, it must be removed since it can influence the horizontal clearance estimation. Not removing the grass can cause the algorithm to use the grass as the bound for the horizontal clearance.

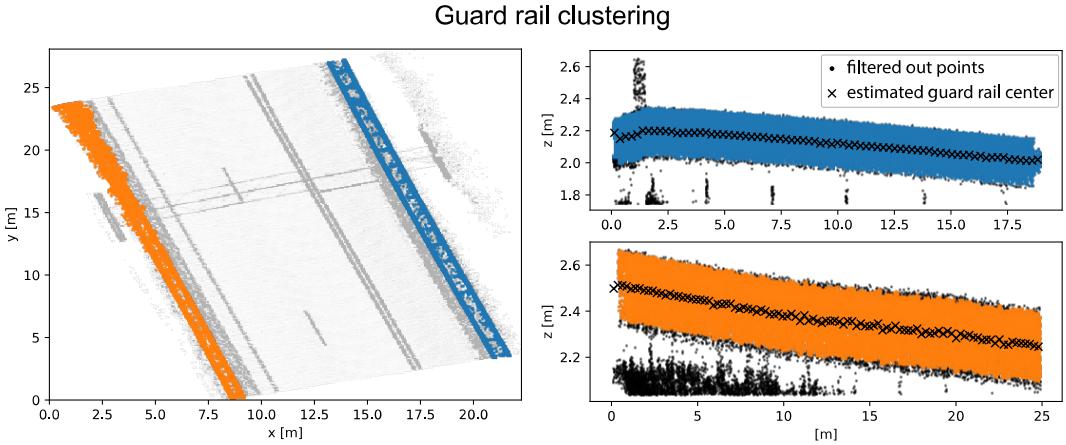

Figure 4.40: (left) A bird's eye view of the road section with the classified guard rails. (right) The individual guard rail clusters. The black cross-markings indicate the approximate center of the rail bumper. The remaining black points are filtered out by using the KDE.

4.5.3 Horizontal clearance estimation

To estimate the horizontal clearance between the guard rails a small section of $10\,cm$ of a guard rail on each side of the road is extracted at the location where the horizontal clearance needs to be estimated. The minimal clearance is then estimated as the minimal horizontal distance perpendicular to the driving direction between the guard rails. The minimal clearance should be determined between a height of $0.5\,m$ and $1.0\,m$ above the asphalt according to the regulations. This area is green shaded in Figure 4.41. The figure shows that there are guard rails present on both sides of the road. The final horizontal clearance is estimated parallel to the road surface.

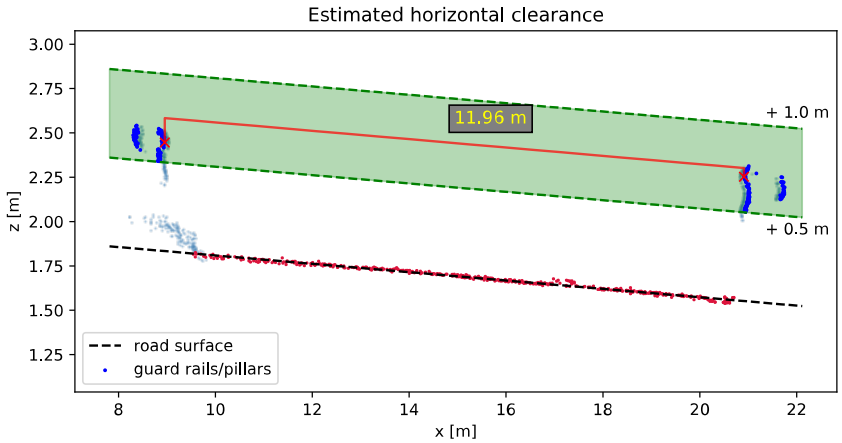

Figure 4.41: The result for a horizontal clearance estimation between two guard rails. The green shaded area indicates where the minimal horizontal clearance is estimated.

4.5.4 Clearance estimation without guard rails

Guard rails are not always present alongside the road under viaducts or traffic gantries. In these situations, there are often other objects that bound the horizontal clearance. Objects such as bridge columns, gantry columns or concrete barriers. If there is no guard rail present on the side of the road, the DBSCAN algorithm is used in the area next to the road to find a cluster of points that can serve as an alternative boundary for the horizontal clearance. Figure 4.42 shows two situations where there is only a guard rail present on the right side of the road.

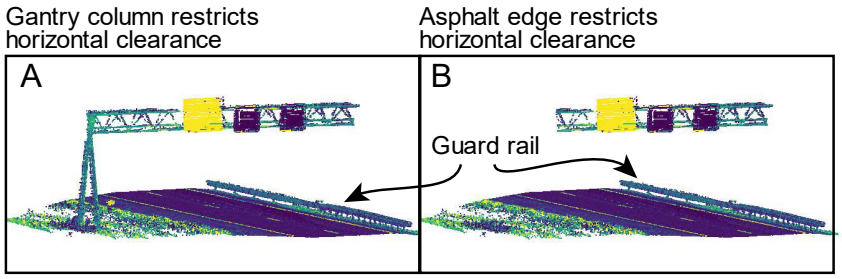

Figure 4.42: Two situations where a guard rail is missing on the left side of the road.

Once an alternative object has been identified at the side of the road that is missing a guard rail, the minimal horizontal clearance is again estimated between $0.5\,m$ and $1.0\,m$ above the asphalt. Figure 4.43 shows that on the left there is no guard rail present but instead a column of a gantry. If the DBSCAN clustering algorithm cannot find an object bounding the horizontal clearance within 10 meters from the asphalt edge, the horizontal clearance is bound by the edge of the asphalt. In the situation of Figure 4.44 no object restricting the clearance could be found on the left side of the road. Now the edge of the asphalt on the left and the guard rail on the right are used as the two objects restricting the horizontal clearance.

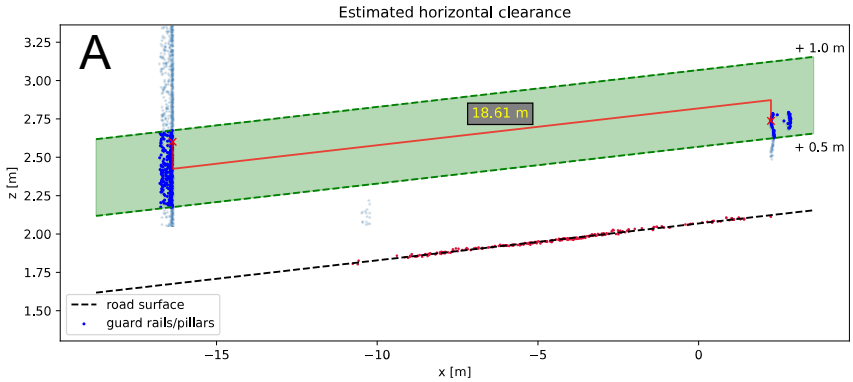

Figure 4.43: Horizontal clearance between a gantry column (left) and a guard rail (right)

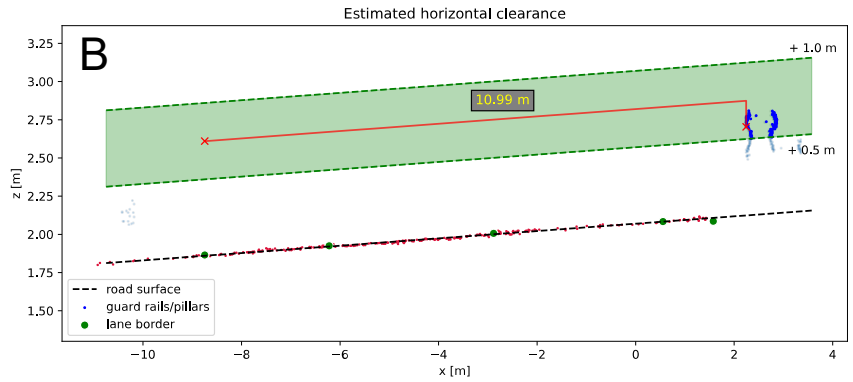

Figure 4.44: Horizontal clearance between the asphalt edge (left) and a guard rail (right)

4.6 Road information classification

The point clouds used for this research contain coordinates in the RD-New (EPSG:28992) reference frame. This information is used to find the nearest hectometer sign to the road section that is being processed. The hectometer sign in Figure 4.45 shows that the sign is located on the A32 highway, at 62.5 kilometers and the direction is 'Re' or right.

Figure 4.45: A hectometer sign. The signs are placed every 100 meters along the highways. 'Re' stands for right and 'Li' stands for left.

A .shp shapefile with the location of all hectometer signs along the Dutch highway network is used as a look up table for the nearest sign. With the Nearest Neighbor implementation in scikit-learn (Pedregosa et al., 2012) the nearest hectometer sign is found. This is often enough to classify the correct road name, but near highway intersections an extra step is needed to obtain the correct road information. When estimating clearances on a road A under a viaduct it should be taken into account that there is also a road B crossing overhead. To make sure that the correct road name is determined, it is also important to determine the orientation of road A. The orientation can be estimated from the road markings that were classified in Section 4.2.

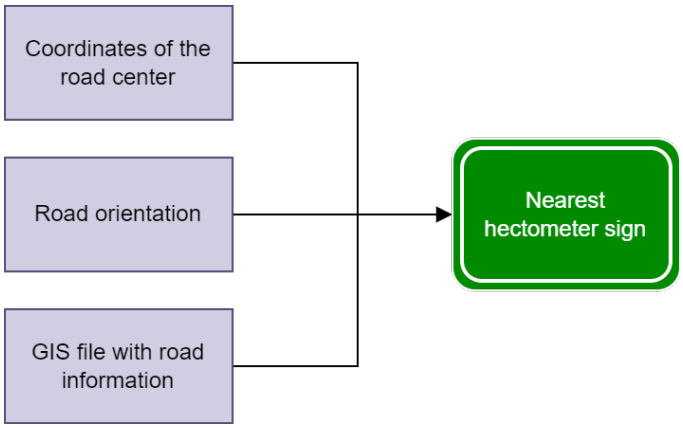

Figure 4.46: The components needed to find the nearest hectometer sign.

5. Case study and results

In this section the proposed method will be applied to a selection of gantries and viaducts. This case study will give insight into the quality of the estimated clearances. The estimated values will be compared to the measurements that were independently obtained by third party contractors.

5.1 Case study area

For the case study two sections of highway in the Netherlands are selected (see Figure 5.47). The reason these two sections are selected is that they fulfill two requirements:

- The section has recently (<1 year) undergone major maintenance, i.e., a new asphalt layer was applied. After the maintenance is completed, the contractor must take new clearance measurements under all gantries and viaducts.
- The most recent point clouds that are available for these sections were obtained after the maintenance was completed. As such, the scanned scene in the point cloud is identical to the scene when the clearance measurements were taken by the contractor.

Combined, the two sections of highway contain 50 gantries and 20 viaducts. The point clouds for these objects are all obtained from dataset A. For 10 gantries along the A50 highway there are also point clouds available from dataset B. These will also be included in the case study.

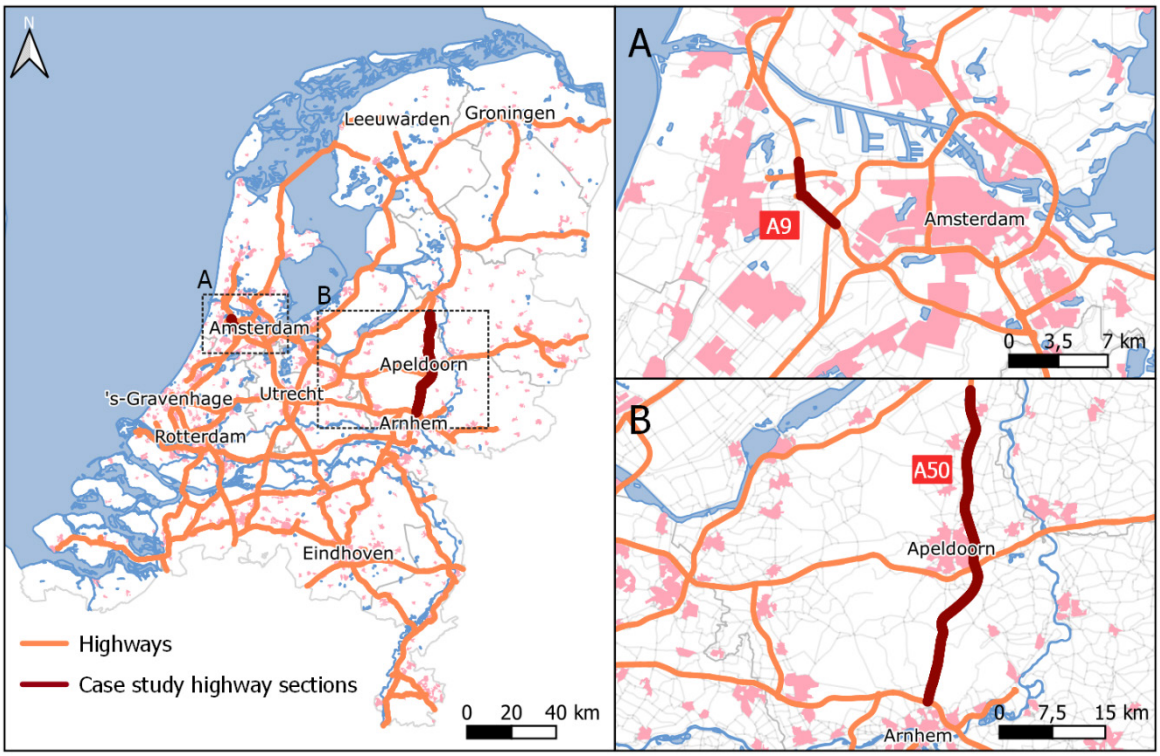

Figure 5.47: Overview of the highway sections selected for the case study.

5.2 Estimated clearances for a single structure

The purpose of this section is to give insight into how the proposed method presents its output to the user. First the clearance estimates for a single gantry are reviewed and subsequently the clearance estimates for a single viaduct are reviewed.

5.2.1 Gantry

5.2.1.1 Vertical clearance

In the top panel of Figure 5.48 the input point cloud for a single gantry from dataset A is presented with annotations for the different objects that are visible. On the left side of the superstructure a section of the high-density dataset B is superimposed. In the bottom panel the three traffic signs that are mounted to the superstructure are displayed along with the bottom edge that was estimated. The bottom edge of sign A is estimated correctly, but the bottom edge of sign B seems unrealistic. The estimated bottom edge follows the contour of the data nicely, but in reality this traffic sign probably has a straight bottom edge. The estimated bottom edge of sign C looks better compared to sign B since this sign has a more realistic horizontal edge.

5.2.1.2 Horizontal clearance

The horizontal clearance in the example of Figure 5.48 is somewhat ambiguous. The left bound of the horizontal clearance is the guard rail that is next to the road. The right bound however could be either the bush/small tree or the column of the gantry. Section 2.1.2 gives the definition that obstacles that serve as a boundary for the horizontal clearance are defined as objects or vegetation that can cause severe damage or injuries to a vehicle or its passengers when a collision occurs. It is difficult to automate this assessment of whether an object will cause severe damage or injuries. The method that is currently proposed will use the small tree as the right boundary. To get the horizontal clearance between the guard rail and the column of the gantry the user can choose to alter the DBSCAN parameters that clusters the objects alongside the road or by simply removing the small tree from the input point cloud. This situation is however very rare as it occurred only once during the case study.

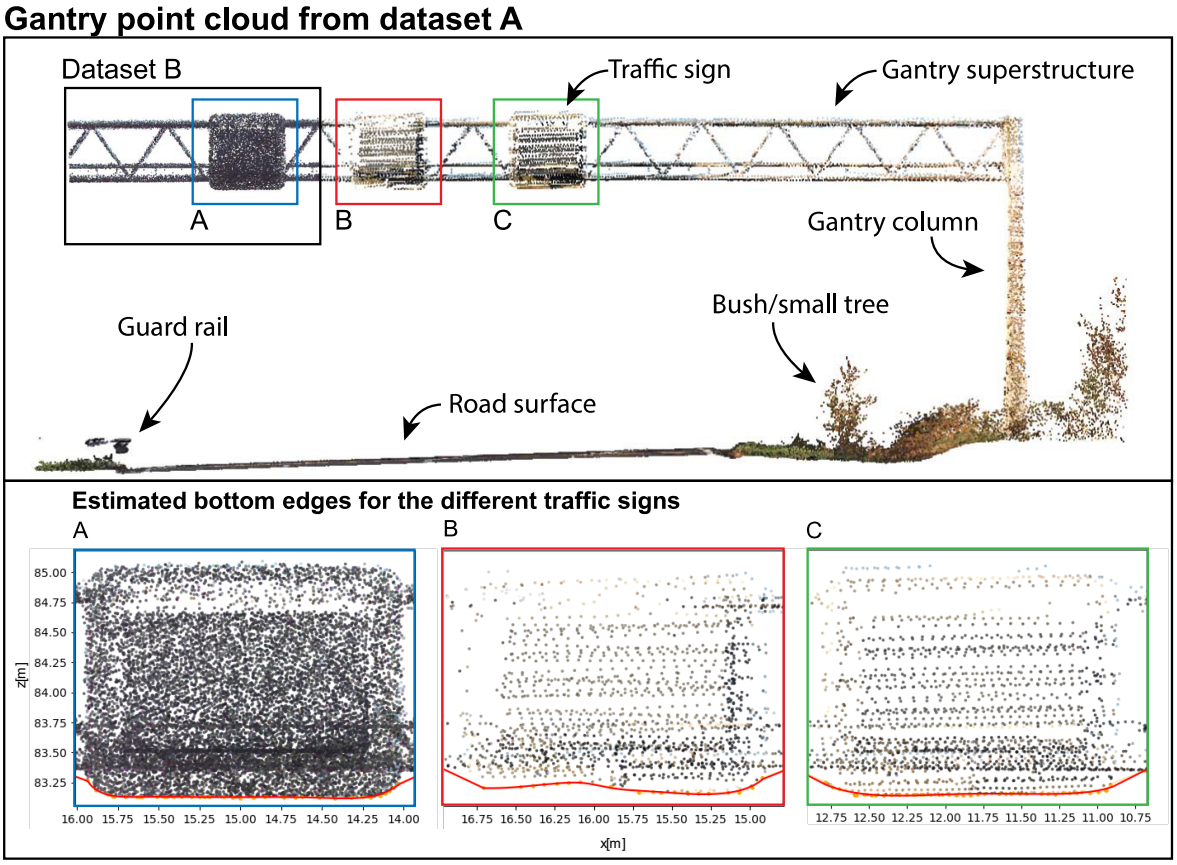

Figure 5.48: Example input point cloud of a gantry. The bottom panel shows the estimated bottom edges of the traffic signs attached to the gantry superstructure.

Figure 5.49 shows the third-party clearance measurements together with the estimated clearance measurements by the proposed method. The comparison between the results is shown in Table 2. This shows that the estimated vertical clearances $c_{V,1}$, $c_{V,2}$ and $c_{V,4}$ are an overestimation of the third-party measurements by approximately $2\ cm$. $c_{V,3}$ has much larger offset with the third-party measurements of almost $6\ cm$. A possible explanation for this large difference is incomplete sampling of the traffic sign by the laser scanner. The estimated horizontal clearance C_H is an underestimation of the third-party measurement by $5\ cm$.

Table 2: Difference between the third-party measurements and the gantry clearances that were estimated by the proposed method.

	Third-party measurement [m]	***Estimated from point cloud [m]***	***Difference [mm]*** $(c_{V,third-party} - c_{V,estimated})$
$c_{V,1}$	6.943	6.964	-21
$c_{V,2}$	6.873	6.852	-21
$c_{V,3}$	6.708	6.766	-58
$c_{V,4}$	6.859	6.875	-16
c_H	22.31	22.26	50

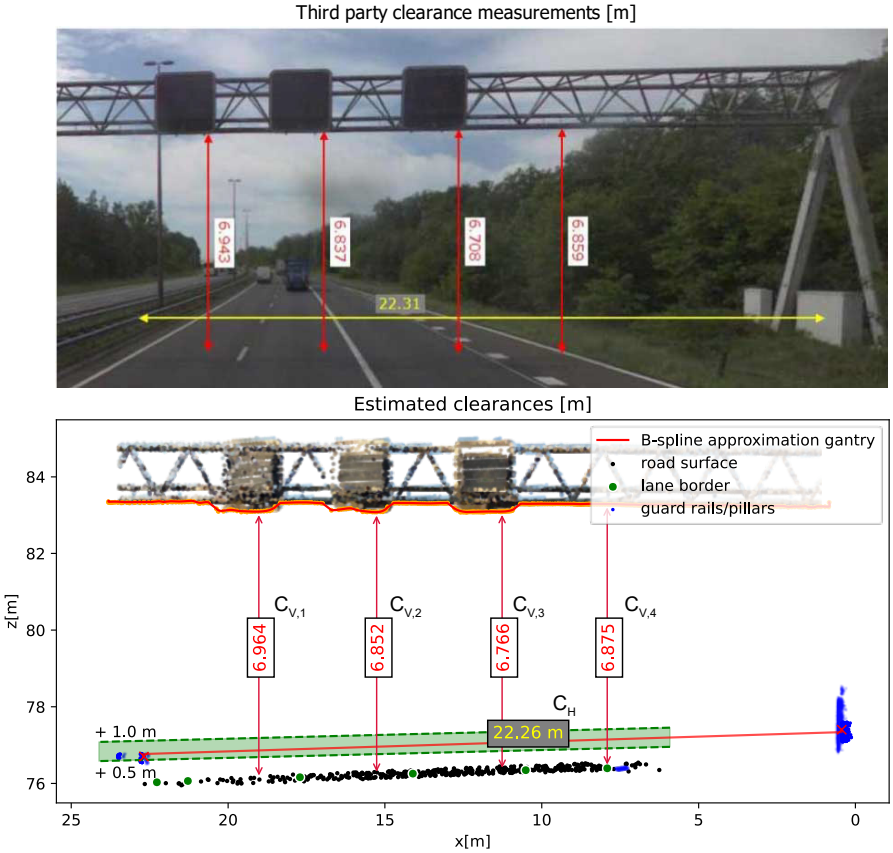

Figure 5.49: The third-party clearance measurements (top) and the estimated clearances from the point cloud from dataset A (bottom).

5.2.2 Viaduct

5.2.2.1 Vertical clearance

The locations at which the vertical clearances under a viaduct are determined are shown in Figure 5.50. The top image shows the third-party measurements for a single side of the viaduct and the bottom image shows the estimated clearances for an entire viaduct. The comparison between the clearances is shown in Table 3. The table shows that all estimated vertical clearances under this viaduct are an overestimation of the clearance measurements provided by the third-party contractor.

5.2.2.2 Horizontal clearance

Under the viaduct there are guard rails present on both sides of the road. These serve as the left and right boundary of the horizontal clearance. The horizontal clearance should be determined at the frond and the back of the viaduct hence the two annotations $c_{H,1}$ and $c_{H,2}$ in Figure 5.50. Both estimated horizontal clearances are an underestimation of the third-party measurements.

Table 3: Difference between the third-party measurements and the viaduct clearances that were estimated by the proposed method.

	Third-party measurement [m]	***Estimated from point cloud [m]***	***Difference [mm]*** $(c_{V,third-party} - c_{V,estimated})$
$c_{V,1}$	4.871	4.950	-79
$c_{V,2}$	4.888	4.953	-65
$c_{V,3}$	5.034	5.065	-31
$c_{V,4}$	5.177	5.193	-16
$c_{V,5}$	5.297	5.327	-30
$c_{V,6}$	5.423	5.450	-27
$c_{V,7}$	5.152	5.200	-48
$c_{V,8}$	5.167	5.209	-42
$c_{V,9}$	5.328	5.365	-37
$c_{V,10}$	5.478	5.507	-29
$c_{V,11}$	5.615	5.634	-19
$c_{V,12}$	5.717	5.760	-43
$c_{H,1}$	17.84	17.78	60
$c_{H,2}$	17.85	17.80	50

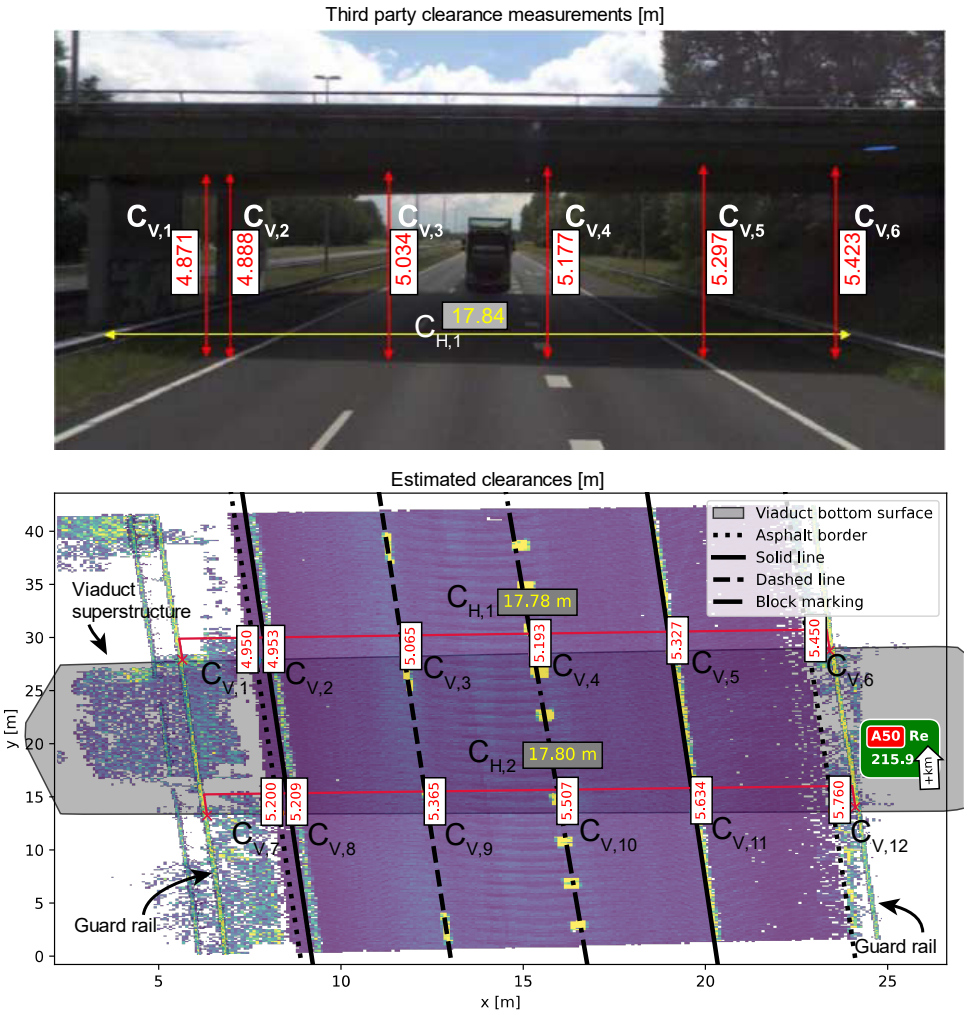

Figure 5.50: Third-party clearance measurements for one side of the viaduct (top) and the estimated clearances from the point cloud (bottom).

5.3 Gantry vertical clearances

This section covers the combined results of all gantries in the case study. The distribution of the vertical clearance estimations is presented here. The case study area contains 50 gantries. These are all gantries with varying traffic sign layouts. On average a gantry spans three lanes: two traffic lanes and an emergency lane. The largest gantries span up to six lanes, which will in that situation yield six vertical clearance estimations. In total the 50 gantries yield 177 clearance estimations. Each gantry was processed separately, and the estimated clearances were compared with the available third-party measurements. By calculating the difference between the third-party measurements and the estimated clearances an offset is calculated. The distribution of these offsets gives a quantitative judgement on the quality of the results. The offset is calculated as:

$$e = c_{V,third-party} - c_{V,estimated}$$

Where $c_{V,third-party}$ is the minimal vertical clearance of a lane as established by the third-party contractor and $c_{V,estimated}$ is the vertical clearance of a lane that was estimated from the point clouds of dataset A. The distribution shows that the median offset of the method is $-23\,mm$. This implies that the method on average overestimates the minimal vertical clearance of a lane under a gantry. To make a robust assessment of the variability of the method the median absolute deviation (MAD) is introduced. The MAD gives a better estimation of the dispersion since it is not affected by outliers. The standard deviation of the offsets is $15\,mm$. The standard deviation is calculated as:

$$\sigma = MAD * k$$

Where $k = 1.4826$ is the scale factor that is needed to convert the MAD to a standard deviation for a normally distributed dataset. The distribution of the offsets is visualized in Figure 5.51.

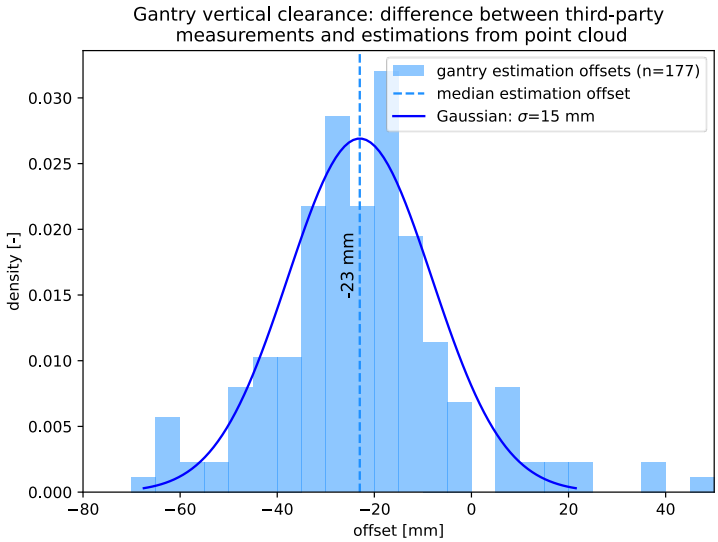

Figure 5.51: The histogram shows the difference between the third-party measurements and the estimated vertical clearances.

5.3.1 Vertical clearance estimations on high density validation point cloud

As stated in Section 3, there are high-density point clouds from dataset B available. This dataset only contains 10 gantries but applying the proposed method to these gantries gives insight in how the point density of a point cloud impacts the offsets with the third-party measurements. The 10 gantries are also present in dataset A, so a comparison between the results can be made. The high-density dataset B has a point density that is up to 20 times higher than dataset A. The estimated clearances from the high-density point clouds show a much lower median offset of $5\ mm$ as well as a lower standard deviation of $9\ mm$ when comparing the results with dataset A. The distributions of the offsets for dataset A and dataset B are visualized in Figure 5.52. Both datasets have an equal population of 10 gantries, which translates to 30 vertical clearance estimations (3 lanes or vertical clearances per gantry).

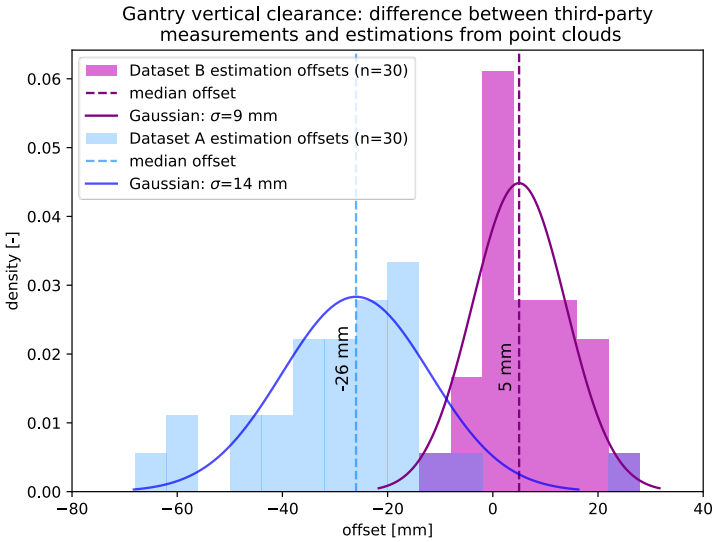

Figure 5.52: The histogram shows the difference between the third-party measurements and the estimated vertical clearances. Dataset A and Dataset B are described in Section 3.

5.4 Viaduct vertical clearances

The case study area contains 20 viaducts. This is less than half of the number of gantries that was processed. However, this deficit is compensated for two reasons:

- Each vertical clearance should be estimated once at the front of the viaduct and once at the back.
- Under viaducts the vertical clearance must be estimated for each road marking instead of each lane. A road with two lanes should have three road markings.

These two factors combined compensate for the lower number of viaducts that were processed compared to the number of gantries. In total the 20 viaducts yield 246 vertical clearance estimations. By calculating the difference between the third-party measurements and the estimated clearances an offset can be calculated. The distribution of these offsets gives a quantitative judgement on the quality of the results. The offset is calculated as:

$$e = c_{V,third-party} - c_{V,estimated}$$

Where $c_{V,third-party}$ is the vertical clearance above a road marking as established by the third-party contractor and $c_{V,estimated}$ is the vertical clearance above a road marking that was estimated from the point clouds in dataset A. The distribution shows that the median offset of the method is $-33\ mm$. This implies that the method on average overestimates the vertical clearance on a point under a viaduct compared to the third-party measurements. To make a robust assessment of the variability of the method the median absolute deviation (MAD) is calculated. By converting the MAD to a standard deviation, a σ of $13\ mm$ is found. The distribution of the offsets is visualized in Figure 5.53.

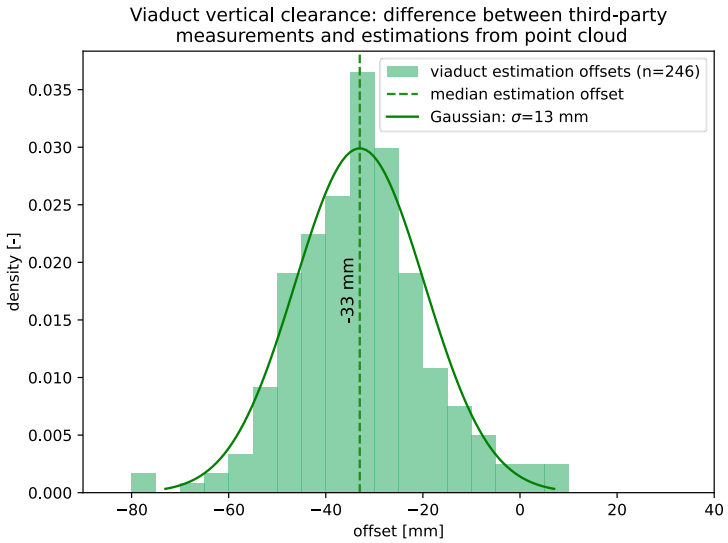

Figure 5.53: The histogram shows the difference between the third-party measurements and the estimated vertical clearances.

5.5 Horizontal clearances

The estimation of the horizontal clearance is not dependent on whether a gantry or a viaduct is processed. The estimated horizontal clearances from the 50 gantries and 20 viaducts can be combined and evaluated as a single set of results. For each gantry one horizontal clearance is estimated and for each viaduct two horizontal clearances are estimated. A viaduct yields two horizontal clearances since it is estimated at the front and at the back of the structure. By calculating the difference between the third-party measurements and the estimated clearances, an offset can be determined. The offset is calculated as:

$$e = c_{H,third-party} - c_{H,estimated}$$

Where $c_{H,third-party}$ is the horizontal clearance under a gantry or viaduct as established by the third-party contractor and $c_{H,estimated}$ is the horizontal clearance that was estimated from the point clouds in dataset A. In Figure 5.54 these offsets are visualized with a probability density function. The distribution shows that the median offset of the proposed method is $30\ mm$. This implies that the method on average underestimates the horizontal clearances. The standard deviation σ here is $34\ mm$. This is calculated based on a population of 90 horizontal clearance estimations.

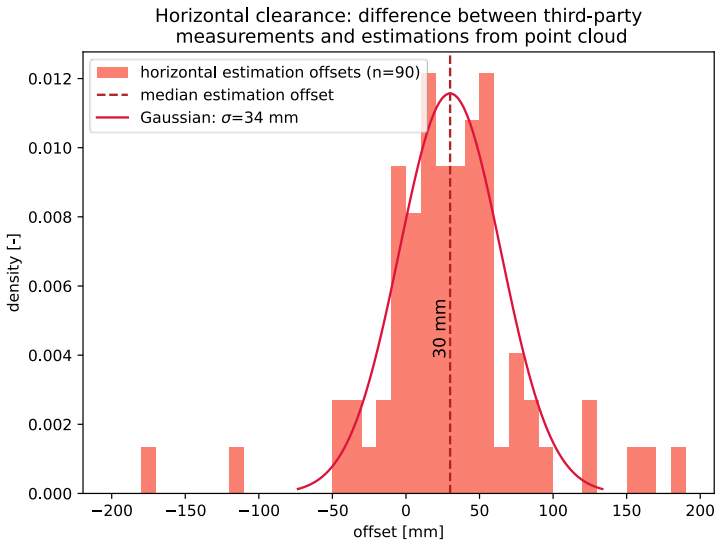

Figure 5.54: The histogram shows the difference between the third-party measurements and the estimated horizontal clearances.

5.5.1 Boundary type

When estimating the horizontal clearance, the proposed method considers three different types of boundaries:

1. Guard rails
2. Other objects (columns, other structural components or vegetation)
3. The asphalt edge

Under all viaducts and gantries that were processed there was at least a guard rail on one side of the road. Figure 5.55 shows the distribution of the horizontal clearance offsets $(e = c_{H,third-party} - c_{H,estimated})$ for the different boundary classes. The figure shows that when guard rails are present on both sides of the road the distribution of the offsets is narrow and has a median around $0\ mm$. When the road edge is used as one of the boundaries, there seems to be a systematic underestimation in the horizontal clearance. When there is no guard rail present on one side, but a different object serves as a boundary for the horizontal clearance, the results are very diverse. The results at marker A and B in Figure 5.55 were caused when in reality there were guard rails on both sides of the road, but the clustering algorithm for segmenting the guard rails could only find one. In both cases the algorithm classified a different object as the boundary for the horizontal clearance. In case of situation C the column of a gantry was supposed to be a boundary for the horizontal clearance, but due to too much vegetation between the column and the road, a large bush was determined by the method to be the boundary of the horizontal clearance.

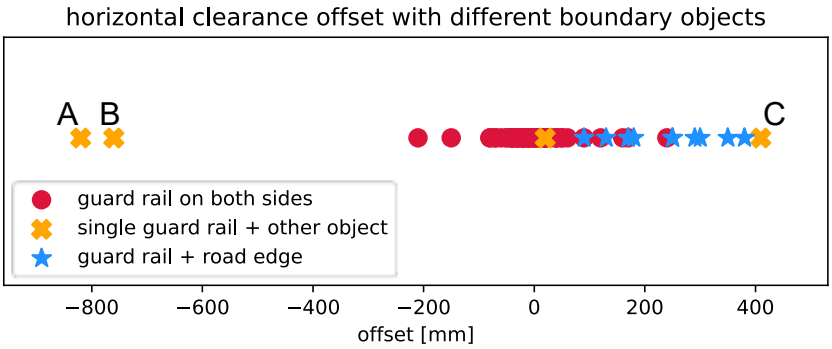

Figure 5.55: Impact of the type of boundary on the horizontal clearance offset. In situation A and B on of the guard rails was not recognized and in situation C there was too much vegetation present which caused a large offset with the third-party measurement.

5.6 Processing time

The processing time is largely dependent on the size of the point cloud used as input. This section covers the relation between the size of an input point cloud and the processing time of the proposed method. Figure 5.56 visualizes this relation for estimating the clearances under a gantry. The figure shows a breakpoint just below 1.500.000 million points. This breakpoint can be found by using piecewise or segmented regression (Muggeo, 2003 and Pilgrim, 2021). This is a regression model where a change in gradient, the breakpoint, and the linear lines are fit iteratively. The general form of a model with one breakpoint according to Muggeo (2003) is:

$$y = \alpha x + c + \beta(x - \psi)H(x - \psi) + \zeta \quad (7)$$

Where given some data x, y the goal is to estimate the gradient α and intercept c of the first segment, the change in gradient from the first to the second segment β and the position of the breakpoint ψ. H is the Heaviside step function and ζ is a noise term. This non-linear function can be solved by performing a Taylor expansion with an initial guess for the breakpoint ψ_0 to obtain a linear approximation:

$$y \approx \alpha x + c + \beta(x - \psi_0)H(x - \psi_0) - \beta(\psi - \psi_0)H(x - \psi_0) + \zeta \quad (8)$$

The linear relation can now be solved by using ordinary linear regression. This regression iterates until the solution is converged beyond an arbitrary stopping criterion.

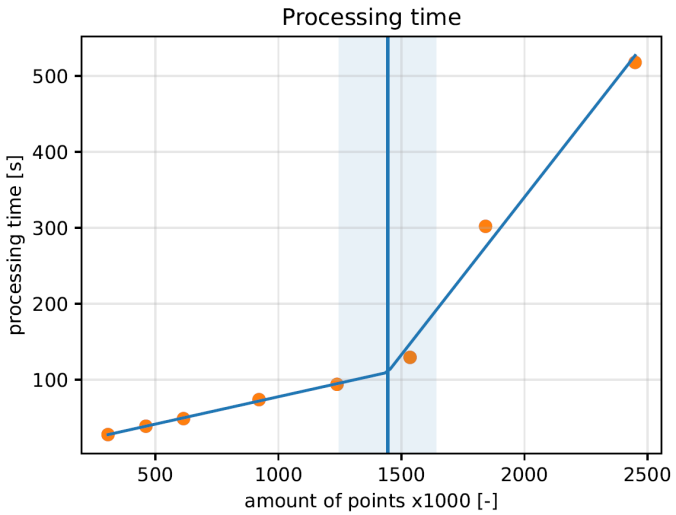

Figure 5.56: Processing time for estimating the clearances of a gantry for different point cloud sizes.

In Section 5.2 the point clouds for obtaining the test results did not exceed a size of 1.000.000 points, thus the breakpoint of 1.500.000 points was not exceeded. The processing times were obtained by using point clouds from dataset B which contains much higher point densities. By taking multiple random subsets of different point sizes from the same gantry point cloud, the data from Figure 5.56 was obtained. The processing times were obtained on a computer with an AMD Ryzen™ 5600u processor with 16GB memory.

6. Discussion

6.1 Third-party measurement data

When comparing the proposed method with existing third-party clearance measurements, it is assumed that these measurements comply with the requirement from Rijkswaterstaat. However, it cannot be guaranteed that the contractor responsible for these measurements has a waterproof approach when measuring the clearances. It can be difficult to judge to which extent the differences between the third-party measurements and the estimations from the point clouds are caused by the proposed method, quality issues with the point clouds or even the measurements from the contractor. A solution to this problem would be to obtain the validation measurements yourself. This way the third-party is taken out of the equation, but this is costly and time consuming.

A clear benefit of the available validation third-party data however is that there are archived measurements available for every gantry and viaduct along the Dutch highway network. Since it is necessary to always take new measurements after maintenance, there should be data of the current situation of each viaduct and gantry in the country. This makes it possible to perform even more and larger case studies.

6.2 Quality of the point cloud

Of the point clouds that were used in this thesis only the 10 high-density point clouds of dataset B were specifically acquired with the purpose of clearance estimation. Therefore, the contractor responsible for performing the laser scans was aware of the requirements that apply to these measurements. Based on these requirements the measurement campaign was designed.

The point clouds from dataset A can be described as a 'general purpose' point cloud. They have not been acquired with the clearance measurement requirements in mind. The point clouds are offered as a service and the customer can download the point cloud of an area of interest whenever and do whatever he wants with it. Each year there are new point clouds available for all roads in the Netherlands, and the old point clouds remain available as historic data. This approach has a much lower cost per scanned viaduct or gantry for the end user since all data is offered as a service to multiple customers. The downside however is that a single customer does not have any influence on how the measurement campaign is designed and what quality is desired from the point clouds.

6.3 Occlusions in the point clouds

A characteristic of the point clouds from dataset A is that they are for the most part obtained by only scanning a road section once. Moreover, the point clouds are collected without road closures which means that overtaking vehicles will obstruct the MLS system. When the laser scanner is obstructed by a small car for only a short duration, the obtained cloud is still usable but the point density in the occluded areas is significantly reduced. When the MLS passes a large truck, the occlusion is much more severe resulting in large empty areas in the point cloud (Figure 6.57). Even in less severe cases of laser scanner obstruction, the resulting point cloud can have a very inhomogeneous point density. This makes it difficult to deploy any density-based clustering algorithms such as DBSCAN since the results can be greatly affected by these irregularities.

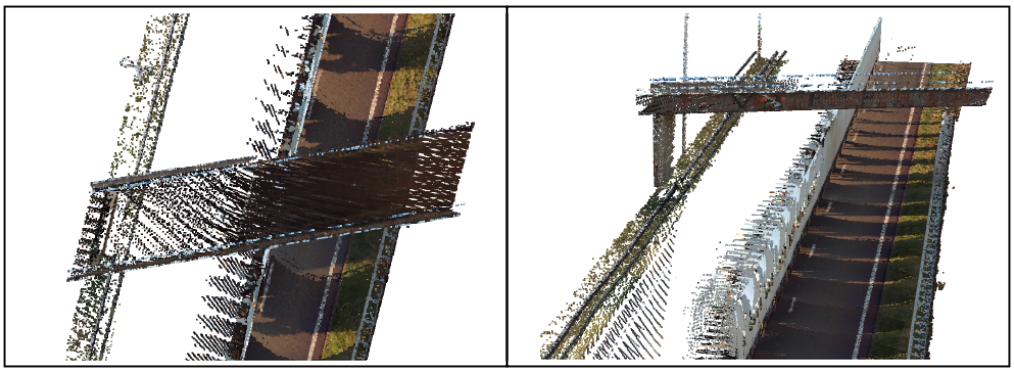

Figure 6.57: Missing area in a point cloud because of an obstructed laser scanner.

This occlusion problem occurs a lot since there are always other vehicles on the road passing or being passed by the MLS. Hence, when the MLS passes a viaduct or gantry it is not guaranteed that the scanner obtained a point cloud that is suitable for the developed method to estimate clearances. This is an expected limitation of the data since the scans are obtained on an open road with other road users.

A less severe reduction in point density in Figure 6.58 shows that besides the reduction in points, the intensity of the road markings on the right side is also reduced. A possible explanation for this reduced intensity could be a consequence of a large incidence angle of the scanner with the scanned surface. The road markings circled in red were occluded by traffic when the MLS was alongside them, but from a distance the MLS was able to get a line of sight with these road markings. Scanning a horizontal plane from a large distance with a large incidence angle can greatly reduce the intensity. This incidence angle effect is already significant for incidence angles $> 20°$ (Kukko et al., 2008). The road markings were still detected in the end, as can be seen in the right image, but the differences in point density and intensity for similar classes of road markings asks for forgiving detection parameters with a high bandwidth. These forgiving parameters cause more noise and can result in errors in the road marking detection.

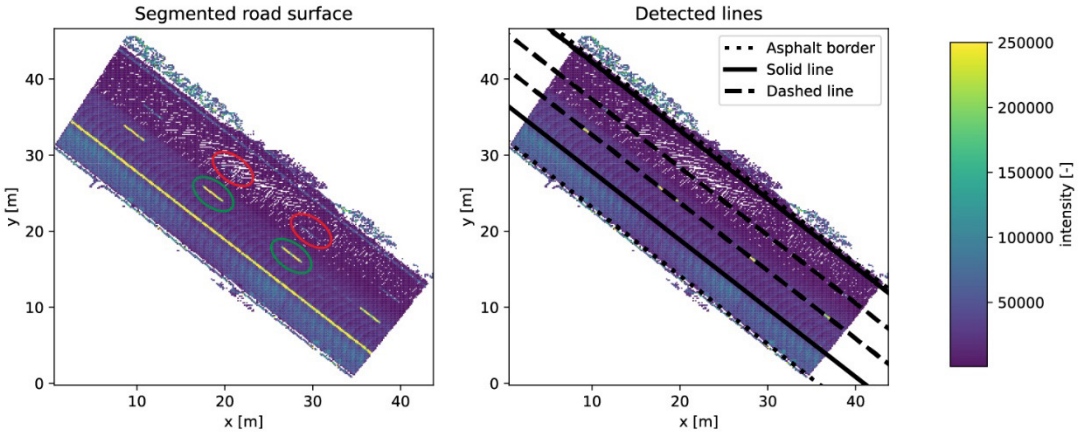

Figure 6.58: Reduces point density on the right lane makes road markings less visible.

6.4 Sensitivity analysis

To make an assessment about how sensitive the method is to a point cloud with a reduced point density, a 50% random subset of a gantry point cloud is processed 100 times. By calculating the dispersion of the obtained clearances from these subsets a quantitative judgement can be presented about how important it is that the proposed method selects the correct edge points.

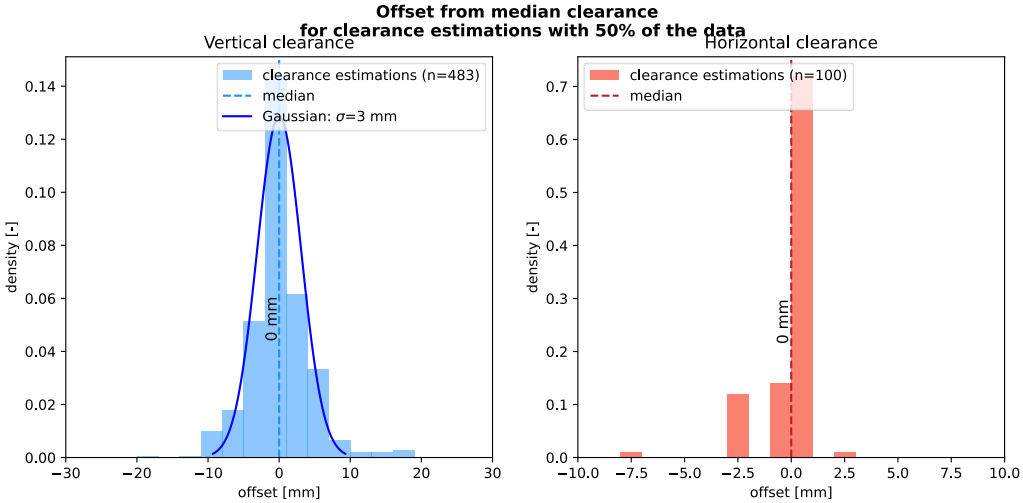

Figure 6.59: Deviations from the median clearance for clearance estimations with a subset of 50% from the original data. Left: Vertical clearances, right: horizontal clearances.

Figure 6.59 shows that if the clearances under a gantry are determined 100 times for a random subset of 50% of the original data, the standard deviation of the clearance offsets ($e = c_{V,third-party} - c_{V,estimated}$) is $3\,mm$. For the horizontal clearances in the right plane, the distribution is even narrower. For 87 out of 100 horizontal clearance estimations the deviation was within $1\,mm$. This supports that the proposed method is stable and is not very sensitive to a homogeneous reduction in points.

6.5 Incomplete laser scanner sampling

When the point density of a sampled traffic sign is too low, it can occur that the line that estimates bottom edge of a sign is not an accurate representation of the reality. In Figure 6.60 it is clearly visible that the estimated bottom edge is very rough. Problems like this can have a significant impact on the vertical clearance estimation under signs that have a low point density. A possible solution here could be to only take the lowest point of a traffic sign and use that point to estimate the bottom edge as a horizontal line.

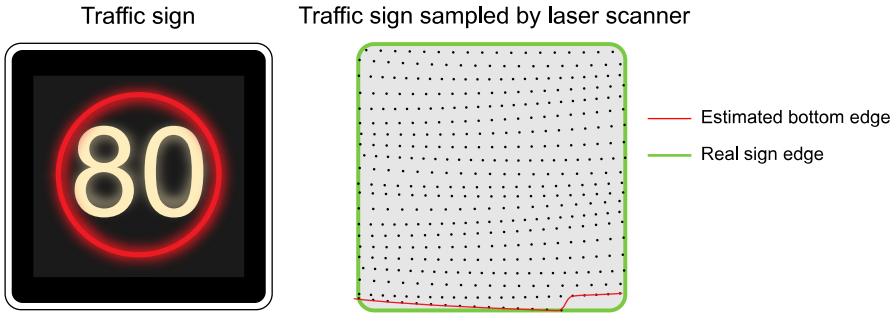

Figure 6.60: A typical example of a bottom edge estimated on a low point density traffic sign.

6.6 Data noise

To get a sense of the noise present in the point clouds of dataset A, a plane can be fitted to a small cutout of points representing a planar surface. This is done with three different object/material types: asphalt, concrete (viaduct) and traffic signs. The plane can be fitted with least squares and the root mean square (RMS) of the distance of all points to the fitted plane is shown in Table 4. The table shows that RMS is the lowest for the concrete of a viaduct and that the RMS is highest for a traffic sign mounted to a gantry. A visualization for distance to the fitted plane for each point on a traffic sign is presented in Figure 6.61.

Table 4: Overview of the RMS for a plane fitted to a group of points from different objects.

	Area [m²]	***Number of points***	***RMS [mm]***
Asphalt	2.25	1387	7.4
Viaduct bottom surface	2.25	1109	3.7
Gantry sign	2.25	1177	9.2

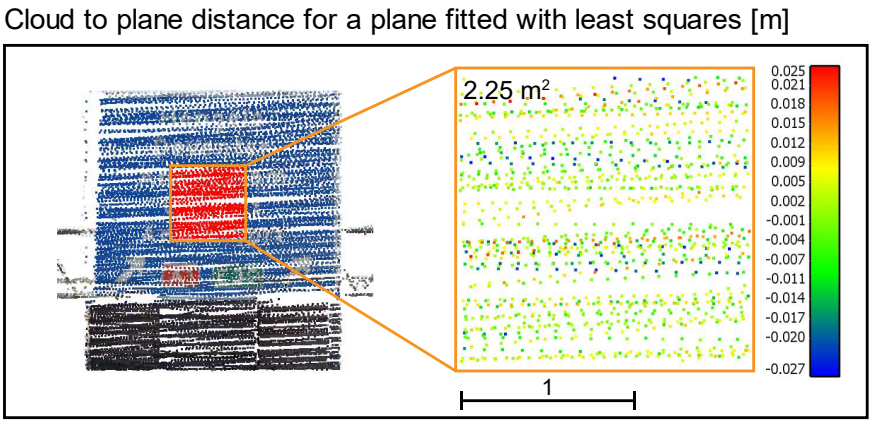

Figure 6.61: The cloud to plane distance for a plane fitted to a set of points in the orange outlined area.

6.7 Applicability

The method developed in this research focuses on Dutch highway infrastructure. Particularly viaducts and traffic gantries. Can the developed method also be applied to other infrastructure objects such as overhead traffic lights or tunnels? Will the method also be applicable to highways in other countries?

A traffic light construction as visualized in Figure 6.62 has a very similar construction to the traffic gantry. It is also mandatory to obtain clearances under traffic light constructions. The proposed approach for segmenting the bottom edge of a traffic gantry should also be applicable to a traffic light construction. A potential issue however could occur when segmenting the road markings. Road markings near a traffic stop are often more complex with arrows or stop lines. This is not something that the method considers currently.

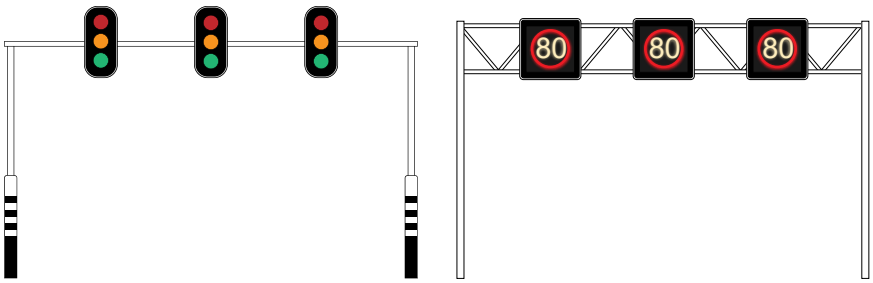

Figure 6.62: The traffic light construction has similar structural characteristics to the traffic gantry.

For tunnels the clearances are also measured and archived by Rijkswaterstaat and its contractors. The tunnel shares some structural characteristics with a viaduct, but they are not similar enough for the method to work. Tunnels often have installations for ventilation suspended from the ceiling which is not accounted for in the proposed workflow. Even more, tunnels don't always have horizontal planar ceilings but can also have curved ceilings.

Is the proposed method also applicable to highway infrastructure in other countries? This is a question that cannot be answered with certainty since there were no point clouds from other countries available but the Netherlands. In general, the viaducts and traffic gantries in other European countries look very similar to their Dutch counterparts. It can be assumed that, all be it with some tuning of different parameters, the proposed workflow can also be applied to infrastructure in other countries.

7. Conclusions and Recommendations

This chapter will conclude this thesis. In Section 7.1 the research questions from Section 1.3 will be answered and Section 7.2 will present a recommendation for future research in the field of automatic clearance estimations of highway infrastructure from LiDAR point clouds.

7.1 Conclusions

In Section 1.3 the following main research question was stated:

- ***How to improve the approach for validating clearance measurements of highway infrastructure with the usage of LiDAR point clouds?***

Currently, clearance measurements are validated by performing manual measurements in a point cloud. In this research a method is proposed that can automatically estimate vertical and horizontal clearances under gantries and viaducts from a point cloud. The clearances are estimated using an intuitive geometrical approach. Initially the road surface is segmented to classify the road markings, subsequently the bottom edge of the overhead structure, or the edge of the guard rails is segmented and finally the vertical and horizontal clearances are estimated. This approach gives the user a good understanding of how the different measurement estimations are obtained. The presentation of the results for a clearance estimation is according to the requirements issued by Rijkswaterstaat.

The main research question is divided into 6 sub-questions. They are answered below:

1. ***How to segment and classify different viaduct and gantry components from the point cloud data?***
   The bottom surface of the viaduct is segmented from the point cloud using a series of operations involving a quadtree representation of the input point cloud, a local surface extraction method by using a kernel density estimation and subsequently cell-based region growing to obtain the bottom surface of the superstructure. The convex hull of this segmented surface is computed to obtain the edges.

   The gantry superstructure is segmented from the point cloud using DBSCAN with PCA and the assumption that the superstructure should be located at least 3 meters above the road surface. The bottom edge of the superstructure is extracted by computing the alpha shape. This yields a set of edge points in $\mathbb{R}^3$ that can be clustered using DBSCAN to obtain the separate clusters representing the bottom edge of the different signs and structural beams that are part of the superstructure.
2. ***How to obtain the highway lane boundaries from the point cloud data?***
   A similar approach to extracting the viaduct bottom surface is used to extract the road surface from the point cloud. A combination of DBSCAN with PCA and the Hough transform for straight lines is used to obtain the different classes of lane boundaries. The input for the Hough transform is first preprocessed with some common image processing steps to increase the robustness of the line detection.
3. ***What objects bound the horizontal clearances under a gantry or viaduct and how can they be segmented from the point cloud?***
   Generally, the horizontal clearance under a gantry or viaduct is bounded by guard rails that are present alongside both road edges. With the assumptions in Section 4.5 and DBSCAN the guard rails can be segmented from the point cloud. These clusters can still contain noise from high vegetation but since the guard rails have a predictable size and location, this information can be used to filter out the grass and other noise with help of a kernel density estimation. When no guard rail is present a different cluster of points

that bounds the horizontal clearance is sought for. Since these other clusters containing objects such as columns, beams or even fences have less predictable characteristics, there is a higher chance that this clusters contains vegetation that is not filtered out. When there is no object restricting the horizontal clearance within 10 meters of the road edge, the edge of the asphalt is used as the boundary where the horizontal clearance is truncated.

4. ***What are the geometric characteristics of a structure's components that determine the clearances?***
   For a viaduct the vertical clearances are restricted by the road surface and the bottom of the bridge superstructure. These are both horizontal planar surfaces. For gantries the bottom edge is a bit more complex since it is dependent on the layout of the mounted traffic signs on the gantry superstructure. In general, a gantry bottom edge is composed of separate edges from the individual traffic signs. The bottom edge is best described by a set of B-splines.
5. ***How to estimate and locate the minimal vertical and horizontal clearances from the point clouds?***
   To estimate the clearances between two segmented point clusters, for instance a road surface and the bottom edge of a traffic sign mounted on a gantry, B-splines are used to approximate the collections of discrete points as a continuous surface or edge. The information about the location of the road markings is then used to determine at what location or between which boundaries the clearances should be estimated. The continuous surfaces and edges now make it possible to estimate the clearance at every location instead of only at the locations of the discrete points in the point cloud.
6. ***How to assess the quality of the inferred clearances and what is the quality difference between data providers?***
   To make an assessment about the quality of the proposed method a case study was performed. The study area contained 50 gantries and 20 viaducts. The proposed method was used to estimate all clearances for these structures and the results were compared with clearance measurements performed by third party contractors. The clearances inferred from the low-density point cloud, dataset A, show a median overestimation of the vertical clearance of $23\,\mathrm{mm}$ under the gantries and $33\,\mathrm{mm}$ under the viaducts. The horizontal clearances show a median underestimation of $30\,\mathrm{mm}$. A comparison with higher density point clouds, dataset B, was made by using a point cloud dataset containing 10 gantries. These point clouds were specifically obtained with the purpose of estimating clearances and had an approximately 20 times higher point density in some areas compared to dataset A. The median vertical clearance estimation offset in these point clouds was an underestimation of $5\,\mathrm{mm}$. The clearances estimated from dataset B also had a lower level of dispersion compared to when the same gantries were processed from dataset A: a standard deviation of $9\,mm$ vs $14\,mm$.

7.2 Recommendations

The proposed method can be used for determining clearances of highway viaducts and gantries. Still, there are several aspects that could be improved upon or could be investigated in future research:

Investigation into the origin of the estimation offsets
The estimated clearances from the proposed method seem to have systematic offset with the third-party measurements. The origin of this offset might lay in the data itself, but there could also be explanation for this difference in the proposed method. The cause is unclear. A further investigation could seek to explain this offset and use that understanding to improve the estimated clearances.

Optimization of Python code and batch processing
The code behind the proposed method was written in Python. The processing time for a single point cloud was covered in Section 5.6 but there certainly are performance gains that can be achieved to improve the processing time. This can become especially beneficial when the goal is to process a large set of gantries and viaducts for future case studies. Currently the code only processes a single point cloud and when it is finished the user must manually edit and run the code again for a new point cloud. It should however not be a major challenge to implement batch processing.

Using large point clouds from other data providers
If the method is used for point clouds with a much higher point density compared to the point clouds used for the case study, it is advisable to investigate a suitable down sampling technique that gives the best ratio between performance and the preservation of the geometric properties of the scanned object. Random subsampling is fast and efficient, but it comes at the tradeoff that it also removes points that are very useful for estimating the clearances. Many more subsampling techniques exist, so exploring other options can be interesting. Even with the point clouds from dataset A it was proven that consistent clearance estimations can be achieved with a random subset of 50% of the data. Here it could also be interesting to investigate other down sampling techniques.

Updating the clearance requirements
The current clearance requirements issued by Rijkswaterstaat are updated every two years or so. However, they only mention requirements for accuracy and the location of the measurements. A lot of contractors already use point clouds to estimate the clearances from, but each contractor might use point clouds with completely different characteristics. Since Rijkswaterstaat can also request these point clouds from the contractors to perform an in-house validation of the measurements, it can be difficult to process all these different point clouds with a single tool. Point clouds are not mentioned in the requirements, though it might be a good addition in future releases to put some sort of standard in place.

Bibliography

Bellekens, B., Spruyt, V., Berkvens, R., & Penne, R. (2015). A Benchmark Survey of Rigid 3D Point Cloud Registration Algorithms. *InternationalJournalonAdvancesinIntelligentSystems*, *8*(1), 118–127. http://www.iariajournals.org/intelligent_systems/

Canny, J. (1986). A Computational Approach to Edge Detection. *IEEE Transactions on Pattern Analysis and Machine Intelligence*, *PAMI-8*(6), 679–698. https://doi.org/10.1109/TPAMI.1986.4767851

Dierckx, P. (1982). Algorithms for smoothing data with periodic and parametric splines. *Computer Graphics and Image Processing*, *20*(2), 171–184. https://doi.org/10.1016/0146-664X(82)90043-0

Duda, R. O., & Hart, P. E. (1972). Use of the Hough Transformation to Detect Lines and Curves in Pictures. *Communications of the ACM*, *15*(1), 11–15. https://doi.org/10.1145/361237.361242

Edelsbrunner, H., Kirkpatrick, D., & Seidel, R. (1983). On the shape of a set of points in the plane. *IEEE Transactions on Information Theory*, *29*(4), 551–559. https://doi.org/10.1109/TIT.1983.1056714

Ester, M., Kriegel, H.-P., Sander, J., & Xu, X. (1996). A Density-Based Algorithm for Discovering Clusters in Large Spatial Databases with Noise. *Proceedings of the 2nd International Conference on Knowledge Discovery and Data Mining*, 226–231.

Gargoum, S. A., & El-Basyouny, K. (2022). Impacts of point cloud density reductions on extracting road geometric features from mobile LiDAR data. *Canadian Journal of Civil Engineering*, *49*(6), 910–924. https://doi.org/10.1139/cjce-2020-0193

Gargoum, S. A., Karsten, L., El-Basyouny, K., & Koch, J. C. (2018). Automated assessment of vertical clearance on highways scanned using mobile LiDAR technology. *Automation in Construction*, *95*(November 2017), 260–274. https://doi.org/10.1016/j.autcon.2018.08.015

Hackel, T., Wegner, J. D., & Schindler, K. (2016). Fast Semantic Segmentation of 3D Point Clouds With Strongly Varying Density. *ISPRS Annals of Photogrammetry, Remote Sensing and Spatial Information Sciences*, *III–3*(July), 177–184. https://doi.org/10.5194/isprsannals-iii-3-177-2016

Heikkilä, R., Kivimäki, T., Mikkonen, M., & Lasky, T. A. (2010). Stop & go scanning for highways - 3D calibration method for a mobile laser scanning system. *2010 - 27th International Symposium on Automation and Robotics in Construction, ISARC 2010*, *Isarc*, 40–48. https://doi.org/10.22260/isarc2010/0005

Hough, P. (1962). *Method and means for recognizing complex patterns*. HOUGH PAUL V C OP - US 1771560 A. https://lens.org/147-492-958-779-046

Kineri, Y., Wang, M., Lin, H., & Maekawa, T. (2012). B-spline surface fitting by iterative geometric interpolation/approximation algorithms. *CAD Computer Aided Design*, *44*(7), 697–708. https://doi.org/10.1016/j.cad.2012.02.011

Kretschmer, U., Abmayr, T., & Thies, M. (2002). Traffic construction analysis by use of terrestrial laser scanning. *Archives*, 232–236.

Kukko, A., Kaasalainen, S., & Litkey, P. (2008). Effect of incidence angle on laser scanner intensity and surface data. *Applied Optics*, *47*(7), 986–992. https://doi.org/10.1364/AO.47.000986

Kunoth, A., Lyche, T., Lyche, T., & Manni, C. (2017). Splines and PDEs: From Approximation Theory to Numerical Linear Algebra. In *Lecture Notes in Mathematics* (Vol. 2219).

Landa, J., Prochazka, D., & Štastny, J. (2013). Point cloud processing for smart systems. *Acta*

Universitatis Agriculturae et Silviculturae Mendelianae Brunensis, *61*(7), 2415–2421. https://doi.org/10.11118/actaun201361072415

Muggeo, V. M. (2003). Estimating regression models with unknown break-points. *Statistics in Medicine*, *22*(19), 3055–3071.

Paffenholz, J. A., Vennegeerts, H., & Kutterer, H. (2008). High frequency terrestrial laser scans for monitoring kinematic processes. *Proceedings CD INGEO*, 1–12.

Pedregosa, F., Varoquaux, G., Gramfort, A., Michel, V., Thirion, B., Grisel, O., Blondel, M., Müller, A., Nothman, J., Louppe, G., Prettenhofer, P., Weiss, R., Dubourg, V., Vanderplas, J., Passos, A., Cournapeau, D., Brucher, M., Perrot, M., & Duchesnay, É. (2012). Scikit-learn: Machine Learning in Python. *Environmental Health Perspectives*, *127*(9), 2825–2830. https://doi.org/https://doi.org/10.48550

Pilgrim, C. (2021). piecewise-regression (aka segmented regression) in Python. *Journal of Open Source Software*, *6*(68), 3859. https://doi.org/10.21105/joss.03859

Prochazka, D., Prochazkova, J., & Landa, J. (2019). Automatic lane marking extraction from point cloud into polygon map layer. *European Journal of Remote Sensing*, *52*(sup1), 26–39. https://doi.org/10.1080/22797254.2018.1535837

Puente, I., González-Jorge, H., Martínez-Sánchez, J., & Arias, P. (2013). Review of mobile mapping and surveying technologies. *Measurement: Journal of the International Measurement Confederation*, *46*(7), 2127–2145. https://doi.org/10.1016/j.measurement.2013.03.006

Rijkswaterstaat. (2019). *Productspecificaties Doorrijprofielen*. https://standaarden.rws.nl/link/standaard/6067

Rijkswaterstaat. (2021). *Staat van de Infra Rijkswaterstaat*. https://open.overheid.nl/repository/ronl-8adf67c9-e3cf-4579-ad69-89c9ca705835/1/pdf/bijlage-rapportage-staat-van-de-infra-rws-definitief.pdf

Soudarissanane, S. (2016). *The Geometry of Terrestrial Laser Scanning: IDENTIFICATION OF ERRORS, MODELING AND MITIGATION OF SCANNING GEOMETRY*.

StreetMapper. (n.d.). *StreetMapper IV*. Retrieved November 15, 2022, from https://www.igi-systems.com/files/IGI/Brochures/StreetMapper/StreetMapper IV.pdf

Talebitooti, R., Shojaeefard, M. H., & Yarmohammadisatri, S. (2015). Shape design optimization of cylindrical tank using b-spline curves. *Computers and Fluids*, *109*, 100–112. https://doi.org/10.1016/j.compfluid.2014.12.004

Truong-Hong, L., Lindenbergh, Roderik, & Amiri-Simkooei, A. (2022). *Automatical estimation of vertical clearance of highway bridges from mobile laser scanning data*.

Truong-Hong, L., & Lindenbergh, R. (2022). Automatically extracting surfaces of reinforced concrete bridges from terrestrial laser scanning point clouds. *Automation in Construction*, *135*(January), 104127. https://doi.org/10.1016/j.autcon.2021.104127

Velodyne. (n.d.). *Velodyne HDL32E*. Retrieved November 3, 2022, from https://velodynelidar.com/products/hdl-32e/

Virtanen, P., Gommers, R., Oliphant, T. E., Haberland, M., Reddy, T., Cournapeau, D., Burovski, E., Peterson, P., Weckesser, W., Bright, J., van der Walt, S. J., Brett, M., Wilson, J., Millman, K. J., Mayorov, N., Nelson, A. R. J., Jones, E., Kern, R., Larson, E., … Vázquez-Baeza, Y. (2020). SciPy 1.0: fundamental algorithms for scientific computing in Python. *Nature Methods*, *17*(3), 261–272. https://doi.org/10.1038/s41592-019-0686-2

West, K. F., Webb, B. N., Lersch, J. R., Pothier, S., Triscari, J. M., & Iverson, A. E. (2004). Context-driven automated target detection in 3D data. *Automatic Target Recognition XIV*, *5426*(September 2004), 133–143. https://doi.org/10.1117/12.542536

Zhang, C., Arditi, D., & Chen, Z. (2013). Using terrestrial laser scanners to calculate and map vertical bridge clearance. *International Archives of the Photogrammetry, Remote Sensing and Spatial Information Sciences - ISPRS Archives*, *XL-2/W2*, 133–138.

https://doi.org/10.5194/isprsarchives-XL-2-W2-133-2013

Zhou, Y., Wang, S., Mei, X., Yin, W., Lin, C., Hu, Q., & Mao, Q. (2017). Railway tunnel clearance inspection method based on 3D point cloud from mobile laser scanning. *Sensors (Switzerland)*, *17*(9), 1–20. https://doi.org/10.3390/s17092055

A

ISPRS Paper

The following paper was presented during the optical 3D metrology workshop at the University of Würzburg from 15 to 16 December 2022.

CLEARANCE MEASUREMENT VALIDATION FOR HIGHWAY INFRASTRUCTURE WITH USE OF LIDAR POINT CLOUDS

Jens P. Meinderts[1,*], Roderik Lindenbergh[1], Daan H. van der Heide[2], Alireza Amiri-Simkooei[1] and Linh Truong-Hong[1]

[1]Dept. of Geoscience & Remote Sensing, Delft University of Technology, the Netherlands - j.p.meinderts@student.tudelft.nl
[2]Rijkswaterstaat Centrale Informatievoorziening, Delft, The Netherlands

Technical Commission II

KEY WORDS: Point Clouds, Segmentation, Clearance estimation, Mobile Laser Scanning, Highway infrastructure, Traffic gantries

ABSTRACT:

This paper introduces a method to automatically estimate vertical and horizontal clearances of highway viaducts and gantries from Mobile Laser Scanner (MLS) point clouds. It is essential to have accurate data on the vertical and horizontal clearances of overhead infrastructure objects along the highway. Accurate clearance data is used for routing oversized transports, infrastructure reconstruction, maintenance and settling legal claims after incidents. The proposed method takes a point cloud of an infrastructure object as input, and as output provides the user with a concise overview of the horizontal and vertical clearances of the object. A point cloud of a highway overpass or gantry is segmented into the different clusters relevant for determining the clearances. The discrete points in these clusters will then be used to approximate their surfaces with B-splines. Subsequently the minimal clearances can be estimated. These clearances are estimated at certain pre-specified locations according to guidelines from the highway authority. The paper also includes a comparison of the inferred clearances from the point clouds with archived measurements performed by third party contractors. For this case study, a Dutch highway section containing 50 gantries and 20 viaducts is selected. Along this stretch of highway the clearances are estimated. The estimated clearances for each structure are then compared with archived in situ measurements. This will give a quantitative analysis of the quality of the estimated clearances. The estimated vertical clearances have an overestimation of 20-30 mm compared to the validation data. The horizontal clearances show a median underestimation of 20 mm.

1. INTRODUCTION

The Dutch highway network contains more than 3.000 kilometers of roads (Rijkswaterstaat, 2021). Spanning these roads are thousands of viaducts and traffic sign wielding gantries (Figure 1). It is essential to have accurate data on the vertical and horizontal clearances under these objects. This data is used when routing oversized transport, carrying out maintenance or settling legal claims after an incident with oversized transport.

Figure 1. A typical traffic sign gantry on a Dutch highway with in the background a highway viaduct. The horizontal clearance is restricted by guard rails on both sides of the road. (Source: Rijkswaterstaat, 2006)

For all overhead structures along the highway network the clearances are documented according to specifications issued by the executive organisation of the Dutch ministry of Infrastructure and Waterways: Rijkswaterstaat. These specifications (Rijkswaterstaat, 2019) describe at what locations under a structure and with what margin of error the clearances should be measured.

Traditionally these measurements are taken in the field with usage of geodetic devices such as a total station, rangefinder or laser scanner. Measurements and documentation are usually performed by a third party contractor and involve a lot of manual work. To guarantee the quality of this data the measurements need to be validated. For the validation of measurements yearly Mobile Laser Scanner (MLS) point clouds are available for the complete Dutch highway network.

This study introduces a method to automatically estimate clearances under viaducts and gantries from MLS-point clouds with a geometric approach (Figure 2). The paper is structured as follows. In the section Background information will be given on related research and guidelines for determining clearances. The section Method will show a step by step workflow for estimating the vertical and horizontal clearances. In the section Case Study and Results the method will be validated on two sections of highway in the Netherlands.

2. BACKGROUND

This section gives some insight into related researches and also provides information on the definition of a 'minimal' clearance used in this research.

* Corresponding author

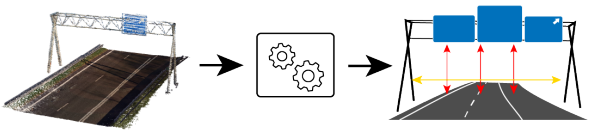

Figure 2. A simplification of the tool to be developed in this research. A point cloud of a gantry is taken as input and processed. The result is a visualization with the estimated clearances.

2.1 Related research

Gargoum et al. (2018) propose an algorithm whereby mobile LiDAR data is used to assess vertical clearance at overhead objects on highways. The algorithm detects and classifies all overhead objects on a highway segment. At each detected object the minimal clearance is determined. This research mainly focuses on vertical clearances under viaducts and power lines and does not cover gantries. The location where the vertical clearance should be determined is manually defined by the user. Differences between estimated clearances and conventional measurements were up to 15 cm.

Point clouds often contain differences in point density. This variation is expected to affect the quality of the information that is inferred from the point clouds. Gargoum and El-Basyouny (2022) investigates the impacts of point density reduction on the extraction and assessment of different geometrical features. The different geometrical features were extracted from a point cloud at varying levels of point density and on a selection of different Canadian highway segments. It was found that clearance assessments on viaducts had low sensitivity to reductions in point density. Reductions to 10% of the original data yielded comparable results to what was obtained at 100% point density. Low point density can however cause an inability to detect accurate clearances under short span overhead objects i.e. power cables or gantries.

In Zhang et al. (2013) a method is proposed to estimate vertical bridge clearances by using terrestrial laser scanners. The study introduces an approach to reduce data noise caused by nearby traffic. The locations of the vertical clearances are determined manually. No quantitative assessment was performed on the accuracy of the estimated clearances.

Railway tunnel clearance is directly related to the safe operation and freight capacity of trains. In Zhou et al. (2017) a tunnel clearance inspection approach is presented based on 3D point clouds obtained by a mobile laser scanner system. A dynamic coordinate system for railway tunnel clearances is introduced. By using a 3D linear fitting algorithm on a segmented point cloud the rail line can be extracted and is used to seamlessly connect all rail segments. Based on the rail alignment and the clearance coordinate system different types of clearance frames are introduced to perform the tunnel clearance inspection. The claimed precision reaches 0.03 m.

In a review of mobile mapping and surveying technologies, (Puente et al., 2013), an analysis is introduced on the performance of some modern mobile terrestrial laser scanning systems. The study presents an overview of the positioning, scanning and imaging devices used in these systems. A systematic comparison of the navigation and LiDAR specifications from the manufacturers is provided. Based on the accuracy requirements for a mapping or surveying project a best solution is found taking into account all scanner specifications.

2.2 Guidelines for clearances

There is not one universal method for documenting minimal clearances under viaducts and gantries. In this research the guidelines of the Dutch highway authority were used as a base (Rijkswaterstaat, 2019).

The **vertical clearance** is a measurement perpendicular to the road surface between a viaduct or traffic gantry and the underlying pavement. The minimal vertical clearance is found where this distance is the smallest. The vertical clearance measurements must meet the following requirements: The precision σ should be $\leq$1.0 cm and the measurements should be presented with 3 decimals. The locations of the clearance heights have different requirements for each type of object.

For a highway viaduct the following applies:

- The vertical clearance should be determined on each lane border road marking and on the asphalt edges.
- For each driving direction two clearance cross sections should be provided. The first one at beginning of the object and the second one at the rear of an object. The location of the front is determined based on in what direction the hectometer signs along the road are increasing in value.
- Double highway bridges less than 3 meters apart are seen as one object. When the gap in between is larger than 3 meters both bridges are seen as individual objects.

For traffic sign gantries the minimal vertical clearances should be determined for each lane including rush hour lanes, entry or exit lanes and emergency lanes. If there is no road sign or lane control sign directly above a lane the vertical clearance is determined from the pavement to the gantry's suspension structure.

The **horizontal clearance** is the minimal horizontal distance perpendicular to the driving direction between obstacles that are positioned alongside the pavement. Obstacles here are defined as guardrails, bridge columns or gantry columns.

The horizontal clearance measurements must meet the following requirements: The precision σ should be $\leq$5.0 cm and the measurements should be presented with 2 decimals. For the location of the horizontal clearance the following applies:

- The horizontal clearance must be determined at a height between 0.5 m and 1.0 m above the pavement. The height of the guardrail should fall within this range.
- In a situation where there is no guard rail on one or either side of the road, the width of the roadway cannot always be clearly defined. If the boundary of the clearance width on one or both sides of the road cannot clearly be indicated, for instance due to the absence of obstacles as stated previously, the edge of the pavement is taken as the boundary.

3. DATA

For this paper mobile mapping data two sections of highway were selected. Along these two sections the clearances will be estimated with the proposed method. In total 20 viaducts and 50 gantries will be processed. The MLS-point clouds that are used are all obtained with similar equipment and thus have similar characteristics.

The point clouds are obtained using a Velodyne HDL-32E LiDAR sensor which generates 700.000 points per second with a claimed relative accuracy of approximately 2 cm (Velodyne, n.d.). GPS combined with an Inertial Measurement Unit is used to present the xyz-coordinates in the RD-New (EPSG:28992) reference frame. The point cloud is delivered as a .laz file and for all points it contains five attributes; intensity, number of returns, return number, GPS time and RGB color. The RGB values are derived from a separate 360° panoramic image sensor.

A typical gantry contains 40.000-50.000 points. This is considerately less than a highway viaduct which contains on average 300.000-500.000 points. This is not including the asphalt.

4. METHOD

To estimate the clearances under a viaduct or gantry, the proposed method is divided into three components: (i) Vertical clearance estimation under a viaduct, (ii) vertical clearance estimation under a traffic gantry and (iii) horizontal clearance estimation. All three components require the location and orientation of the road markings, therefore the segmentation of the road surface and the road markings is the first step.

4.1 Step 1: Surface segmentation

The workflow for extracting the road surface consists of multiple steps briefly explained below:

1. A quadtree representation (Truong-Hong and Lindenbergh, 2022) aims to reduce the complexity of the original point cloud. The quadtree is carried out to recursively subdivide the initial point cloud into increasingly smaller 2D cells. This is carried out until the termination criterion is reached i.e. when a subdivided cell contains fewer points than a predefined threshold.

2. For all cells the local surfaces are extracted. When the input point clouds contains a viaduct, the remaining cells can contain multiple horizontal surfaces; the road and the bridge superstructure. Since the surfaces are expected to be concentrated in different groups in vertical direction, a kernel density estimation (KDE) (Truong-Hong and Lindenbergh, 2022) is used to establish the location of the local surfaces. These local surfaces are assumed to be nearly horizontal.

3. In this step planes are fitted to the different surfaces in each cell. Cell-based region growing (Truong-Hong and Lindenbergh, 2022) is applied to group the planes from the different patches that belong to the same surface. Some additional patch filtering is applied to obtain appropriate surface edges.

4. Now that multiple surfaces have been extracted it is necessary to classify them with the correct class. Road and bridge surfaces are extracted from the set of surfaces derived in the previous step.

When the input point cloud contains a traffic gantry, the output of the road surface segmentation will only contain a single horizontal surface; the road surface. When the input point cloud contains a highway bridge, the surface extraction will output two surfaces; the road surface and the bottom of the bridge superstructure.

4.2 Step 2: Road marking segmentation

Segmentation of the road markings gives information on the orientation of the road and the location of the lane borders, which are useful since the vertical clearance is determined for each lane. This step distinguishes 4 types of markings: (1) dashed markings, (2) block markings, (3) continuous markings and (4) the asphalt edge. The asphalt edge is not a painted-on road marking, but it often defines the right border of an emergency lane. The workflow for segmenting the markings is as follows:

4.2.1 Dashed markings The dashed lines are very distinguishable from the dark asphalt surface in the point clouds. The white paint that is used for applying the road markings give points on these surfaces a much higher intensity value than the surrounding asphalt. Applying a simple intensity filter on the extracted road surface from step 1 and subsequently using the DBSCAN clustering algorithm (Ester et al., 1996) yields a set of clusters containing different kinds of road markings. To filter out only the dashed markings a cluster-based feature filter is used with PCA features. Several features have already been proposed by West et al. (2004) & Hackel et al. (2016). The following geometrical features are selected and give information on what type of road marking a cluster potentially belongs to:

- **Orientation:** With the assumption that all road markings are parallel (only small sections of road are considered at once) all markings should have the same orientation. The orientation is defined by the first eigenvector corresponding to the largest eigenvalue λ_1.

- **Length:** The largest eigenvalue λ_1 of a cluster gives information about the variance in the direction of the first eigenvector. Dashed lines as well as block markings have generic dimensions which should suggest that all dashed markings and all block markings should have similar characteristics.

- **Width:** Similar to the length, the second eigenvalue λ_2 gives information about the variance in the direction of the second eigenvector perpendicular to the first eigenvector.

- **Roughness/height:** The third eigenvalue λ_3 gives information about the variance in the direction of the third eigenvector. Since road markings usually correspond largely to 2D planes on the road surface, the variance in the direction of the third eigenvalue should be very small ($\lambda_3 \ll \lambda_1$).

- **Linearity:** The linearity of a cluster is a geometrical feature that can be derived from the eigenvalues. To describe the linearity of a cluster:

$$\textbf{linearity} = \frac{\lambda_1 - \lambda_2}{\lambda_1} \tag{1}$$

- **Planarity:** The planarity is a cluster is described as:

$$\textbf{planarity} = \frac{\lambda_2 - \lambda_3}{\lambda_1} \tag{2}$$

4.2.2 Block markings The segmentation of block markings has a similar approach to the segmentation of dashed markings. The PCA filters uses the same features with different thresholds for the length, width and linearity.

4.2.3 Continuous lines For continuous lines it is also possible to segment and classify them from the point cloud using a method similar to the method for dashed markings. However, an approach using a Hough transform (Hough, 1962) for detecting lines is more simple and gives more reliable results. The Hough method used here takes as input a 2D image. The point cloud itself is a collection of points in 3D space, so some pre-processing has to be done in order to obtain a 2D image of the point cloud that can be fed to the Hough algorithm.

First the 3D point cloud is converted to a 2D image from a bird's eye perspective with full and empty pixels. Some basic opening and closing morphological operations, (Vincent, 1993), are performed to remove noise and improve the visibility of the painted markings in the input image.

4.2.4 Asphalt edge The asphalt edge is not a painted road marking but to detect it a similar approach to the continuous line detection can be used with one extra pre-processing step. After the opening and closing operations a silhouette of the asphalt remains. The edges of the asphalt need to be converted to distinct lines. With a Canny filter, (Canny, 1986), an edge detection algorithm, the asphalt silhouette is transformed into an asphalt outline. This outline is detectable by the Hough algorithm.

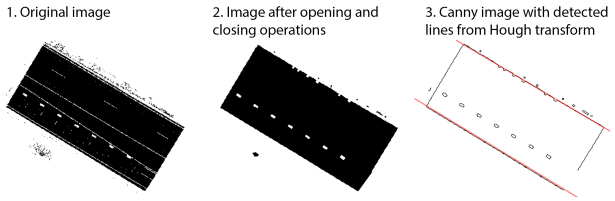

Figure 3. An overview of the pre-processing steps taken for the detection of the asphalt edges. (1) is the original 2D image obtained from the point cloud. (2) the result of a closing-opening operation. (3) the final input image for the Hough transform after applying the Canny operation overlapped with the detected Hough lines.

4.3 Viaduct vertical clearance estimation

Assuming that step 1 yielded a surface for both the road and the bottom of the bridge superstructure, it is now possible to approximate both surfaces with a 2D B-spline and infer the minimal vertical clearances for each lane from these B-splines. B-splines are suitable to represent smooth, non-planar surfaces. The goal here is to find the surface best approximating the points in the segmented surface. By taking the tensor product of two 1D sets of basis functions that describe the surface in the x and y direction, a basis for the 2D polynomial describing the 2D surface is obtained. This is also known as the 2D bi-cubic approximation method, see (De Boor, 1978).

The minimal vertical clearance is now estimated as the minimal vertical distance between the estimated bridge and road surfaces. This clearance is estimated for each traffic lane.

4.4 Traffic gantry vertical clearance estimation

A gantry has a more complex shape than the bottom of a highway bridge, which means that a 2D B-spline is not suitable to describe the bottom edge. This method will use multiple 1D B-splines to describe the irregular bottom edge of the gantry superstructure. Assuming that the road surface already has been segmented in step 1, the steps to determine the vertical clearance under a gantry are as follows:

1. A DBSCAN clustering algorithm is used to cluster the point cloud remaining after the removal of the road surface. To classify the gantry cluster correctly, PCA features are calculated for all clusters similarly to Section 4.2.1.
2. By performing a Hough transform on a top-down 2D image of the classified gantry cluster, the orientation can be determined. Its orientation should be perpendicular with the road trajectory in the xy-plane.
3. The skeleton of a gantry's superstructure can be characterized as an extruded triangle with the point facing downwards. Along the extruded edges there are steel tubes. The bottom steel tube is always present and defines the upper limit of the bottom edge. A kernel density estimation of the z-values in the remaining point cloud is used to identify the location of the bottom tube. All points above this steel tube are discarded since they are not relevant for estimating the bottom of the superstructure.
4. To identify the edge points of the remaining cluster, its alpha shape, (Edelsbrunner et al., 1983), is computed. The bottom edge of this alpha shape contains all the points needed for estimating the bottom of the gantry.
5. The remaining clusters (see Figure 4) are a collection of edges from different signs and tubes. For each edge a B-spline is computed that closely follows the points.
6. The vertical clearance is now estimated as the minimal vertical distance between the 2D road B-spline surface and the B-splines at the bottom of the gantry. The minimal vertical clearance is determined for each traffic lane.

4.5 Horizontal clearance estimation

Most often the horizontal clearance under a viaduct or gantry is restricted by guard rails on either side of the road. Hence, the workflow for finding the horizontal clearance starts with looking for guard rails. If there is no guard rail present the algorithm will look for other objects restricting the horizontal clearance. The process for finding the horizontal clearance is as follows:

4.5.1 Classification of guard rails Guard rails are predictable structures. Their height above the road surface and the horizontal distance from the asphalt edge do not vary much. A first step in segmenting the guard rails from the point cloud is by using the DBSCAN clustering algorithm. Before using the clustering algorithm a few assumptions are used:

1. Assumption 1: The guard rail is located at a height of at least 30 cm above the road surface.
2. Assumption 2: Points more than 2 m above the road surface are not considered for the horizontal clearance.
3. Assumption 3: The road surface is already classified in the lane detection step. These points can be disregarded when searching for the guard rails.

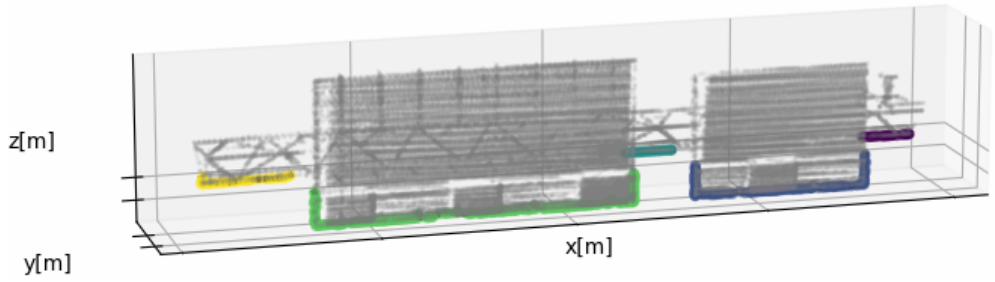

Figure 4. Each color/cluster represents part of the gantry bottom edge.

The clustering algorithm can do a good first segmentation step, but often the clusters containing the guard rails also contain a lot of grass. This is not odd since grass can easily grow high enough to make it difficult for the clustering algorithm to find a border between the guard rail and the grass. To resolve this problem some knowledge of the dimensions of standard guard rails is used.

A candidate cluster possibly containing a guard rail and possibly grass is divided into multiple sections along its main axis with a length of approximately 25 cm. For each section a kernel density estimation is performed of the z-values with a Top-hat filter (Laefer and Truong-Hong, 2017). This Top-hat filter has a total bandwidth of 30 cm. Since the height of a guard rail bumper is also 30 cm the KDE should give the highest signal on a height equal to the center of the bumper as shown in Figure 5. The information on the approximate center of the guard rail bumper can now be used to remove grass from the guard rail cluster candidates.

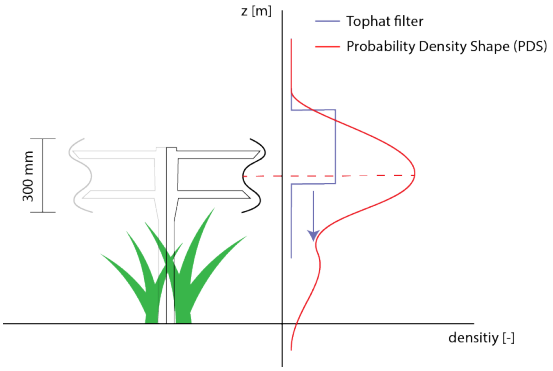

Figure 5. PDS of KDE along the z-axis with a Top-hat filter moving in the z-direction.

4.5.2 Other objects restricting the horizontal clearance If no guard rail is present on the side of the road, the algorithm will look for other clusters of points located alongside the asphalt. Other objects restricting the horizontal clearance are bridge columns, gantry columns, concrete barriers, etc. The same assumptions from Chapter 4.5.1 are used.

4.5.3 Determining the minimal horizontal clearance Assuming that an object restricting the horizontal clearance has been found on either side of the road, the horizontal clearance can now be estimated. The location of the estimated horizontal clearance along the road trajectory is determined by the location of the viaduct or gantry superstructure.

5. CASE STUDY AND RESULTS

The case study consists of a set of gantries and viaducts from two separate Dutch highway sections (Figure 7). These sections have been selected since they have recent (<1 year) validation data available. To analyze the accuracy of the estimated clearances, the developed method is applied to an amount of 50 traffic gantries and 20 viaducts. Each gantry yields a single horizontal clearance and for each lane 1 vertical clearance (Figure 9). A viaduct yields 2 horizontal clearances and for each lane 2 vertical clearances since the clearances are determined on both sides of the bridge as seen in Figure 8. The highway location sign on the right in green gives information on the road name, the direction ('Re' for Right and 'Li' for Left) and the location in kilometers. The white arrow on the sign indicates in what direction the kilometer value is increasing. The results for the clearance estimation errors are shown in Table 1.

Table 1. Statistics of the results [mm]

	Median Error	**MAD**
Vertical clearance gantry	-23	10
Vertical clearance viaduct	-33	7
Horizontal clearance	20	30
Vertical clearance gantry (50% subset)	0	7
Horizontal clearance ganrty (50% subset)	0	0

The median absolute deviation (MAD) is given instead of a standard deviation since the MAD is a more robust estimator of dispersion; it is not affected by outliers. The distribution of the errors is shown in Figure 10. The results in Table 1 and Figure 10 show that the proposed method overestimates the vertical clearances by 23-33 mm. However, the horizontal clearances show a median underestimation of 20 mm.

The outliers of the vertical clearance errors in Figure 10 at -80 and 40 mm are caused by an inaccurately detected asphalt edge. If the detected asphalt edge line is not located on the asphalt but instead just outside of the paved surface, there can be a significant difference in the estimated vertical clearance. Moreover, the road surface 2D B-spline also gives inaccurate results (z-values) when evaluated outside of the road surface.

To assess the sensitivity of the method to a more sparse point cloud a single gantry point cloud is randomly sub-sampled 100 times with 50% of the data. On these subsets the clearances are determined. This shows a MAD of 0 mm for the horizontal clearances and a MAD of 7 mm for the vertical clearances.

Figure 6 shows that the bottom edge of a sign is not always accurately estimated. In this situation the MLS point cloud did not

cover the complete traffic sign surface leaving gaps in between scan lines and a rough bottom edge. A possible explanation could be occlusion by a passing vehicle or because the used laser scanning device has a sparse scan line spacing. This sparse scan line spacing is also apparent on other parts of the sign since there are multiple 'empty' areas visible in the figure.

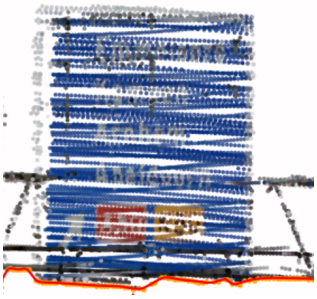

Figure 6. An inaccurately estimated sign bottom edge in red.

6. CONCLUSION AND RECOMMENDATIONS

This paper presented a method for estimating clearances under highway bridges and gantries with point clouds obtained from a Mobile Laser Scanner. The relevant surfaces and edges that determine the horizontal and vertical clearances are estimated with B-splines. The results from the case study show an apparent overestimation in the vertical clearances. This does assume that the validation data is accurate and serves as a ground truth.

The overestimation could be a consequence of the relatively sparse MLS point clouds that are used in this research. Gantries and traffic signs are slender structures and it sometimes difficult for the laser scanner to cover a bottom edge of an object that is only a centimeter thick.

The horizontal clearances is not sensitive to a significant decrease in point density. Vertical clearances however seem more sensitive. A possible explanation is that a gantry superstructure is only sparsely represented in the MLS point clouds with individual points on the bottom edge of a gantry superstructure often not covering the true bottom edge. Guard rails on the side of the road are more densely covered in points and also have a more constant profile.

There are a lot of parameters in this method that can be tuned in order to achieve a higher clearance accuracy. A sensitivity analysis on different parameters for the B-splines, DBSCAN, Hough transform and PCA could give better surface and edge estimation. This could yield better and more consistently accurate clustering results.

The point cloud data used in this research has a limited density and relative accuracy. It would be interesting to estimate and validate the clearances on point clouds with a higher density and relative accuracy. This higher relative accuracy can be reached by using a more high end laser scanner.

References

Canny, J., 1986. A Computational Approach to Edge Detection. *IEEE Transactions on Pattern Analysis and Machine Intelligence*, PAMI-8(6), 679–698.

De Boor, C., 1978. *A Practical Guide to Splines*. Springer New York.

Edelsbrunner, H., Kirkpatrick, D., Seidel, R., 1983. On the shape of a set of points in the plane. *IEEE Transactions on Information Theory*, 29(4), 551–559. http://ieeexplore.ieee.org/document/1056714/.

Ester, M., Kriegel, H.-P., Sander, J., Xu, X., 1996. A Density-Based Algorithm for Discovering Clusters in Large Spatial Databases with Noise. *Proceedings of the 2nd International Conference on Knowledge Discovery and Data Mining*, 226–231.

Gargoum, S. A., El-Basyouny, K., 2022. Impacts of point cloud density reductions on extracting road geometric features from mobile LiDAR data. *Canadian Journal of Civil Engineering*, 49(6), 910–924.

Gargoum, S. A., Karsten, L., El-Basyouny, K., Koch, J. C., 2018. Automated assessment of vertical clearance on highways scanned using mobile LiDAR technology. *Automation in Construction*, 95(November 2017), 260–274. https://doi.org/10.1016/j.autcon.2018.08.015.

Hackel, T., Wegner, J. D., Schindler, K., 2016. Fast Semantic Segmentation of 3D Point Clouds With Strongly Varying Density. *ISPRS Annals of Photogrammetry, Remote Sensing and Spatial Information Sciences*, III-3(July), 177–184.

Hough, P., 1962. Method and means for recognizing complex patterns.

Laefer, D. F., Truong-Hong, L., 2017. Toward automatic generation of 3D steel structures for building information modelling. *Automation in Construction*, 74, 66–77. http://dx.doi.org/10.1016/j.autcon.2016.11.011.

Puente, I., González-Jorge, H., Martínez-Sánchez, J., Arias, P., 2013. Review of mobile mapping and surveying technologies. *Measurement: Journal of the International Measurement Confederation*, 46(7), 2127–2145. http://dx.doi.org/10.1016/j.measurement.2013.03.006.

Rijkswaterstaat, 2019. Productspecificaties Doorrijprofielen. https://standaarden.rws.nl/link/standaard/6067.

Rijkswaterstaat, 2021. Staat van de Infra Rijkswaterstaat. https://open.overheid.nl/repository/ronl-8adf67c9-e3cf-4579-ad69-89c9ca705835/1/pdf/bijlage-rapportage-staat-van-de-infra-rws-definitief.pdf.

Truong-Hong, L., Lindenbergh, R., 2022. Automatically extracting surfaces of reinforced concrete bridges from terrestrial laser scanning point clouds. *Automation in Construction*, 135(January), 104127. https://doi.org/10.1016/j.autcon.2021.104127.

Velodyne, n.d. Velodyne HDL32E. https://velodynelidar.com/products/hdl-32e/.

Vincent, L., 1993. Grayscale Area Openings and Closings: their Applications and Efficient Implementation. *EURASIP Workshop on Mathematical Morphology and its Applications to Signal Processing*, 22–27. http://www2.vincent-net.com/luc/papers/93barcelona

West, K. F., Webb, B. N., Lersch, J. R., Pothier, S., Triscari, J. M., Iverson, A. E., 2004. Context-driven automated target detection in 3D data. *Automatic Target Recognition XIV*, 5426(September 2004), 133–143.

Zhang, C., Arditi, D., Chen, Z., 2013. Using terrestrial laser scanners to calculate and map vertical bridge clearance. *International Archives of the Photogrammetry, Remote Sensing and Spatial Information Sciences - ISPRS Archives*, XL-2/W2, 133–138.

Zhou, Y., Wang, S., Mei, X., Yin, W., Lin, C., Hu, Q., Mao, Q., 2017. Railway tunnel clearance inspection method based on 3D point cloud from mobile laser scanning. *Sensors (Switzerland)*, 17(9), 1–20.

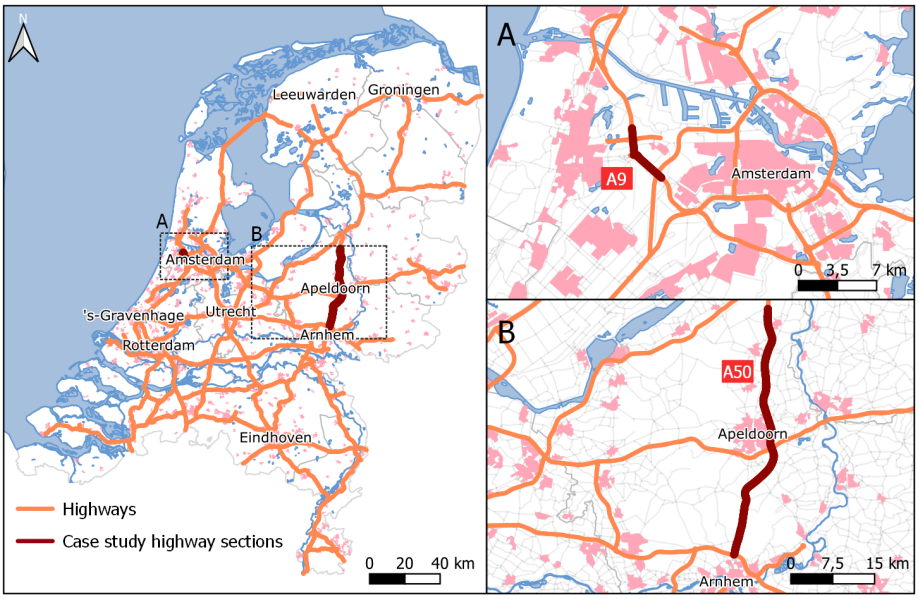

Figure 7. Overview of the selected sections for the case study.

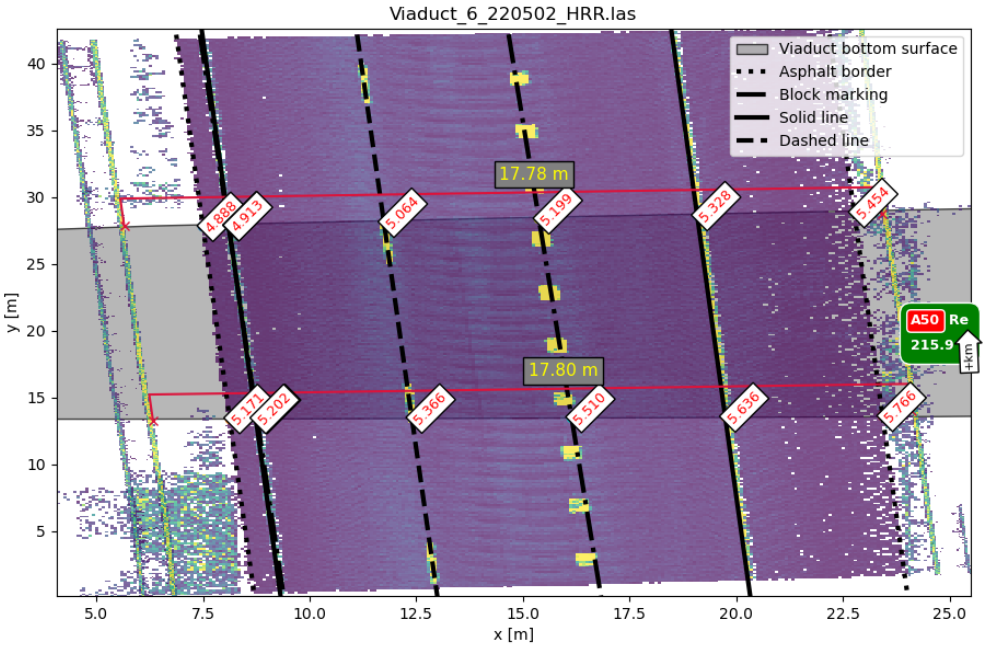

Figure 8. Example of the estimated clearances under a viaduct. The vertical clearances are shown in red and the horizontal clearances in yellow.

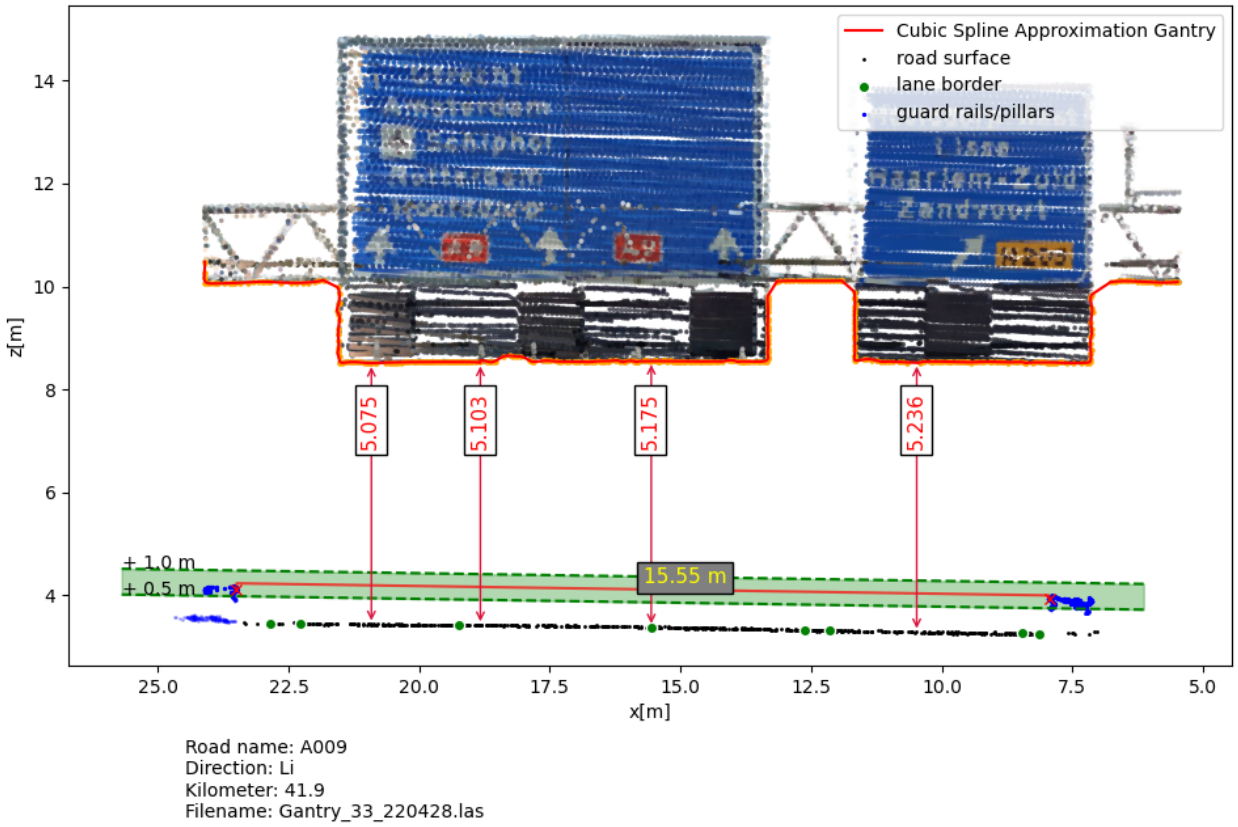

Figure 9. Example of the estimated clearances on a single gantry. The measurements are given in meters.

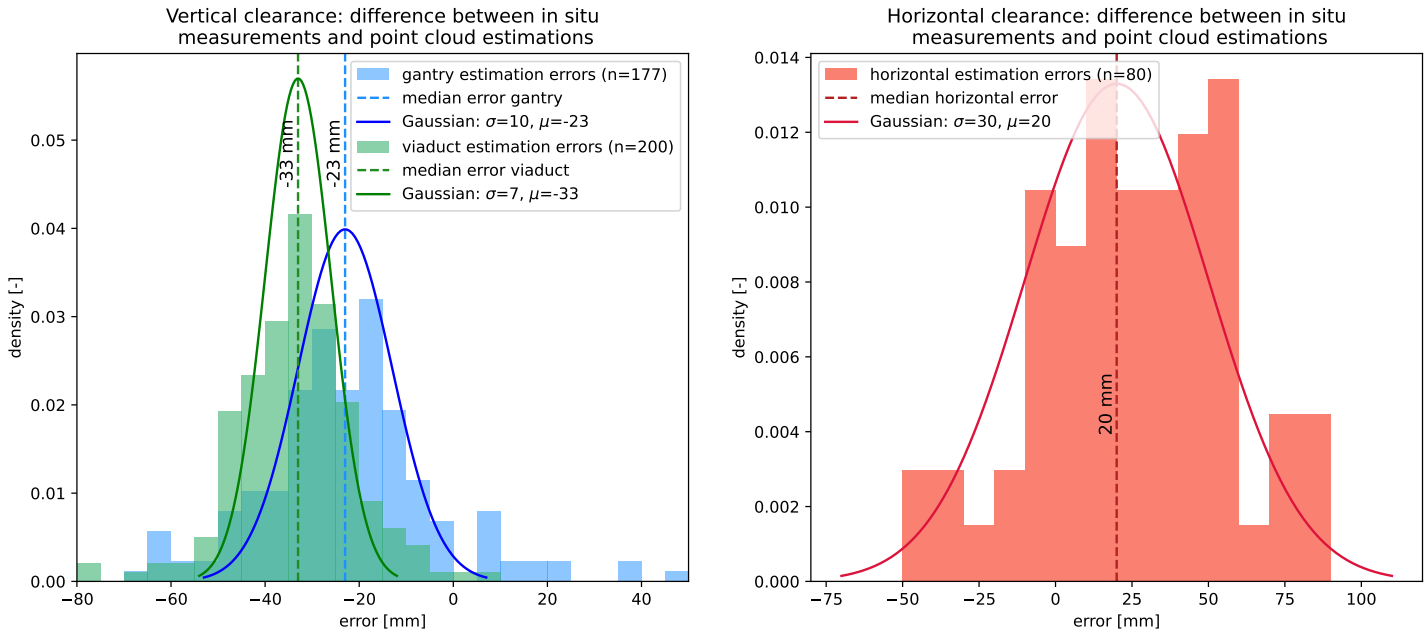

Figure 10. Histogram of errors of the estimated clearances.